POLITECNICO DI TORINO

Collegio di Ingegneria Chimica e dei Materiali

Master of Science Course in Materials Engineering

Master of Science Thesis

Rubber nanofibrous membranes obtained by electrospinning: preparation, functionalization, and application as filters for oil/water separation

Tutors

Prof. Alessandra Vitale
Prof. Roberta Maria Bongiovanni

Candidate

Jessica Alexandra Talamo Ruiz

October 2023

Abstract

Offshore oil spills, industrial oily wastewater, and domestic oil pollution are some of the most serious global challenges and are leading environmental causes of morbidity and mortality. The development of effective methods to separate oils from water surfaces and oil/water mixtures is thus crucial.

Electrospinning is a unique technique to produce nonwoven membranes formed by fine submicrometric fibers from polymer solution or melt through the application of high electrostatic forces. Electrospun nanofibrous membranes are considered a promising candidate for oil/water separation, with competitive advantages including a large specific surface area, high porosity, good pore channel connectivity, facile tunability of surface wettability, and easily scalable fabrication from various materials. In particular, the fabrication of rubber nanofibrous membranes by electrospinning has recently attracted significant attention owing to their interesting properties, such as high elasticity, extensibility and abrasion resistance, low hysteresis loss and excellent resilience.

This research work concerns the preparation and functionalization of rubber electrospun membranes for oil/water separation. Suspension electrospinning (i.e., electrospinning of a stable dispersion of polymer micro-/nano-particles in water using a small quantity of an easily electrospinnable water-soluble polymer acting as a template) of a styrene-butadiene rubber (SBR) latex and polyethylene oxide (PEO) as template polymer is carried out. Then, a thiol-ene photo-induced chemical crosslinking process of the fibrous membranes is applied to inhibit the movement of the polymeric macromolecules and thus prevent the collapse of the fibers due to cold flow. This combination of processes allows the easy production of stable and insoluble rubber nanofibrous membranes exhibiting high hydrophobicity (contact angle with water ≈100°) and oleophilicity (contact angle with hexadecane <10°). After a few minutes of continuous contact with water, however, the membranes become gradually hydrophilic, losing their oil/water separation capacity.

To overcome this limitation, a surface functionalization of the electrospun rubber membranes is designed and developed with the aim of tuning and stabilizing their wettability. In particular, a vinyl terminated polydimethylsiloxane (PDMS) is used as functionalizing agent.

In order to study and optimize the membranes functionalization process, characterization techniques such as FT-IR, optical microscopy and FE-SEM analyses are used. In addition, quantitative tests are conducted to evaluate the wettability properties and the oil/water separation efficiency of the functionalized membranes. The developed PDMS-functionalized rubber nanofibrous membranes demonstrate to maintain their hydrophobicity with time (water contact angle of 123.4° after 30 minutes, and water-in-oil contact angle of 121.6° after 24 hours) and to successfully separate oil from water (efficiency of separation of 99.3 %), showing an outstanding application potential for the treatment of polluted oily water.

Index

Index of figures

Index of tables

1 Introduction

The constant growth of industrial activities has led to a reduction in the availability of clean water sources worldwide due to the serious pollution generated by waste products. In fact, supply shortages, scarcity of drinking water, escalation of diseases and destruction of marine ecosystems are some of the main problems currently affecting society with alarming consequences. Among the activities responsible for water pollution, the petrochemical and oil industry is undoubtedly one of the most significant. Indeed, oil is a severe pollutant for any aqueous system, as it is capable of covering large areas of clean water in a very easy and fast way. On the other hand, conventional techniques for the treatment of oily wastewater currently available are often demanding in terms of energy and financial capital, and require considerable space and personnel to operate the treatment facilities. As a result, the purification phase of the polluted water is often neglected. Certainly, it would be unfeasible to contemplate a restriction of industrial activities in a world that depends mainly on these production cycles and commercial activities. For this reason, the current challenge for society is to develop prevention strategies and new water treatment techniques capable of dealing with pollution problems while being effective, sustainable and economically viable.

The search for alternative techniques for the treatment of oily wastewater has led to the use of innovative materials capable of separating oil and water with a reduced environmental and economic impact. Among the approaches proposed for this category of materials, the production of membranes with tunable surface characteristics has emerged. Indeed, the most important properties that determine the separation efficiency of a membrane include its specific surface area and the possibility of modifying its wettability behavior. Thus, in this work, electrospinning and a subsequent photo-induced functionalization process are proposed for the fabrication of hydrophobic/oleophilic fibrous membranes for oil/water separation. In fact, electrospun membranes are nonwoven structures consisting of submicrometer fibers assembled from a polymeric solution through the application of high electrostatic forces and their main characteristics include a large specific surface area, high porosity, good pore channel connectivity, and easily scalable fabrication from various materials.

Notably, rubbery materials have arisen as a valid option for the fabrication of nanofibrous membranes as they possess interesting properties such as high elasticity, extensibility and abrasion resistance, low hysteresis loss and excellent resilience. However, the possibility of using such polymers to fabricate membranes through electrospinning is limited by the low glass transition temperature of the material, as it leads to a tendency to cold flow over time, resulting in an increase in the diameter of the fibers and eventually in the structure collapse. To solve this problem, it is possible to apply a chemical crosslinking capable of preventing the movement of the polymeric macromolecules and thus stabilize the fibrous structure. In this regard, this research work concerns the preparation of electrospun membranes for oil/water separation through a suspension electrospinning process, in which a styrene-butadiene rubber (SBR) latex and a small quantity of an easily electrospinnable water-soluble polymer acting as a template (polyethylene oxide, PEO) are combined to obtain a stable deposition of the fibers without the use of toxic or flammable solvents (water is the only solvent used). The membranes are then stabilized through a photoinduced chemical crosslinking process in which a thiol-ene reaction is triggered thanks to the presence of a photoinitiating system and a multifunctional thiol crosslinker.

For the application as filter for wastewater treatment, a selective wettability of the membranes, i.e., the ability to preferentially interact with a specific liquid, is envisaged. In fact, one of the possible options for the oil/water separation is the use of hydrophobic and oleophilic membranes. For this reason, SBR-based membranes can be functionalized using an agent capable of increasing and stabilizing the hydrophobicity of the surface to obtain membranes that allow the passage of oil while retaining water. In this case, a vinyl terminated polydimethylsiloxane (PDMS), recognized for being a strongly hydrophobic polymer, is used as functionalizing agent, and is chemically grafted on the nanofibrous membranes by a photo-induced thiol-ene reaction.

The aim of the research work is to fabricate and functionalize nanofibrous membranes to be used as filters for oil/water separation, and to study their structure from a morphological and chemical point of view, as well as in terms of wettability and filtration capacity (efficiency of separation of oil/water mixtures and oil flux).

The results obtained demonstrate the efficiency of the fabrication of rubber nanofibrous membranes by coupling suspension electrospinning and thiol-ene photo-induced crosslinking, and of the surface functionalization with PDMS, capable of conferring stable hydrophobic and oleophilic properties. In fact, the developed functionalized nanofibrous electrospun membranes present a considerably high and competitive filtration capacity for oil/water mixtures with respect to other membrane filtration systems found in literature.

The thesis includes Chapter 2, which describes the state of the art on the use of membranes for the treatment of oily water as well as the electrospinning technique applied to the fabrication of nanofibrous membranes for oil/water separation. Chapter 3 presents the materials and methods used in the experimental phase of the work and Chapter 4 shows and discusses the results obtained. Finally, the conclusions and the perspectives of the work are presented in Chapter 5.

2 State of the art

2.1 Membranes for oil/water separation

2.1.1 Oily wastewater: Impact and future scenarios

The identification and preservation of clean water sources has been a major priority since the beginning of humankind. However, with the growth and development of production processes in almost any field of industry, this has now become a real environmental problem, and water pollution is currently a significant challenge. Indeed, increasing amounts of oily water are produced as waste from daily human activities and industrial processes, such as metallurgy, palm oil production, water treatment, food processing and, of course, accidental oil spills in marine and terrestrial environments [1]. In fact, oil is one of the most severe contaminants affecting any type of aqueous system and the oil industry, which includes the refining, treatment, storage, transportation, and distribution of oil, as well as petrochemical industries, generates enormous quantities of oily wastewater. This generates an unrestrainable cycle between the use of water in the industry and the stability and conservation of the environment, as illustrated in Figure 2.1.

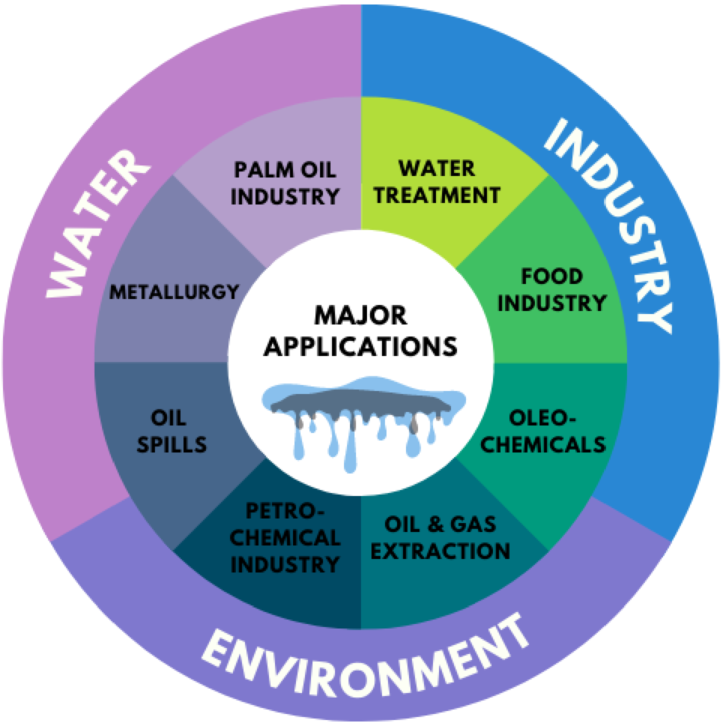

Figure 2.1: Schematic illustration of different applications that involve the production of oily wastewater. (Figure adapted from [1]).

The reason why oil is one of the worst water pollutants is that it can spread over very large areas. In fact, one liter of oil can contaminate a million liters of water, as it is able to form a very thin layer that covers the surface of clean water [2]. Most common oily contaminants for water are fuel oils (e.g., heavy fuel oil, diesel fuel, heating oil, light fuel oil), fats, lubricants and cutting fluids [3].

In general terms, the main impact of this water contamination are environmental damages and economic losses, which inevitably have consequences for society as a whole. This is because oil chokes off the oxygen supply for all species of animals and plants, making oil spills a potentially fatal accident for marine ecosystems. Furthermore, once the oil reaches the first level of the ecosystem, it does not just settle there, but rather moves up from level to level through the entire food chain. This means that even if the oil does not reach all species directly, it is still transmitted through the survival mechanisms of animals, reaching, inevitably, also humans.

On the other hand, oil adheres to the fur and coat of marine and flying animals as well. As a result, the intrinsic mechanisms that animals have to protect themselves from extreme environmental conditions, whether hot or cold, are restricted by a layer of oil from which they are often unable to release. This means that oil modifies the thermal insulation and water-resistant properties of their external coat, which can result in life-threatening consequences [2], as the degree of oiling decreases the animal's chances of survival.

Therefore, oily wastewater undoubtedly represents a hazard to human health as it can be carcinogenic and metagenic, but it is actually a risk that affects multiple levels of the environment: it affects fresh water and groundwater resources, implying a danger for aquatic ecosystems, contributes to atmospheric pollution, deteriorates the natural landscape, endangers animal and plant species and affects food and crop production [4]. In addition, the discharge of oily wastewater without adequate treatment reduce sunlight penetration into the water and leads also to an increase in the chemical oxygen demand (COD) and the biological oxygen demand (BOD) of the water body [5], which are the amount of oxygen required for oxidation of organic and inorganic compounds and the amount of oxygen consumed by aerobic bacteria growing on the organic material present in water, respectively. The COD/BOD ratio identifies the biodegradability of wastewater, and it is higher in industrial discharges in which non-biodegradable organic substances predominate [6].

Furthermore, oil contamination represents an additional factor that worsens water scarcity. Indicatively, although water covers about 70% of our planet, only 3% of that percentage is actually clean, drinkable water [7] and almost all of it is found in hard-to-reach sources, such as glaciers. As a result, about 4 billion people —i.e., about two-thirds of the world's population— experience severe water shortages for at least one month a year and more than 2 billion people live in areas with inadequate water supply [8]. In addition, the lack of adequate techniques to purify contaminated water affects about 2.4 billion people suffering from diseases such as typhoid fever, cholera, diarrhea and other water-borne illnesses. Moreover, the effects of the ongoing climate change have significantly altered water sources and weather patterns worldwide. This has caused lakes, rivers and aquifers to dry up or become too polluted to use. The United Nations Educational, Scientific and Cultural Organization (UNESCO) declared that over 80% of the wastewater is released to the oceans without being treated at all [9].

Considering current consumption rates and existing wastewater purification and recycling techniques, the future scenario seems to be very complicated. Just to mention a few of the possible problems that society could face [8]:

- By 2025, two-thirds of the world's population could face water supply shortages and the consequences on ecosystems worldwide will worsen.
- By 2030 about 700 million people may have to leave their current location because of intense water scarcity in certain areas.
- By 2040, 1 over 4 children worldwide will be living in areas with extremely limited access to water.

However, it is clear that with the current level of industrial progress worldwide, many of the activities that produce oily wastewater are impossible to avoid, not to mention that they are often essential for the normal development of the commercial activities of modern society. Nonetheless, wastewater treatment is often neglected by industries due to the high operational costs, the need for considerable space in the area close to the industry, the high installation costs of water treatment equipment and the limitations of the laws on discharge standards.

For this reason, it is necessary to develop preventive strategies and new treatment techniques to deal with the problem of water pollution. With this purpose in mind, many nations have started by setting regulatory limits on the maximum oil concentration in oily wastewater discharges (ranging from 5 to 100 mg/L) [10], which are reported in Table 2.1. However, it should be observed that, depending on the type of process and industry, the concentration of grease and oil in a discharge that is not subjected to sanitation treatments can reach values as high as 200,000 mg/L [11]. Therefore, research efforts are now focusing on the development of effective and economically viable techniques to treat oily wastewater and these often involve innovative materials as main solutions.

Table 2.1. Region-specific limits of oil and grease discharge in wastewater [5].

Entity or Regulation	Limits of Oil Discharge (mg/L)
Paris Convention	40 (to the sea) 5 (to offshore fields)
Oslo-Paris (OSPAR) Convention	30
Environmental Protection Agency (EPA) in USA	72
China Government	10
Department of Environment, Environment Quality Act 1974 in Malaysia	10
UAE Environmental Regulation	100
Central pollution Board of India (CPCB)	35

2.1.2 Conventional treatment techniques of oily wastewaters

Conventional techniques for oily wastewater treatment can be mainly classified into chemical, physical, mechanical and biological methods.

Fundamentally, the main principle that can be exploited when treating oily wastewater is the fact that oil and water are practically immiscible and have different densities, which facilitates the separation process. However, oil can be found in the aqueous medium in different forms [12]:

- **Free oil:** the oil forms a dispersion with droplets with a diameter of more than 150 μm. Such dimensions of the oil droplets facilitate the separation of the two components even with less demanding conventional methods.
- **Dispersed oil:** the droplets present diameters ranging from 50 to 100 μm. In this case, conventional separation methods can be applied, but factors such as the presence of destabilizing agents and the dimensional distribution of the droplets are also relevant and can complicate the separation process.

- **Emulsions:** the oil droplets have a diameter of less than 50 μm. The dimensions start to become too small to ensure the full efficiency of conventional separation methods.
- **Dissolved oil:** the dimensions of the droplets make it excessively difficult to separate the two components, so biological and/or chemical separation techniques are used.

In addition to the droplet size and the densities of the two components, the difficulty involved in the separation process also depends on temperature, pH, droplet size distribution and the presence and amount of other contaminants and chemicals.

Physical methods

Techniques based on physical principles for the treatment of oily wastewater can be applied when dealing with free or suspended oil in the aqueous phase. Overall, physical methods consist of the separation of the components through the application of mechanical, electrical or thermal action [13].

Among the most commonly used techniques in this category are dissolved air flotation (DAF), gravity separation, coagulation separation method as well as evaporation through thermal treatments, filtration, and separation by gravity sedimentation tanks, cyclones, centrifuges and industrial boilers.

The *DAF process* is based on the lack of oil/water interaction. In fact, pressurized air bubbles are introduced to transport the suspended molecules to the top of the mixture, as they adhere to the bubbles through a mechanism called "shock". Generally, the bubbles have sizes between 20 and 100 μm [5]. In this way, the solute accumulates on the surface and is then collected by using a surfactant. However, it is necessary to take into account that both pressure and air saturation in the wastewater are factors that determine the outcome of the process and, for microbubbles to be effectively generated and brought to the surface, the pressure must be close to the atmospheric pressure, so an excess of dissolved gas is used.

On the other hand, the *gravity separation technique* relies on the density difference between oil and water to separate the components: the greater the density difference, the greater the separation efficiency [14]. However, it is currently used only as pretreatment or primary treatment of oily wastewater. For this reason, it is usually coupled to the *coagulation separation method*. This technique consists of increasing the probability of collision of the oil particles with the aim of creating increasingly larger particles [5]. Aggregation of the small particles takes place through two different mechanisms: shielding of the negatively charged sites leading to precipitation or the interaction of the negatively charged colloids and the positively charged coagulants and subsequent neutralization of the charge [15].

Chemical methods

The most widely used chemical methods for the treatment of oily wastewater include adsorption, flocculation and electrochemical technologies. In the first case, materials such as zeolite and activated carbon are used to adsorb oil molecules of small or medium size on their surface, since they have a high specific surface area and a porosity suitable for promoting the separation of water and oil. Currently, materials such as sponges, nanoporous graphene, chitosan, biomass, cotton and metal-organic structures have emerged as innovative materials to promote adsorption [11].

Coagulation-flocculation is considered both a physical and a chemical method. In fact, it consists of adding chemical substances called flocculants that reduce the repulsive interaction between the double layers of electrical charges of the particles leading to their agglomeration, as described above. This process takes place due to a chemical reaction between the positive charge of the coagulating agents and the negatively charged colloidal particles [13]. The efficacy of the technique depends mainly on the pH of the wastewater, the oil concentration, the temperature and the amount and type of flocculants, which can be inorganic salts, natural or organic synthetic polymeric flocculants [16].

As for *electrochemical technologies (ET)*, they can be classified into electroflocculation, electroflotation and electrocoagulation, and it is usually necessary to combine more than one of these methods to treat oily wastewater. The general idea of the technique consists of oxidizing the oil to obtain H_2O, CO_2 or other biodegradable products, and for this purpose an electrolysis process is implemented. The process consists of using electrochemical cells in which sacrificial electrodes (usually made of iron or aluminum) are immersed and a specific potential difference is applied. Thus, through a redox reaction, the Al^{3+} or Fe^{3+} cations react spontaneously with the OH^- formed by the cathode, generating polyhydroxides that act as flocculants to remove the oil by flotation or sedimentation. In addition, H_2 gas microbubbles can also be generated, and the oil droplets progressively adhere to them until they form flocs that can be easily removed. The efficiency of this process depends on the pH and electrical conductivity of the wastewater, the concentration of the contaminants, the current density, and the retention time [17].

Biological methods

Biological methods are based on the ability of microorganisms to use the hydrocarbons present in an oil/water emulsion as nourishment. Thus, the hydrophobic cell surfaces and the various biochemical structures of these microorganisms, composed mainly of lipids and proteins, are used to reduce the interfacial tension facilitating the separation of the two phases.

These techniques can be classified into aerobic or anaerobic methods. In the first case the presence of oxygen and a significant amount of basic nutrients is necessary to complete the water treatment, while in the second case the system requires less nutrients and the organic pollutants are converted into methane (CH_4) [13]. Among these biological technologies, the microbial metabolism method, the activated sludge method, and the biofilm method are the most employed [11].

Mechanical methods

Mechanical methods are based on the use of mechanical coalescers in which the oil droplets collide and adhere, forming progressively larger droplets that are then separated by flotation due to the difference in density of the components in the oily wastewater. In particular, the purification process consists of four main phases: adhesion of the oil droplets, approach, coalescence and release.

Coalescers can be packing, plate, filter or fiber coalescers and their application depends on the operating conditions and the type of mixture being treated: for emulsions with droplet sizes above 20 μm, mainly plate and packing coalescers are used, while for droplet sizes below 10 μm, filter separators and fibrous coalescers are used [5].

Although most of the techniques described above can be optimized to achieve excellent levels of oily wastewater treatment, they are generally ineffective for treating oil/water emulsions with oil droplets smaller than 20 μm and require additional systems in order to pretreat wastewater [5]. Furthermore, they also involve problems related to energy and economic resources consumption, large footprint, secondary pollution, in addition to limitations inherent to the specific characteristics of each technique, as shown in Table 2.2.

Table 2.2. Limitations of conventional techniques for the treatment of oily wastewater.

Technique	**Disadvantages**	**Reference**
Flotation	Complex control of size distribution and amount of microbubbles generated in a given volume. High cost of retention tanks and pumps for microbubbles. Inefficient to separate ultrafine oil droplets.	[5] [18]
Gravity separation	Inefficient for emulsified oil separation. Large equipment, high operating and maintenance costs. Limited separation efficiency.	[12] [13]
Coagulation Flocculation	Large amount of sludge produced with metal hydroxides (aluminum or iron) or organic demulsifiers. Very long residence times and high energy consumption. Inorganic flocculants (aluminum sulfate, polymerized ferrous sulfate, and poly-aluminum chloride) have low flocculating efficiency. Organic polymeric flocculants possess health and environmental hazard since they do not biodegrade.	[5] [19]
Biological methods	Oxygen and nutrients must be present in large quantities. High temperatures are required. Production of high contaminant content due to accelerated biodegradation kinetics.	[13]
Adsorption	Conventional adsorbents (zeolite and activated carbon) have limited adsorption capacity and long adsorption time.	[11]
Electro-Chemical Technologies	Corrosion of the electrodes which causes a reduction in the system efficiency and high maintenance costs.	[20]

2.1.3 Emerging treatment techniques for oily wastewaters

To overcome the limitations and enhance the efficiency of conventional techniques for the treatment of oily water, current research trends are the combination of innovative materials that generally do not generate toxic residues and can biodegrade. For instance, to prevent toxicity of polymeric organic flocculants, materials such as chitosan and extracellular polymeric substances have been studied, as they do not generate hazardous residues and can help to produce sludge that can be biodegraded [21].

On the other hand, to improve the separation capacity of mechanical coalescers, materials such as carbon steel, fiberglass, polypropylene (PP), and styrene-butadiene rubber (SBR) are being considered to create fibrous coalescers [5].

Another interesting example of such optimization in wastewater treatment is the use of synthesized nanoporous activated carbon fibers (ACFs) and single-walled carbon nanotubes (SWCNTs), which present a higher adsorption capacity with respect to non-nanostructured materials due to the higher surface area along with smaller particle/fiber size [22], lower production cost and vast availability. Actually, these and several polymer-based nanomaterials can be used as individual devices or integrated into specially fabricated structures for wastewater treatment such as membranes.

Techniques involving membranes as a filtering device have become increasingly attractive for the treatment of oily wastewater due to their ease of operation and separation efficiency. In addition, they can be used to treat different industrial streams without significantly modifying their permeate quality. For this reason, research is currently focused on the optimization of membranes, especially to generate selective wettability by producing superoleophilic and superhydrophobic funzionalized membranes [10].

2.1.4 Fundamentals of membrane technology

Compared to conventional oily wastewater treatment methods, membrane separation techniques are convenient as they require moderate operating temperatures and usually do not require the use of toxic agents. Consequently, the treatment method involves less energy consumption and a more sustainable separation, as well as having a lower capital cost. In addition, membranes are structures that can be easily implemented before, after or in combination with other separation processes in order to improve the quality of treated water and allow to obtain oily sludge that could be reused or properly disposed for further handling.

In general terms, a membrane can be defined as a thin, semipermeable barrier through which certain substances pass, while suspended solids and other substances are prevented from being transferred. This phenomenon can be activated either by mechanical action or due to the effect of a driving force, which can be a pressure, concentration or thermal gradient, or the application of electric potential on both sides of the membrane. Therefore, the operation of a membrane, illustrated in Figure 2.2, depends on a feed stream which is divided into two products of different composition: a permeate, which represents the material passing through the membrane, and a concentrate, represented by the retained substance [23]. In the case of oil/water separation, the membranes normally allow water to pass through while retaining the oil droplets contained in the mixture.

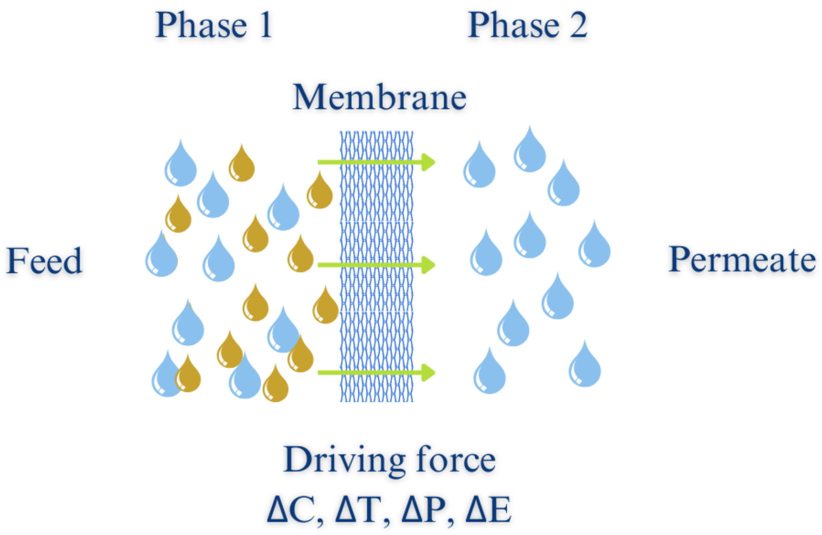

Figure 2.2: Schematic representation of the operation of a membrane for the separation of a two-phase mixture (Figure adapted from [23]).

Membranes can be homogeneous or heterogeneous, natural or synthetic, and these categories present completely different structure and functionality. In fact, depending on the morphology or structure of the membranes, the performance of the separation mechanism changes. Regarding synthetic membranes, they can be symmetrical or asymmetrical. The first category has a thickness ranging from 10 to 200 µm and can be porous or non-porous. In the second case instead, the thickness of the porous layer varies between 50 to 150 µm, but the membrane can be combined with a dense layer or skin with a thickness of 0.1 to 0.5 µm. The main difference between these structures lies in the fact that the decrease in membrane thickness usually determines an increase in permeation rate [23].

On the other hand, membranes can also be produced in different configurations such as flat sheets, plate, tubular and frame structures. Tubular membranes can be made of capillary systems or hollow fibers, while plate and frame membranes can be pillow- or spiral-shaped [24].

Another important classification of membranes refers to the type of driving force applied for the separation of the input flow. In particular, among those mentioned above, the most commonly used methods are pressure-driven and electric field-driven membranes, which are referred to as electrodialysis. However, when it comes to oil/water separation, the most frequently used process is the pressure gradient.

Pressure-driven membranes can be further classified for different applications including microfiltration, ultrafiltration, nanofiltration and reverse osmosis. The distinction depends mainly on the molecular weight or size of the particles that the membrane is able to filter and on the pressure gradient applied, as summarized in Table 3.1 [23, 25].

Table 2.3. Size cut-off range and pressure range in different membrane processes.

Membrane process	Pressure range (bar)	Size cut-off range (μm)
Microfiltration (MF)	0.1 - 2.0	0.05 - 1.5
Ultrafiltration (UF)	1.0 - 5.0	0.002 - 0.05
Nanofiltration (NF)	5.0 - 20	0.0005 - 0.007
Reverse osmosis (RO)	10 - 100	0.0001 - 0.003

In addition to the size of the particles that can be separated, membranes can also be characterized by important concepts that determine their performance, including flux and recovery [24]. The system flux (J) is defined by Equation 2.1:

$$J = \frac{Q_P}{A_m} \tag{2.1}$$

where Q_P represents the filtrate flux and A_m represents the surface area of the membrane.

The membrane recovery (R) is the ratio between the amount of filtrate flux (Q_P) and the amount of feed flux (Q_f) and, thus, it can be expressed by Equation 2.2:

$$R = \frac{Q_P}{Q_f} \tag{2.2}$$

Furthermore, when dealing specifically with membranes for the separation of oil and water, ideally the continuous phase passes through the membrane while the dispersed phase is retained. However, it is necessary to consider that the liquid droplets can be deformed, so they could penetrate the membrane pores if the applied pressure exceeds a certain value. For this reason, in the case of separation of oil/water emulsions, the separation efficiency (f), defined by Equation 2.3, must be considered:

$$f = 1 - \frac{C_P}{C_f} \tag{2.3}$$

where C_P is the oil concentration in permeate and C_f is the oil concentration in feed.

In oily wastewater treatment, UF and MF processes are the most widely used since they guarantee a higher separation efficiency. However, some applications have been limited by *fouling*, a mechanism involving adsorption and surface charge of membranes that generate a low long-term permeation flux: foulants clog pores and the retained aggregates form a polarization layer and/or a thin cake on the membrane surface, as illustrated in Figure 2.3.

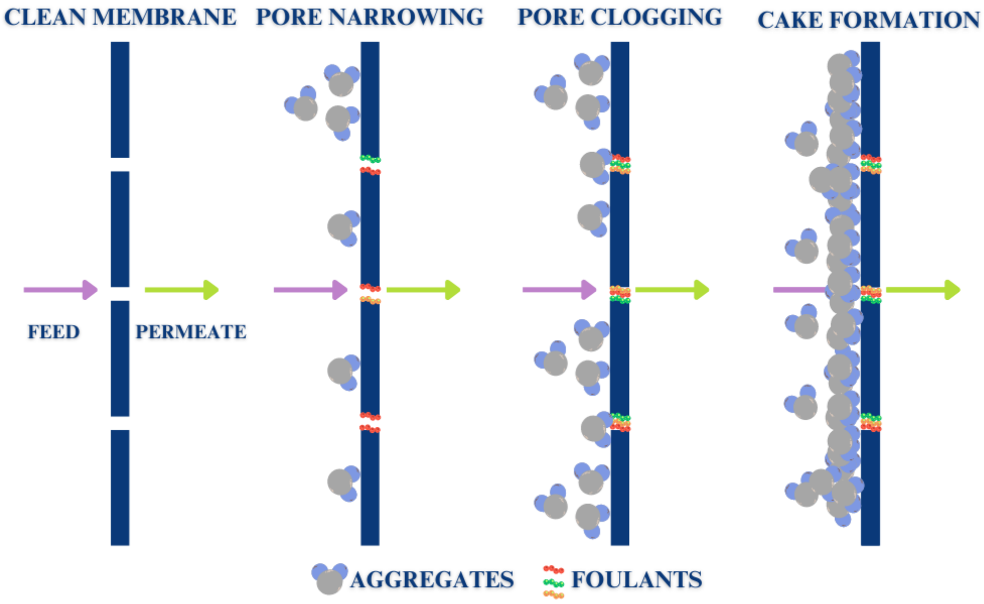

Figure 2.3: Schematic representation of fouling in membranes (Figure adapted from [26]).

This results in lower flux, lower separation efficiency and reduced membrane lifespan with consequent increased maintenance costs. Thus, the advantages offered by membrane technology for oily wastewater treatment can be limited by the extra cleaning, chemicals and energy requirements due to fouling.

2.1.5 Advanced membranes for oil/water separation with controlled wettability

Considering the above mentioned difficulties, in the last decades many works have been focused on the modification of membranes in order to reduce fouling. So far, the solution has been oriented to the search for methods to prepare membranes with tunable surface characteristics. In particular, wettability has proved to be an interesting property capable of improving the separation efficiency of membranes. It is in fact a property that determines the degree of affinity of the material with a liquid, thus, the possibility of controlling it would allow to design devices capable of favorably interacting with one of the components of the mixture while rejecting the other.

In this sense, polymers have emerged as a valid option for wastewater treatment due to their flexibility, ease of processing and adaptation, mechanical characteristics, chemical stability but, especially, because of the availability of techniques that make it possible to modify their properties. A wide variety of polymers have been studied and used to manufacture membranes to treat stable emulsions, specifically when dealing with particularly water-soluble oily wastes [23], including chitosan, polyamide, polyacrylonitrile (PAN), polyvinyl chloride (PVC), polyethylene (PE), cellulose acetate (CA), polyvinyl alcohol (PVA), polypropylene (PP), polyether sulfone (PES) and polyvinylidene fluoride (PVDF) [25, 27]. Moreover, to modify the wettability of polymeric membranes, techniques such as blending of different polymers, pre-adsorption of water-soluble polymers, plasma deposition to enhance solute rejection, fabrication of composite membranes and photochemical grafting have been used [25].

On the other hand, nanotechnology offers new interesting techniques for the preparation of membranes for oil/water separation. This way of manipulating matter refers to the nanometric scale, i.e., to the science, engineering and technology and use of materials with at least one of the dimensions with sizes between 1 and 100 nm [28]. In this field, natural structures and organisms have inspired the design of new alternatives based on the nanohierarchy of the surface of the materials to obtain a special wettability (e.g., superhydrophobic surfaces), allowing to create membranes with higher permeate flux, stability and resistance to fouling [29].

To understand the potential of membrane surface modification for oil/water separation, it is essential to understand the general theories of wettability. Wettability is defined as the extent to which a liquid is able to interact with a solid surface through intermolecular interactions [30]. In general, when it comes to the separation of liquid mixtures, the resistance to mass transfer and the efficiency of the process depend on the wettability phenomenon, which in turn is related to the size, number and distribution of pores, roughness and surface energy of the membrane. In the case of oil/water mixtures, the separation process occurs precisely through wettability mechanisms that take place at the interface between the solid phase of the membrane surface and air, water and oil.

To have a quantitative measure of wettability, the contact angle (CA) formed by a given liquid on a solid surface is used. Geometrically, the CA is defined as the angle formed by the liquid at the three-phase interface where it meets a gas and a solid. Equation 2.4, known as Young's equation [31], relates this angle (θ) to the surface tension between the different phases:

$$cos\theta = \frac{\gamma_{SV}-\gamma_{SL}}{\gamma_{LV}} \tag{2.4}$$

where γ_{SV}, γ_{SL} and γ_{LV} represent the surface tensions at the solid-vapor, solid-liquid, and liquid-vapor interfaces per unit length of the contact line, respectively [32], as illustrated in Figure 2.4 (a).

However, Young's equation considers an ideally smooth and chemically homogeneous surface. In reality, surfaces exhibit inevitably a certain chemical heterogeneity, roughness, and variable stiffness, therefore, alternative theories were developed considering these aspects.

First of all, Wenzel [33] proposed a model based on the assumption that the liquid is able to penetrate into the roughness grooves of the surface, as illustrated in Figure 2.4 (b). The result of this consideration is that increasing surface roughness causes an amplification of the wetting properties of the smooth material. Indeed, as show in Equation 2.5, Wenzel's CA (θ_W) takes into account a roughness factor (r), defined as the ratio of the actual surface area to the apparent surface area [27]:

$$cos\theta_W = rcos\theta \tag{2.5}$$

The area of the solid-liquid interface is increased by the roughness of the solid surface, and r varies as a function of surface roughness; in particular, r>1 for a rough surface, while r=1 for a smooth surface [1].

Nevertheless, in this case, an approximation that does not correspond precisely to reality is also made. In fact, Wenzel's theory considers the surface to be homogeneous. Considering the wettability on a heterogeneous rough surface, Cassie-Baxter [34] proposed a more complicated model, illustrated in Figure 2.4 (c) and defined by Equation 2.6:

$$cos\theta_W = \varphi_S\,(cos\theta + 1) - 1 \tag{2.6}$$

where φ_S and (1- φ_S) are the solid fraction and the air fraction at the surface, respectively.

In this case, then, the effect of the solid-liquid and solid-air fraction below the contact area is considered [1]. Thus, when a liquid gets in contact with the surface, the droplet is actually suspended at a composite interface made of the solid and the air trapped by the surface roughness and the liquid droplet.

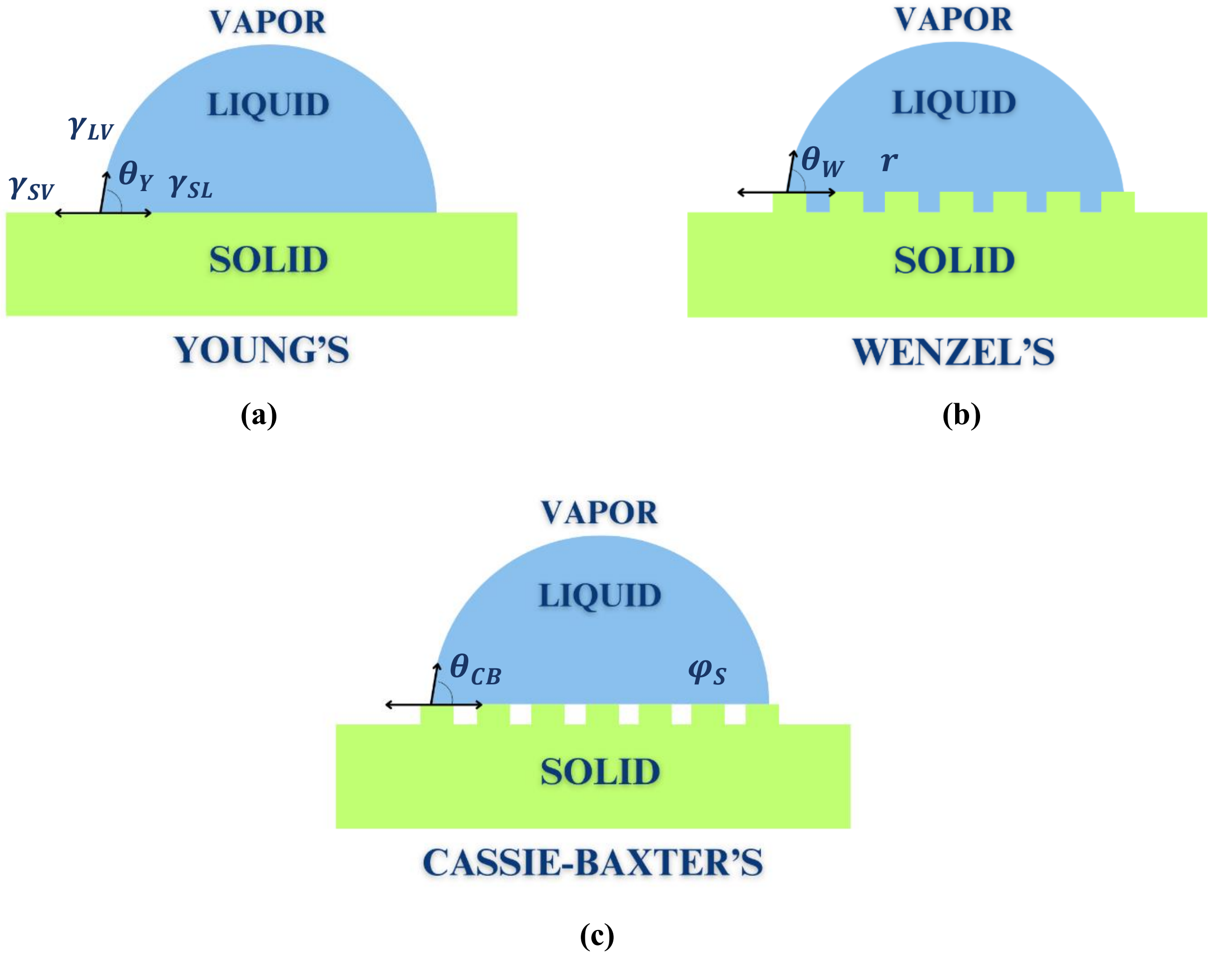

Figure 2.4: Schematic representation of contact angle models: (a) Young's, (b) Wenzel's, and (c) Cassie–Baxter's (Figure adapted from [1]).

The contact angle defined above is determined under static conditions and is therefore defined as static contact angle (SCA). However, there are other measurement methods that provide information on a dynamic contact angle. In this case, it is possible to perform contact angle tests by adding or removing liquid from the droplet that is deposited on the surface. In the first case, the droplet moves forward, so the contact angle is defined as the advancing contact angle (θ_{adv}), while in the second case, the droplet moves backward, so it is defined as receding contact angle (θ_{rec}), as illustrated in Figure 2.5 (a). In addition, it is possible to measure the angle that is formed when the surface is inclined and the droplet starts to slide, as shown in Figure 2.5 (b), which is called indeed the sliding angle (α or SA). The difference between θ_{adv} and θ_{rec} determines the contact angle hysteresis, which can also be measured just before droplet sliding occurs [27].

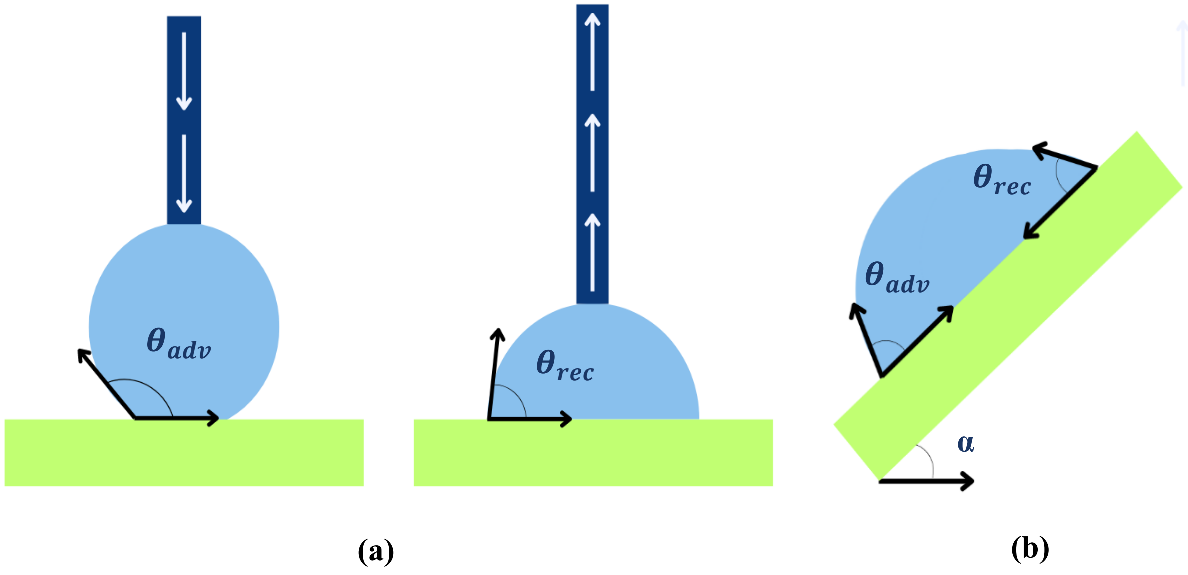

Figure 2.5: Schematic representation of (a) advancing and receding contact angle and (b) sliding angle (Figure adapted from [1]).

On the other hand, when applying membranes for the separation of liquid mixtures, it is important to consider a physical characteristic known as the breakthrough pressure (ΔP_c). This is the maximum pressure that can be applied to the membrane before the pores are wetted by the liquid. Considering small pores with a cylindrical and uniform geometry, it is possible to define the breakthrough pressure with Equation 2.7, better known as the Laplace-Young equation:

$$\Delta P_c = \frac{2\gamma_L \cos\theta_Y}{r_p} \tag{2.7}$$

where γ_L and r_p represent the surface tension of the liquid and the maximum pore radius of the membrane, respectively.

Although this is an approximation that neglects the characteristics of a real membrane, it is also a measure of how much the wettability of a membrane affects the filtration process.

These concepts are essential since they allow defining the nature of a surface on the basis of its wettability behavior. In fact, depending on the value of the contact angle, the hysteresis and the sliding angle, it is possible to classify the different types of surfaces with special wettability suitable for the treatment of oily wastewater. A first classification of surfaces can be made by considering the range in which the contact angle varies. In particular, when θ=0° is considered a condition of complete wettability, while when θ=180° is considered complete dewettability. Moreover, in the case of oily wastewater, the two main liquid components are precisely water and oil. Therefore, considering the wettability of water on a solid surface, two different behaviors can be distinguished, i.e., hydrophilicity (θ<90°) and hydrophobicity (θ>90°). Within this classification, advanced behaviors can be further defined. For instance, when θ exceeds 150° and the contact angle hysteresis is low, the surface is considered superhydrophobic, while when θ ≈ 0° for at least 0.5 s of contact the surface is considered to be superhydrophilic [27].

Similarly, surfaces can be oleophilic or oleophobic, but in this case the threshold separating the two behaviors is different and depends on the intermolecular forces of the substance. Indeed, oil molecules are bound together through weak van der Waals forces, so the bond is not as strong as in the case of water and this has a direct impact on the surface tension. For this reason, for a surface to be hydrophobic, the free energy of the surface of the solid must be less than 72.8 $mN\cdot m^{-1}$ (surface tension of water) [35], while for a surface to be oleophobic the free energy of the surface must be less than approximately 20-60 $mN\cdot m^{-1}$ (average value of the surface tension of oil) [1]. This results in a greater challenge when modifying surfaces, from a chemical and roughness perspective, to obtain oleophobic surfaces.

Superhydrophobic and superoleophilic membranes

A typical example of tested materials for oil/water separation are porous membranes that combine superhydrophobic (SHB) and superoleophilic (SOL) properties. A surface is considered SHB-SOL when the contact angle with oil is approximately 0° and the contact angle with water exceeds 150° [36]. These types of membranes allow oil permeation while retaining water [1] and are usually fabricated to exhibit micro- and nanoscale surface roughness [37]. For this purpose, two main methods are used to enhance the hydrophobicity and oleophilicity of the surface: firstly, roughness is introduced to an already hydrophobic surface and subsequently the chemical composition of the surface is modified with a low surface energy material [1]. Although this type of membranes with special wettability has proven to have a high efficiency in the separation of oil/water mixtures and emulsions, they are subject to fouling effects caused by oil adsorption on the pores and surface of the membranes, especially when the viscosity of the mixture increases [1, 27].

Superhydrophilic and superoleophobic membranes

In contrast to the first case described, superhydrophilic and superoleophobic membranes present a contact angle with oil greater than 150° while the contact angle with water is approximately 0°. The membrane retains the oil molecules due to the formation of a thin layer of water on the rough surface of the material, which repels the oil droplets, inspired by the structure of the rough scales of fish and clam shells which have oil repellent properties under water [29]. These membranes usually overcome the fouling problem and offer a high level of separation (99%). However, they must be used under water, because the membrane must be perfectly wetted in order to avoid oil permeation, which otherwise can proceed very easily [1].

Superomniphobic membranes

This type of membranes has no selective superwetting capacity when in contact with water and oil, but rather behaves as superantiwetting materials. In fact, superomniphobic surfaces present a contact angle greater than 150° both with water and oil, in addition to a low CA hysteresis to substances with low surface tension (i.e., oils) [1]. Superomniphobic membranes are typically applied for oil aerosol removal and membrane distillation technique [27].

Superamphiphilic membranes

Superamphiphilicity defines surfaces that present nearly null contact angle with both water and oil, thus presenting contemporaneously superhydrophilic and superoleophilic properties. In addition, this type of materials exhibits switching behavior depending on the medium in which it is found [38]. In the case of oil-in-water emulsions, the membrane allows the passage of water while retaining oil. On the contrary, when the membrane is immersed in oil, it is this substance that permeates the surface [27]. As a result of these characteristics, superamphiphilic membranes offer a versatile behavior that provides them with anti-fogging and self-cleaning properties. However, they have limited mechanical and chemical resistance, resulting in significant deterioration of the surface.

Membranes with smart wettability and Janus wetting properties

Smart membranes are able to modify their behavior depending on external stimuli. Unlike superamphiphilic membranes, which switch as a consequence of a pre-wetting mechanism, smart membranes can respond to a wider range of stimuli, such as temperature, electric fields, light and pH, modifying their wettability behavior [1].

A Janus structure has two faces with different properties and nature presents several examples of this behavior, such as the lotus leaf, which is a typical Janus interface: one side is superhydrophobic and the other is superhydrophilic [39]. This duality has inspired the development of many innovative materials, among which Janus membranes. These are two-dimensional materials with an asymmetric wettability on each side. This structure allows opposing surface properties to generate particular transport mechanisms. Thus, such membranes have been employed for mass transfer and ionic transport, in addition to unidirectional separation of water and oil, as they act as a switchable interface. However, the production and manipulation of the characteristics of these membranes is complex, as capillary effects can be generated in the pores of the structure promoting the diffusion of modifiers at the interface [40].

2.2 Electrospinning for the fabrication of membranes

Electrospinning is a technique based on a set of electromagnetic concepts used to obtain fibrous materials. In particular, an electric field is applied to overcome surface tension and generate a rotating jet from melts, solutions or suspensions of polymers (natural and synthetic), metals and ceramics. This versatile technique allows the fabrication of micro- and nanomatrials with complex structure and specific surface topology, specifically nanotubes, nanofibers and nanowires with continuous length, as well as random or highly oriented nonwovens [41]. Moreover, it allows the functionalization of nanofibers during their preparation, offering the possibility to incorporate functional agents such as, for instance, drugs, enzymes, metal nanoparticles and catalysts [42].

The functional principle and characteristics of electrospinning lead to the production of materials with great potential for applications ranging from tissue engineering, food packaging, sensors and textiles, to filters and mixture separation techniques. For this reason, it is an extremely interesting technique for the fabrication of nanofibrous membranes that can be used for oily wastewater treatment.

2.2.1 Operating principle and set-up of electrospinning

The electrospinning set-up is quite simple and requires moderate economic investments compared to other spinning techniques. However, it is an extremely complex method from a theoretical and experimental point of view and the material obtained depends on many factors that modify its morphology, surface characteristics and, therefore, its properties. In general, the set-up consists of five fundamental elements, as illustrated in Figure 2.6 for solution electrospinning. First, there is a syringe (I) that acts as a reservoir for the spinning solution/melt and is connected to a metallic needle (II). The latter allows the ejection of the solution, and also acts as the primary electrode. Initially, the solution is slightly extruded through the needle in order to form a droplet at the tip of it which remains stable due to the surface tension.

The feed rate is regulated by a piston/peristaltic feeding pump (III) and can vary from a few microliters per hour to many milliliters per hour, depending on the viscosity of the solution. Then, at a distance that normally varies between 10-25 cm from the primary electrode, a collector (IV) is positioned serving as a secondary electrode. The collector can be stationary (to obtain randomly oriented fibers) or rotating (to obtain fibers aligned according to the rotation speed). Conventionally, aluminum foil or glass plates are the most commonly used materials for the collector, but other types of collectors such as filters, disks or metal frames, or even liquids or baking paper can be used under controlled temperature conditions [41]. Finally, a high-voltage power supply is required (V) [43], which generates an electric field between the primary and the secondary electrode (with a voltage generally ranging from 10-30 kV).

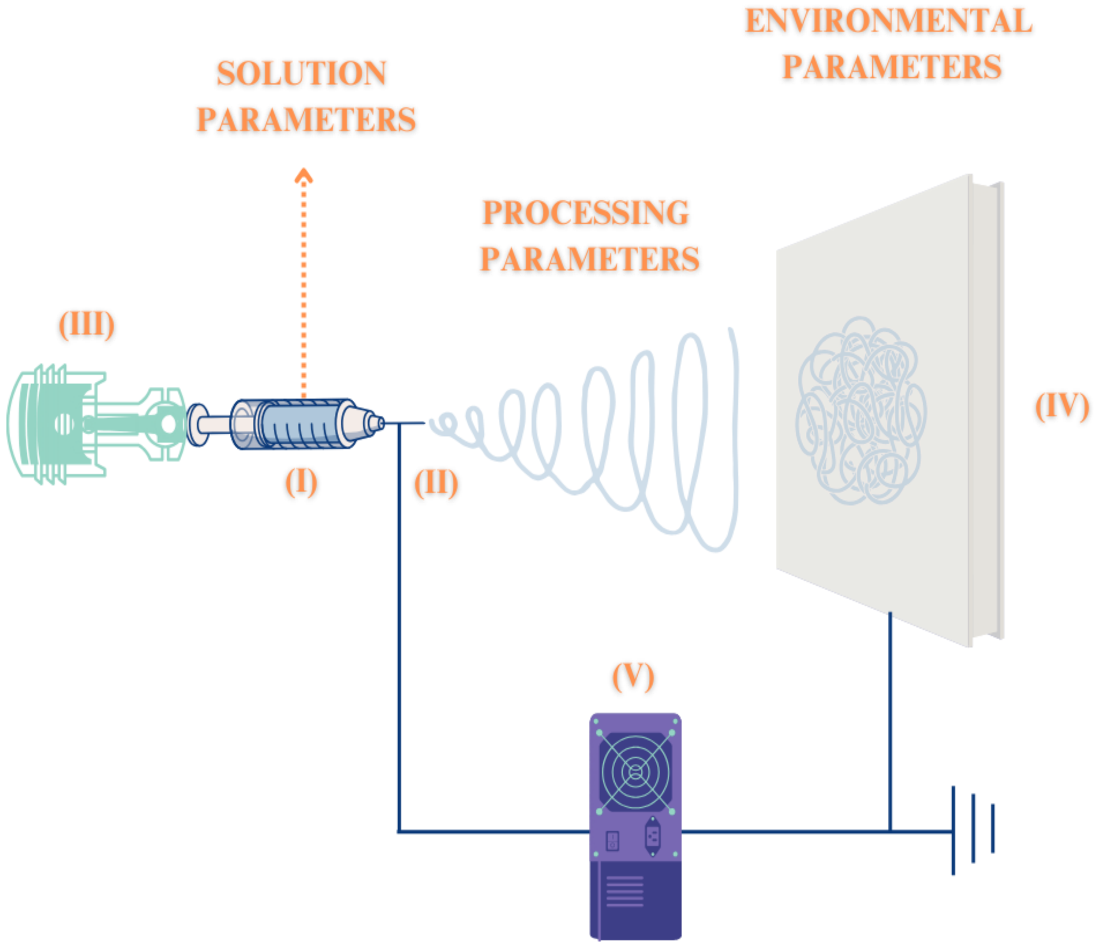

Figure 2.6: Schematic representation of electrospinning set-up.

One of the advantages of electrospinning over other fiber-forming processes (such as extrusion and elongation, melt blowing or other spinning techniques) is that the fibers are not formed by mechanical forces but rather by electrical forces. For this reason, the fiber is formed by a peculiar self-organizing mechanism controlled by the electrostatic interactions between the charged elements of the fluid [43], and the force involved (*F*) follows Coulomb's law described by equation 2.8:

$$F = \frac{k\,Q_1 Q_2}{d^2} \tag{2.8}$$

where k is Coulomb's constant ($9.0 \cdot 10^9$ Nm^{2}C^{-2}), Q_1 and Q_2 are the charges of the two bodies (C), and d is the distance between them (m).

Once the electric field reaches a critical level and becomes strong enough for the electrostatic force to overcome the surface tension, the fluid is expelled, and the fibers are deposited on the collector. In particular, the process occurs in well differentiated stages: initially, when the high voltage is applied, the droplet at the tip of the metal needle becomes electrostatically charged and the electrostatic repulsion between the surface charges results in a deformation of the spherical shape, which eventually elongates towards the secondary collector. Thus, the droplet acquires a particular conical shape, called Taylor cone, which leads to the onset of jetting.

Ideally, a single, rectilinear, stable jet of solution is formed. However, the number of jets formed per drop depends on the equilibrium between the applied tension and the surface tension, and the trajectory is actually not perfectly rectilinear but is influenced by deformation phenomena that cause loop or spiral deviations.

In particular, initially the jet follows a straight trajectory driven by a linear (ohmic) current flow for a relatively short distance. Then, due to charge migration processes, a convective current flow is generated, and the jet trajectory becomes increasingly loopy, as illustrated in Figure 2.7.

The jet can then exhibit instabilities that affect the fiber geometry, known as Rayleigh instabilities, and electrically driven axisymmetric instabilities causing diameter undulations [41], in addition to other characteristic instabilities, such as branching processes and the formation of physical beads [44].

As the jet proceeds along its trajectory, the solvent evaporates and a stable fiber is formed and deposited on the collector. During the process, a mat or membrane is progressively formed, resulting from the overlapping of randomly oriented fibers.

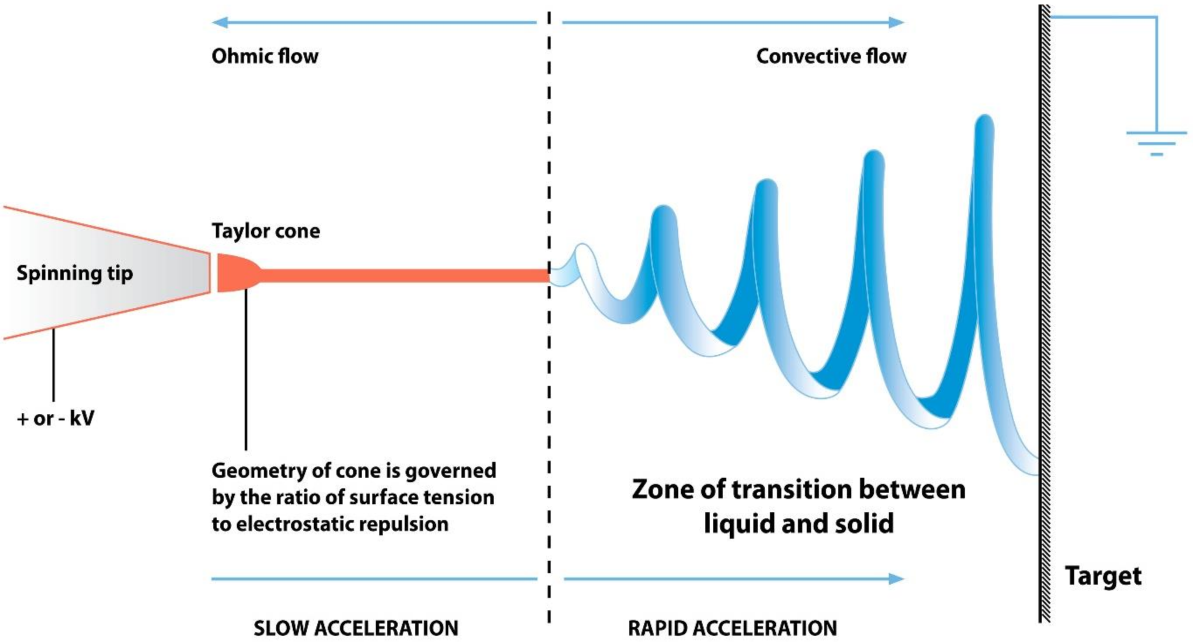

Figure 2.7: Schematic representation of the trajectory and undulatory instabilities of the jet during the electrospinning process [45].

2.2.2 Parameters affecting the electrospinning process

While requirements in terms of morphology vary according to the target application, in general, an electrospinning process is considered to be successful when continuous fibers with uniform diameters and no beads or droplets in their structure are obtained. To achieve this, many different parameters need to be considered and carefully modulated. Each of them has a precise effect on the morphology, diameter and arrangement of the fibers, which results in the modification of the macroscopic characteristics of the final structure.

It is possible to divide these parameters into three macro-categories that include parameters related to the composition and nature of the spinning solution, environmental variables, and factors related to the experimental set-up, i.e., variables that regulate the operation of the devices involved in the electrospinning process.

Solution parameters

Overall, there are two fundamental prerequisites that determine the adaptability of a polymer for an electrospinning process: firstly, a sufficient molecular weight and, secondly, the availability of a suitable solvent to dissolve the polymer [46]. However, the solution-related parameters that influence the final fiber morphology and characteristics are many.

First of all, the most important factor affecting the electrospinning process is the concentration of the polymer as it has an effect on many properties of the solution such as viscosity, surface tension and conductivity. In fact, to obtain continuous and stable electrospun fibers, it is necessary to use an appropriate concentration range. If the polymer concentration is too low, the viscoelastic strength of the polymer jet will be too weak to form a fiber, so it will split into individual sections which, due to the high surface tension, will become droplets. In addition, as the solvent evaporates, the droplet will start to reduce in size, leading to an increase in surface charge density. With the increase in electrostatic repulsion, the droplets tend to split into smaller droplets. On the other hand, if the concentration is too high, the viscosity of the solution may increase to a point where the jetting becomes very difficult. Thus, there is a range of polymer concentration in which the viscoelastic forces in the jet are such as to give it a stability to resist the rapid change of shape. The result is that the jet stretches uniformly, giving rise to a continuous and homogeneous fiber structure. This is because the concentration and the molecular weight of the polymer has a direct impact on the viscosity of the solution, which is determined by the entanglement of the polymer chains and the polymer-polymer, polymer-solvent and solvent-solvent intermolecular interactions. In fact, in order to have an indication of the morphology of the electrospun fibers, it is possible to refer to the solution entanglement number (n_e), described by Equation 2.9:

$$(n_e)_{sol} = \frac{M_W}{(M_e)_{sol}} = \chi \frac{M_W}{M_e} \tag{2.9}$$

where M_e is the entanglement molecular weight in the melt/solution, M_W is the polymer average molecular weight and χ is the polymer volumen fraction.

In the case of Newtonian fluids, different morphologies are obtained for different ranges of n_e:

- When $n_e < 2$, the polymeric chains do not entangle, so polymeric drops and particles (beads) are obtained, as illustrated in Figure 2.8 (a).
- When $2 < n_e < 3.5$, the entanglement of the chains is not sufficient and structures known as beads-on-string are produced, as illustrated in Figure 2.8 (b).
- When $n_e > 3.5$, the entanglement of the chains within the polymer solution is sufficient and the electrospinning process results in continuous and uniform fibers, as illustrated in Figure 2.8 (c).

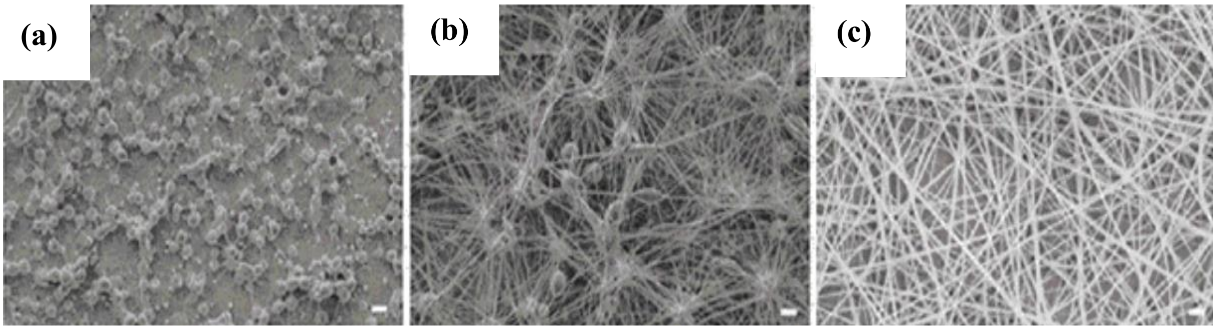

Figure 2.8: Example of different morphologies obtained through electrospinning using different polymer concentrations: (a) Individual polymeric beads, (b) Beads-on-strings structures, (c) Uniform electrospun fibers [47].

Furthermore, solution properties such as conductivity, viscosity and surface tension also depend on the choice of solvent. In fact, these characteristics are affected by intrinsic factors related to the solvent such as its polarity, boiling point, conductivity, dielectric constant, vapor pressure and dipole moment. From an experimental point of view, it is necessary to consider that the solvent must evaporate during the electrospinning process to obtain dry fibers on the collector and this means that the volatility of the solvent must coincide with the time and distance of jet displacement. If these factors are not synchronized, the solvent may evaporate before fiber deposition, resulting in the formation of irregularly porous surfaces, or it may not evaporate properly, resulting in the production of wet fibers.

As electrospinning is governed by electrostatic phenomena, the conductivity of the solution is essential. Also in this case there is a range of suitable values to promote the success of the electrospinning process. Thus, the solution cannot be electrically insulating because the electrostatic phenomena that lead to the formation of the jet would not be generated, but it must not have a too high conductivity value because the formation of the Taylor cone would be difficult, and the process would be unstable [46]. In this latter case, the jet loses its stability because of the strong electric fields, so that electric discharges could occur in the surrounding environment [47].

Environmental parameters

The environment in which the electrospinning process is conducted also plays a fundamental role in the morphology of the fibers obtained. In particular, humidity impacts on the volatility and evaporation mechanism of the solvent, and therefore modifies the structure and dimensions of the fibers. In addition, the interaction between humidity and solvent in the spinning solution determines the pore size distribution and number, which, generally, increase with increasing humidity level. When the humidity level is too low, the evaporation rate of the solvent in the jet increases as a consequence of the large difference between the partial pressure in the electrospinning chamber and the vapor pressure of the solvent. The result is that the fibers solidify in a short period of time and thus larger diameters are obtained. When humidity increases, the pressure difference is reduced and solvent evaporation occurs more slowly, which results in the stretching of the jet that generates finer fibers.

On the other hand, the properties of both the polymer and the final solution are correlated with temperature, so this is another environmental factor that affects the electrospinning process. In general, an elevated temperature causes a reduction in the viscosity and surface tension of the solution, as well as an increase in its electrical conductivity. This leads to the enhancement of jet stretching, resulting in fibers with smaller diameters. However, an increase in temperature also accelerates the evaporation process of the solvent, so that the advancement and stretching of the jet may be limited, favoring the formation of thicker fibers. For this reason, it is important to modulate the temperature range at which filamentation is carried out [47].

Processing parameters

The performance of an electrospinning process clearly depends also on the processing parameters settings. These mainly include the flow rate of the solution, the applied voltage and the distance between the needle and the collector (working distance).

The relevance of the applied voltage lies in the fact that it is the main factor determining the jet formation. Thus, to initiate the electrospinning process it is necessary to apply a certain voltage value that is able to generate the electric field to activate the electrostatic phenomena that lead to the formation of the Taylor cone and the subsequent generation of the jet. However, the voltage applied must be carefully regulated. On the one hand, a high value of applied voltage facilitates the formation of thinner fibers, but exceeding a critical value could generate a much more accelerated jetting, which results in the increase of the diameter dimensions of the fibers obtained and the possibility of obtaining irregular structures. This is due to the fact that the increase in tension promotes the electrical instabilities of the jet, which results in a much less uniform process.

Similarly, the solution flow rate influences the jet ejection and therefore impacts the solvent evaporation rate as well. Hence, it is necessary to find a minimum value of feeding in order to compensate the solution consumption and to maintain the continuous generation of the jet. In particular, when the flow rate is too low, an insufficiency of solution in the feeding phase of the system could be verified, obtaining irregular fibers. On the other hand, if the flow rate is too high, a dripping of the solution could be generated due to the deformation of the Taylor cone in view of the excess of material being expelled. Furthermore, if the flow rate is too high, the solvent may not have enough time to evaporate before deposition.

Lastly, the working distance influences the intensity of the generated electric field and the traveling time of the jet. Therefore, it is necessary to set a distance between the primary and secondary collector that ensures electrical and dynamic equilibrium. A smaller distance implies the generation of a larger electrostatic force and a shorter jet traveling time. Within certain limits, this results in an effective stretching of the jet and therefore in the formation of more stable and uniform fibers. However, if the solvent does not have enough time to evaporate during the jet travel time, the result is diametrically opposite: unstable jetting that generates defective or wetted fibers [46, 47, 48].

2.2.3 Electrospinning of polymer latexes

Among the main limitations of the application of electrospinning at industrial scale is the use of toxic and flammable organic solvents, incompatible with sustainable objectives related to the preservation of the environment. A possible alternative to overcome this problem is the use of water as a solvent, but this approach implies the exclusive use of water-soluble polymers, such as poly (vinyl alcohol) (PVA) or poly (ethylene oxide) (PEO). Electrospun fibers with such polymers would dissolve rapidly in water, a characteristic that could be limiting for many industrial applications [48], such as filtration and treatment of oily wastewater. Thus, there are techniques such as crosslinking that allow increasing the water resistance of water-soluble nanofibers, but this would still imply the use of energy, high temperatures and toxic crosslinkers, all of which are environmentally unfriendly.

On the other hand, another important limitation of the electrospinning process is the concentration of the polymer in the solution, as the maximum critical concentration is around 10-15 wt. % of polymer [49], depending on its viscosity. These values of concentrations are a declining factor in the productivity of the process. In fact, many polymers have been used to produce electrospun membranes (e.g., PAN, PP, PVDF), intended for filtration systems, and, although most of these structures have a very high filtration efficiency, the production of secondary pollution and resource costs has diminished their potential for practical applications.

Furthermore, there are certain materials that have very interesting characteristics but, due to their properties, can scarcely be electrospun. An example of this case are rubber polymers (e.g., polybutadienes). In fact, rubber nanofibrous membranes would be suitable for the development of efficient systems for filtration due to their porosity, stretchability, low weight, breathability, elasticity, low hysteresis loss and abrasion resistance, but the spinning ability of such polymers is very poor.

For this reason, the challenge of finding more sustainable methods for the production of electrospun fibers has arisen.

As a result, green electrospinning, a novel alternative that consists of combining a small amount of a water-soluble polymer (template) that is easily electrospun with the main polymer (e.g., latex) to formulate the electrospinning solution, has been developed. Using this technique, it is possible to overcome the drawbacks previously mentioned, since water is used as the medium for electrospinning and it allows the dispersion of higher polymer concentrations, which translates into a higher productivity [50, 51]. Generally, the required amount of template ranges from a few % up to 20 wt. % relative to the latex [49]. Once the fibers are obtained, the template is removed without disintegration of the latex fiber, as illustrated in Figure 2.9. After the removal of the template, the particles forming the fibers are held together by the van der Waal attractive forces between them, thus, the structure remains stable [48].

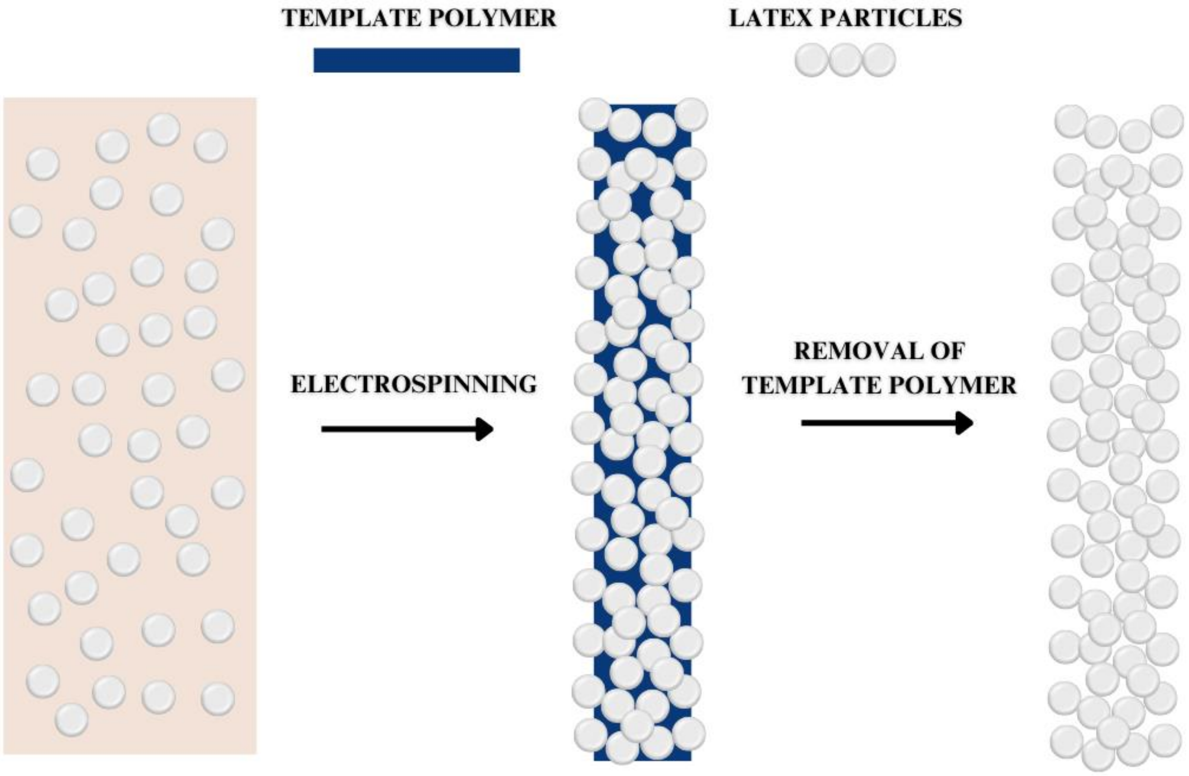

Figure 2.9: Schematic representation of the latex electrospinning process (Figure adapted from [48]).

Stability, morphology, and water resistance of the obtained fibers depend on the particle size of the dispersion: larger the latex particles, faster the disintegration of the fibers after the removal of the template [52]. The particle/template weight ratio and the efficiency of the crosslinking process are also important parameters of the process, in addition to the composition, chemistry and glass transition temperature of the polymer. Therefore, compositional and experimental parameters must be well understood and balanced to obtain the stability of the final fibers [48].

2.2.4 Electrospun membranes for water-oil separation

Once deposited on the collector, the electrospun nanofibers can spontaneously form a non-woven mat with a particularly interesting surface-to-volume ratio and a high interconnected porous structure. These features make it possible to obtain electrospun membranes that, compared to conventional fibrous materials, offer benefits that make them useful for filtration applications [46]. In fact, nonwoven structures composed of electrospun polymeric nanofibers present a porosity of about 80-95%, which allows them to select solid particles, aerosols, dust particles and fine droplets of fluids [43]. Thus, a gas or liquid stream can flow through an electrospun membrane without experiencing excessive resistance. For this reason, this type of structures, especially those that can be tunable or functionalized at surface level, have been studied as advanced filtration systems. They offer high selectivity and stability, and can be manufactured with materials suitable for recycling, representing another environmental advantage.

Electrospun membranes are thus very promising for the treatment of oily wastewater. The properties of nanofibrous membranes determine the efficiency of oil/water separation. These include surface morphology, amount and distribution of voids between fibers, porosity, surface tension and fiber diameter.

Firstly, the fiber morphology can be smooth or rough. According to the principles of wettability discussed in the previous chapters, it is known that roughness increases the hydrophobocity/hydrophilicity or oleophobocity/oleophilicity behavior of surfaces. Indeed, in the case of electrospun membranes this fundamental factor can be regulated to promote the adhesion of the particles of one of the two components to the membrane surface, improving the separation efficiency depending on the desired result. Indeed, the superhydrophobicity and superoleophilicity behaviors of a fiber are related to the natural properties of the material and to a high surface roughness of the fibers, which is particularly interesting in the treatment of oily wastewater.

In addition, the amount of voids between the fibers that make up the membrane is also a fundamental factor in improving the sorption capacity of the system. In fact, if it is possible to obtain an adequate size of the interconnected voids of the membrane, a faster sorption rate and a much higher droplet retention capacity can be obtained thanks to the capillary action established in the porous interior of the membrane fibers [53,54].

Furthermore, porosity can also be obtained in the cross section of the electrospun fibers. This allows the production of membranes with a hierarchical and porous structure at nanometric scale that improves the separation capacity by increasing the specific surface area available for adsorption processes: a large specific surface area directly leads to a large number of adsorption sites and high adsorption capacity [43].

On the other hand, the diameter of the fibers also influences the separation capacity of the membranes. In particular, when the fibers have smaller diameters and the porosity of the structure is high, the sorption and adhesion capacity of the droplets increases. In contrast, membranes composed of fibers with larger diameters have larger voids between them and, therefore, comparatively low capacities for the separation of liquid droplets [53].

Thus, by modeling the fibers morphology and properties, efficient filtration systems can be created. Selective removal of a specific contaminant can be achieved either by immobilizing the agent by physical mechanisms so that it is captured in the membrane structure or by tailoring the surface wettability. For example, a membrane composed of electrospun nanofibers with a low surface energy and a rough surface structure can remove oil, providing a suitable system for the treatment of oily wastewater [43, 54].

3 Materials and Methods

Considering the fundamental aspects described in the previous chapter regarding the use of membranes as a method for the treatment of oily wastewater, the main objective of the research work was to prepare by electrospinning hydrophobic-oleophilic nanofibrous membranes with the capacity to filter and separate oil/water mixtures. In this chapter the materials and the procedures used for the preparation of the membranes will be described, as well as the techniques employed to characterize them.

3.1 Materials

A styrene-butadiene rubber (SBR) latex was used as the main material to produce electrospun membranes. SBR is produced from the random copolymerization of styrene and butadiene and its chemical structure is illustrated in Figure 3.1. It is a synthetic elastomer with a wide range of industrial applications due to its excellent abrasion resistance and stability, excellent properties of aging and thermostability, crack resistance, good compressive strength and resistance to surface defect formation compared with other materials, such as natural rubber [55, 56]. In addition, it is also recognized for its low cost and availability, which makes it a suitable material for a sustainable green electrospinning process [57].

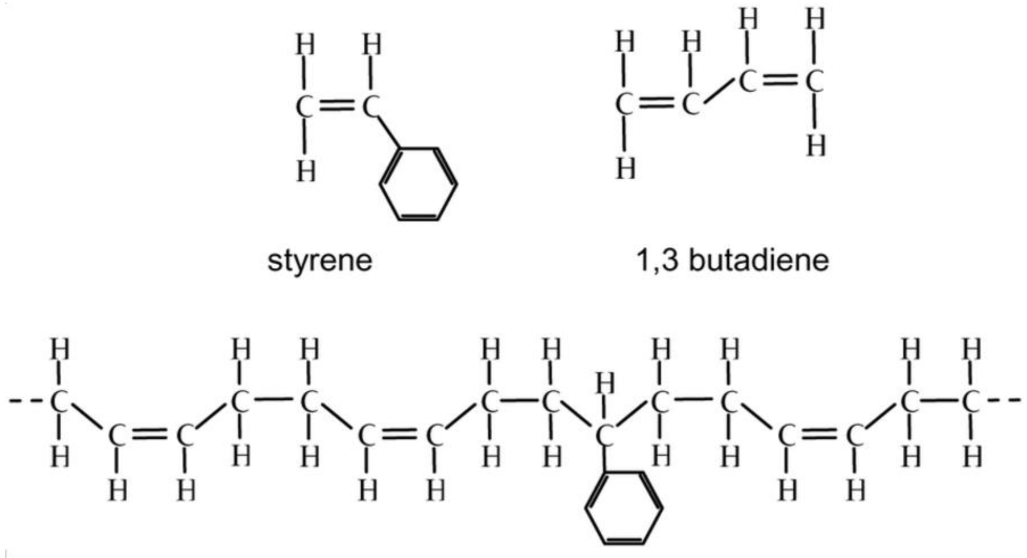

Figure 3.1: Chemical structure of SBR obtained from the random copolymerization arrangement of styrene and butadiene.

For this project, the SBR latex Elastolan S19 provided by RESCOM srl was used. It is a 50 wt. % aqueous dispersion of SBR copolymer (100–200 nm particle size) and visually it appears as a dense, white liquid. Its main characteristics include a glass transition temperature (T_g) of 6 °C and viscosity of 300 cP s at 25°C.

Polyethylene oxide (PEO) was used as template polymer for the electrospinning of the SBR latex. PEO is a water-soluble polymer prepared by polycondensation of ethylene oxide and water catalyzed by acidic or basic catalysts [58] and its chemical structure is shown in Figure 3.2. Specifically, in this work, PEO with a molecular weight (M_w) of 1,000,000 g/mol, which appears as a fine white powder, was purchased from Sigma-Aldrich.

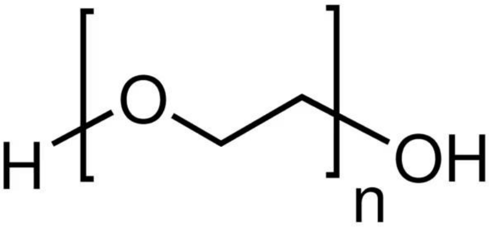

Figure 3.2: Chemical structure of polyethylene oxide (PEO).

In order to promote the photo-induced cross-linking reaction of the SBR membranes, a photoinitiating system was added. A mixture of diphenyl (2,4,6-trimethylbenzoyl) phosphine oxide (TPO), whose chemical structure is illustrated in Figure 3.3, and 2-hydroxy-2-methyl-1-phenyl-propan-1-one (Darocur 1173), whose chemical structure is illustrated in Figure 3.4, was used.

TPO is a monoacylphosphine oxide-based photoinitiator, and it appears as a light-yellow powder. Darocur 1173 is a versatile highly efficient liquid photoinitiator with an excellent compatibility, so it is especially suitable to be combined with other photoinitiators. Regarding its physical properties, it is an olorless slightly yellow liquid. Both photoinitiators were provided by Ciba Specility Chemicals Corp.

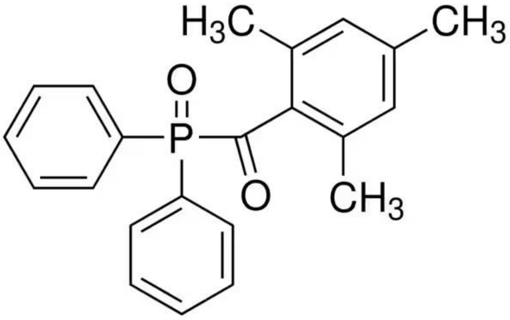

Figure 3.3: Chemical structure of diphenyl (2,4,6-trimethylbenzoyl) phosphine oxide (TPO).

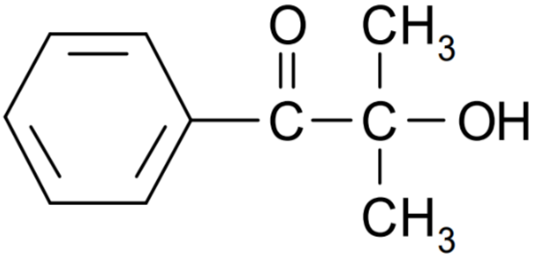

Figure 3.4: Chemical structure of 2-hydroxy-2-methyl-1-phenyl-propan-1-one (Darocur 1173).

In addition, trimethylolpropane tris(3-mercaptopropionate) (TRIS), a trifunctional thiol (-SH) monomer [59] provided by Bruno Bock Group, was used as crosslinking agent.

It is a colorless transparent or slightly yellowish liquid, and its chemical structure is shown in Figure 3.5.

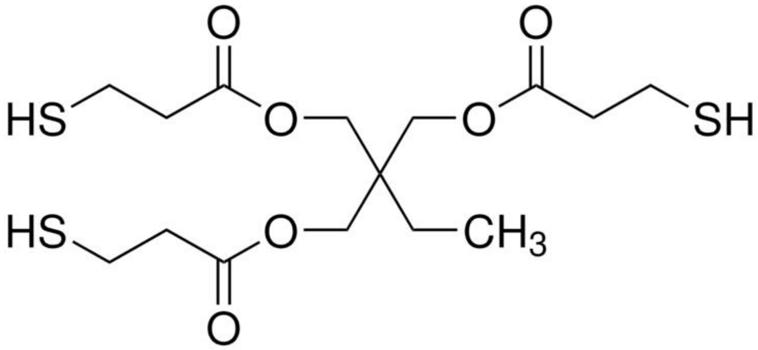

Figure 3.5: Chemical structure of trimethylolpropane tris(3-mercaptopropionate) (TRIS).

With the aim of improving the surface properties of the membranes to adapt them to water and oil filtration, polydimethylsiloxane (PDMS) was used as a functionalizing agent.

It is a widely used silicon-based organic polymer known for its versatile and interesting properties. Indeed, it is strongly hydrophobic, thermally stable, permeable to gases, optically transparent, simple to handle and manipulate, as well as non-toxic and non-flammable [60]. In addition, PDMS has a low surface energy (19–21 $mJ \cdot m^{-2}$) [61].

For this work, a bifunctional vinyl terminated PDMS (molecular weight: 28000 g/mol, wt. % vinyl: 0.18-0.26, vinyl (eq/kg): 0.07-0.10, viscosity at 25 °C: 1,000 cSt, density: 0.97 $g \cdot mL^{-1}$), with the chemical structure shown Figure 3.6 was supplied by Gelest Inc. It appears as a clear viscous liquid.

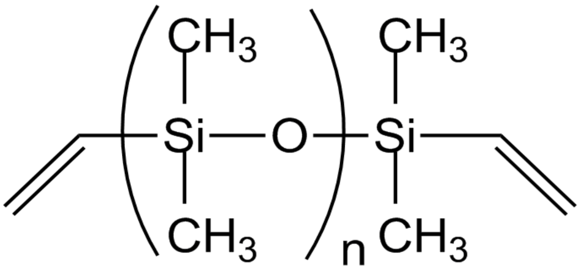

Figure 3.6: Chemical structure of polydimethylsiloxane (PDMS).

All other chemicals used were supplied by Sigma-Aldrich.

3.2 Production of the rubber nanofibrous membranes

3.2.1 Preparation of the solution

The first step in the production of the membranes consisted of preparing the solution for the electrospinning process. Firstly, a primary aqueous solution of PEO at 5 wt. % was prepared. This was magnetically stirred overnight at room temperature. In this way, a transparent, viscous and homogeneous solution was obtained. Elastolan S19 (50 wt. % aqueous dispersion of SBR) was then mixed with the PEO aqueous solution previously obtained, using an SBR/PEO mass ratio of 10:3. In this case, the solution was magnetically stirred for 2 hours at room temperature. On the other hand, TPO was dissolved in Darocur 1173 with a 1:1 mass ratio obtaining the photoinitiators system. Then, the mixture was added to the solution at 1 wt. % with respect to SBR and the solution was magnetically stirred for 15 minutes at room temperature. Finally, TRIS was added at 10 wt. % with respect to SBR and the solution was magnetically stirred for 5 minutes at room temperature. The composition of the solution is summarized in Table 3.1.

Table 3.1. Composition of the solution used to produce the electrospun membranes.

Material	Quantity
PEO	PEO 5% in water
Water	
Latex	Latex: 50 wt. % SBR
SBR	SBR/PEO mass ratio of 10/3
TPO	TPO/Darocur 1173 mass ratio of 1/1
Darocur 1173	Photoinitiators mixture: 1 wt. % with respect to SBR
TRIS	10 wt. % with respect to SBR

In this way a homogeneous, viscous and milk-white colored solution was obtained as shown in Figure 3.7.

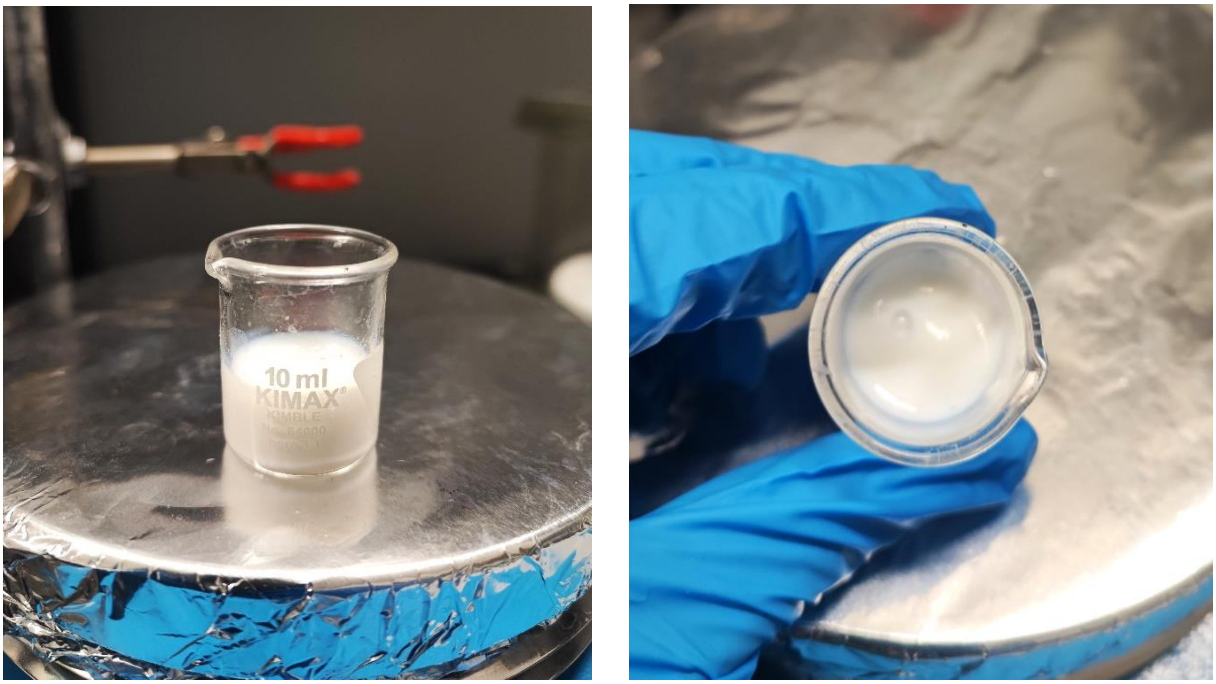

Figure 3.7: Final solution used to produce the electrospun membranes.

3.2.2 Electrospinning

For the production of the nanofibrous membranes, an electrospinning system with a horizontal configuration was used. Specifically, an E-fiber system by the SKE Research Equipment, shown in Figure 3.8 (a) and (b), was employed. The main applied setting of the system were:

- a flow rate of 0.35 ml/h;
- a diameter of the needle of 1 mm;
- a working distance between the two electrodes of 15 cm;
- a plane stationary collector (with an aluminum foil as substrate). In some cases, it was necessary to position a polytetrafluoethylene (PTFE) mesh or a polypropylene (PP) film on the aluminum foil to facilitate the removal of the membrane in the successive phase of the experimental procedure;
- a tension ranging from 13 to 17 kV. Since the dynamics of the process depends on the combination of many factors (including the ambient temperature and relative humidity), the tension had to be increased or decreased depending on the stability of the jet;

- environmental parameters ranging from 16 to 24 °C in terms of temperature and from 30 to 50 % for relative humidity.

The deposition of the fibers was carried out for an hour or an hour and a half for the production of each membrane.

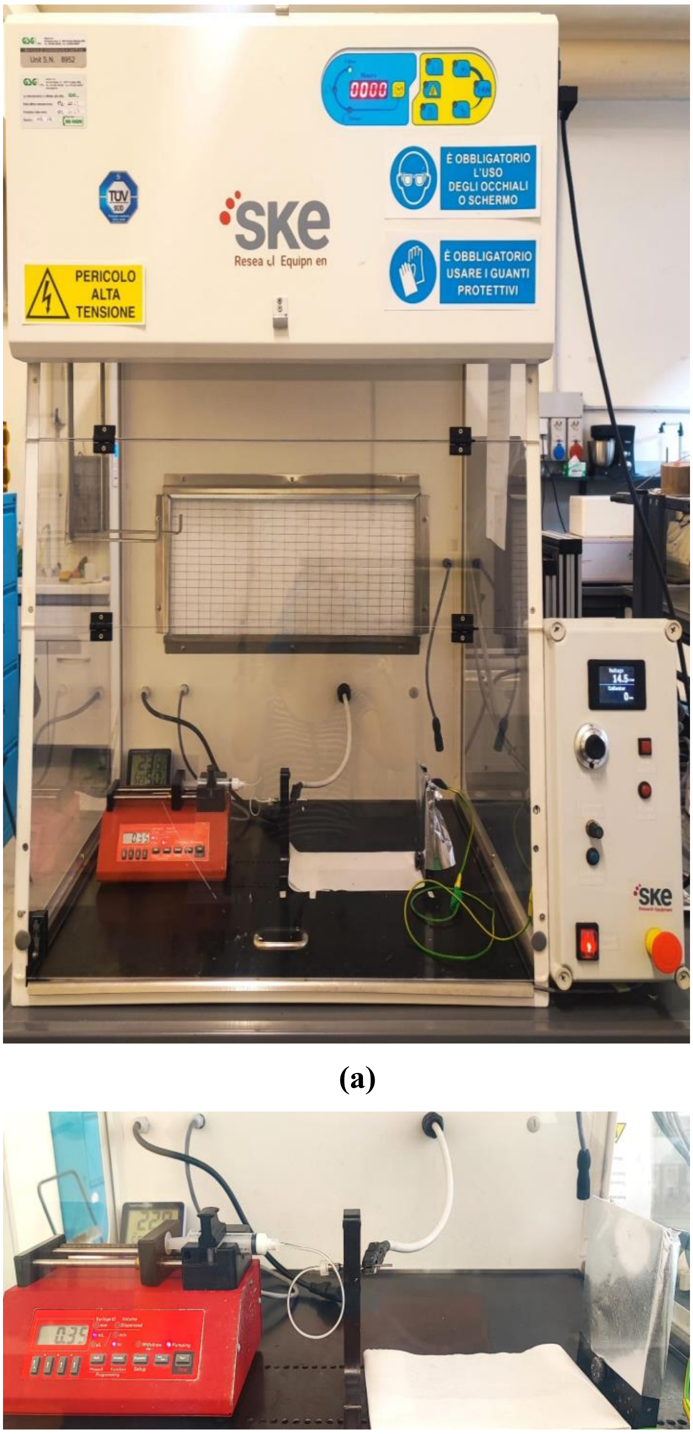

(a)

(b)

Figure 3.8: (a) Electrospinning set-up used to produce the nanofibrous membranes. (b) Detail of the set-up.

Once the nanofibrous membranes were obtained, they were carefully removed from the aluminum foil using precision blades and tweezers so as not to damage the structure, as shown in Figure 3.9 (a). Thus, free-standing membranes were obtained, as shown in Figure 3.9 (b).

(a)

(b)

Figure 3.9: (a) Removal of the electrospun membrane from the aluminum foil used as electrospinning collector. (b) Free-standing membrane obtained.

3.2.3 Photoinduced cross-linking

After production, the samples were irradiated by UV light using a high-pressure mercury-xenon lamp with an optical fiber LIGHTNINGCURE Spot Light source LC8, Hamamatsu, shown in Figure 3.10 (a). To determine the appropriate intensity, the UV radiometer Power Puck® II from EIT® Instrument Markets, shown in Figure 3.10 (b), was used. The membranes were irradiated at ambient conditions with an intensity of around 32 mW·cm^{-2} for 5 minutes to promote the thiol-ene photoinduced cross-linking process.

(a) **(b)**

Figure 3.10: (a) UV light source. (b) UV radiometer.

3.2.4 Water treatment and membrane functionalization

As explained in the previous chapters, green electrospinning consists of the use of an easily electrospinnable and water-soluble polymer as a template for the formation of the fibers.

Once the membranes are obtained and photo-crosslinked, it is necessary to remove the template. For this reason, the samples were immersed in distilled water for 24 hours in order to remove the PEO present in the structure, obtaining SBR-based membranes. The samples were then dried for 5 hours in air condition, allowing the water present in the structure to evaporate.

Once dried, the SBR-based membranes were subjected to surface functionalization using the siloxane monomer (PDMS). For this, a 5 wt. % solution of PDMS in toluene was prepared and then the membranes were immersed in the solution for 1 minute. After removal from the solution, they were dried using a compressed air gun.

Subsequently, they were subjected to UV light irradiation using the same instrument as described in the previous section. Also in this case, they were irradiated with an intensity of 32 mW·cm^{-2} for 5 minutes. The membranes were then immersed for 1 minute in the solvent used to prepare the functionalizing solution, i.e. toluene, in order to remove the excess of monomer that did not react. Finally, they were left to dry in air condition for 24 hours.

Using a digital micrometer, it was possible to measure the thickness of the functionalized membranes in at least five different spots. By calculating the average of these measurements, a range of 25-50 μm of thickness was calculated.

3.3 Characterization of the nanofibrous membranes

3.3.1 Optical Microscopy

With the purpose of observing the morphology of the membranes, the Olympus BX53M optical microscope shown in Figure 3.11 was used, with different magnifying lenses ranging from 5x to 50x.

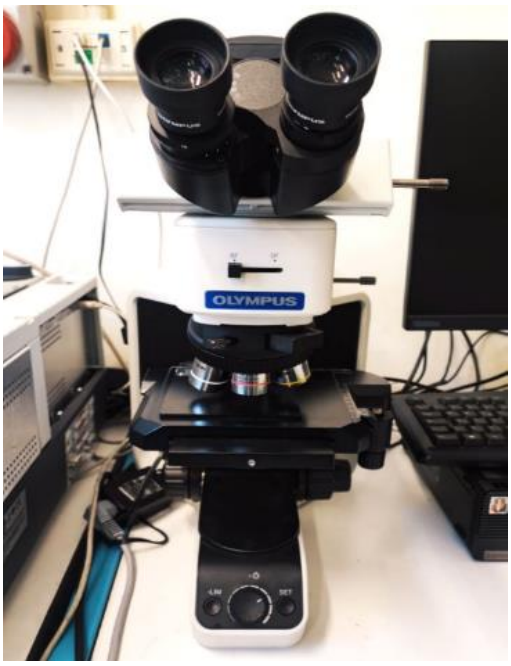

Figure 3.11: Optical microscope used to observe the morphology of the electrospun membranes.

3.3.2 Field Emission Scanning Electron Microscopy (FE-SEM)

The morphology of the nanofibrous membranes was also analyzed by means of the Supra 40 Field Emission Scanning Electron Microscopy (FE-SEM), ZEISS, shown in Figure 3.12. The samples were previously prepared for observation with the instrument through cathodic sputtering in order to create a thin film of Pt of approximately 10 nm. A Quorum Q150T ES was used to perform the coating.

In addition, the fiber diameters were obtained by ImageJ software analyzing the FE-SEM images.

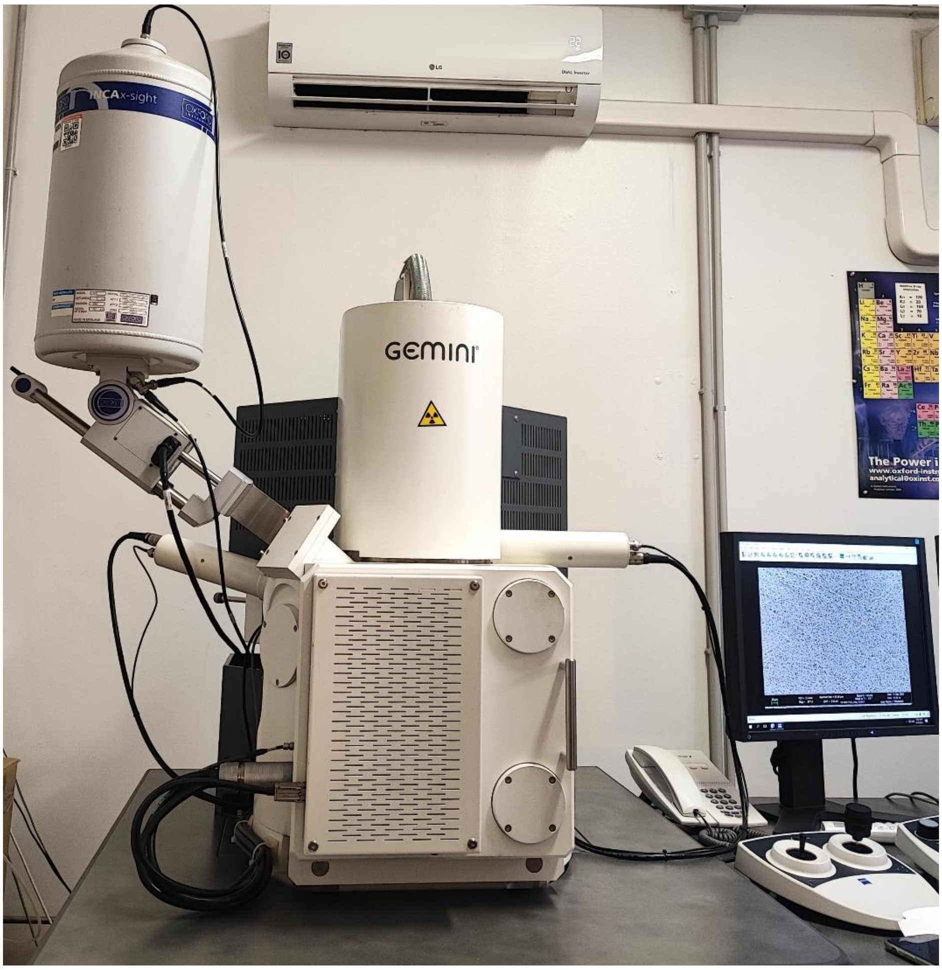

Figure 3.12: Supra 40 FE-SEM used to analyze the morphology of the fibers.

3.3.3 Fourier Transform Infrared Spettroscopy (FT-IR)

The chemical structure and composition of the membranes was analyzed through Fourier Transform Infrared (FTIR) spectroscopy by using a Thermo Fisher Scientific Nicolet^{TM} iS50 spectrometer (shown in Figure 3.13). In particular, the spectra were obtained in attenuated total reflectance (ATR) mode with an accumulation of 32 scans at a resolution of 4 cm^{-1} in the spectral range of 4000-400 cm^{-1}.

In order to study the compositional changes generated in the membranes through the different treatments applied and to follow the UV-induced crosslinking and grafting reactions, the spectra of the membranes before and after irradiation with UV light were acquired and analyzed.

Percent functional groups conversion was calculated by Equation 3.1:

$$Conversion\ (\%) = \left(1 - \frac{\left|{}^{A}/_{A_{ref}}\right|_{t}}{\left|{}^{A}/_{A_{ref}}\right|_{t=0}}\right) \times 100 \tag{3.1}$$

where the absorption band area of the reactive groups (A) was normalized by the area of a constant absorption peak used as reference (A_{ref}). The reactive groups are the C=C double bonds of the SBR (vinyl group absorbing at 910 cm^{-1}), while the reference peak is at 698 cm^{-1} and is related to the out-of-plane bending of the CH groups in the aromatic ring. The peak areas were quantified using the Omnic^{TM} software.

Figure 3.13: Thermo Fisher Scientific NicoletTM iS50 FTIR spectrometer.

3.3.4 Contact angle test

Concerning the wettability behavior of the membranes, different tests were performed to measure the contact angle using the FTA1000 Drop Shape Instrument, shown in Figure 3.14.

A camera and video system made it possible to record the evolution of the deposited drop of the testing liquid on the surface of the membranes and through the FTA32 software it was possible to determine the contact angle formed with the surface by the sessile drop technique using different theoretical models (i.e., Laplace-Young or spherical fit).

The first set of tests was performed in air and two different liquids, i.e., water and hexadecane, were used to evaluate the contact angle on the membranes before and after functionalization. The evolution of the contact angle as a function of time was investigated, and a test time of 30 minutes was considered. Measurements were repeated at least in four different spots on the same membrane.

Moreover, the evolution of the contact angle was measured considering the behavior of a drop of water on the functionalized membranes immersed in hexadecane (water-in-oil contact angle) and of a drop of hexadecane on the membranes immersed in water (oil-in-water contact angle). In this case, a transparent container was filled with the oil or water respectively, the membrane was attached to a sample holder which in turn was fixed to the container and then the drop of the second liquid was deposited using a glass micropipette. Measurements were taken immediately after depositing the drop of the liquid on the membrane, 30 minutes, and 24 hours after deposition.

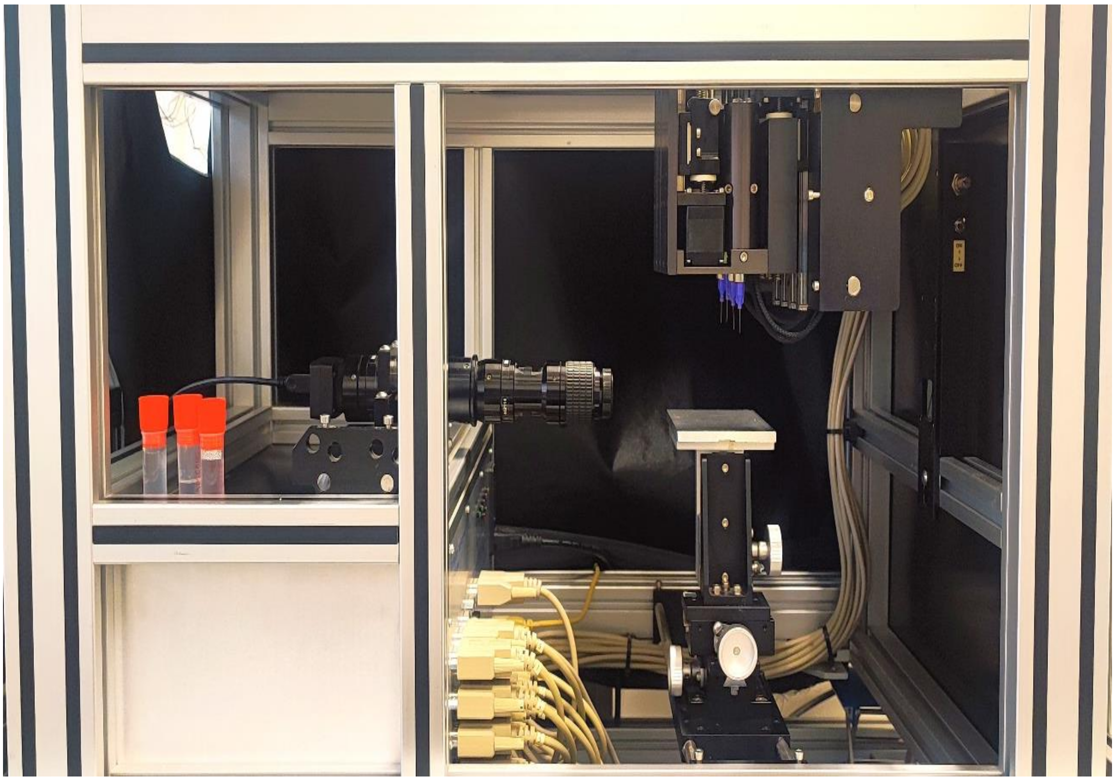

Figure 3.14: FTA1000 Drop Shape Instrument used for contact angle testing.

3.3.5 Tensile testing

In order to analyze the mechanical properties (elastic modulus E, elongation at break and ultimate tensile strength, UTS) of the functionalized electrospun membranes, standard tensile tests were performed using the INSTRON 3360 Series Dual Column Tabletop Testing System, illustrated in Figure 3.15, and the BlueHill software.

Sample preparation consisted of cutting membrane rectangles approximately 28 mm long, 17 mm wide and 0.025 mm thick. The measurements used to analyze the data were an average of three measurements for each dimensional direction of the membranes, obtained using a digital micrometer. Then, the samples were positioned in the clamps of the tensile machine with the help of parafilm to avoid slipping. In particular, three tests were performed for the same membrane type with a test speed of 5 mm/min, a load cell of 10 kN and at room temperature.

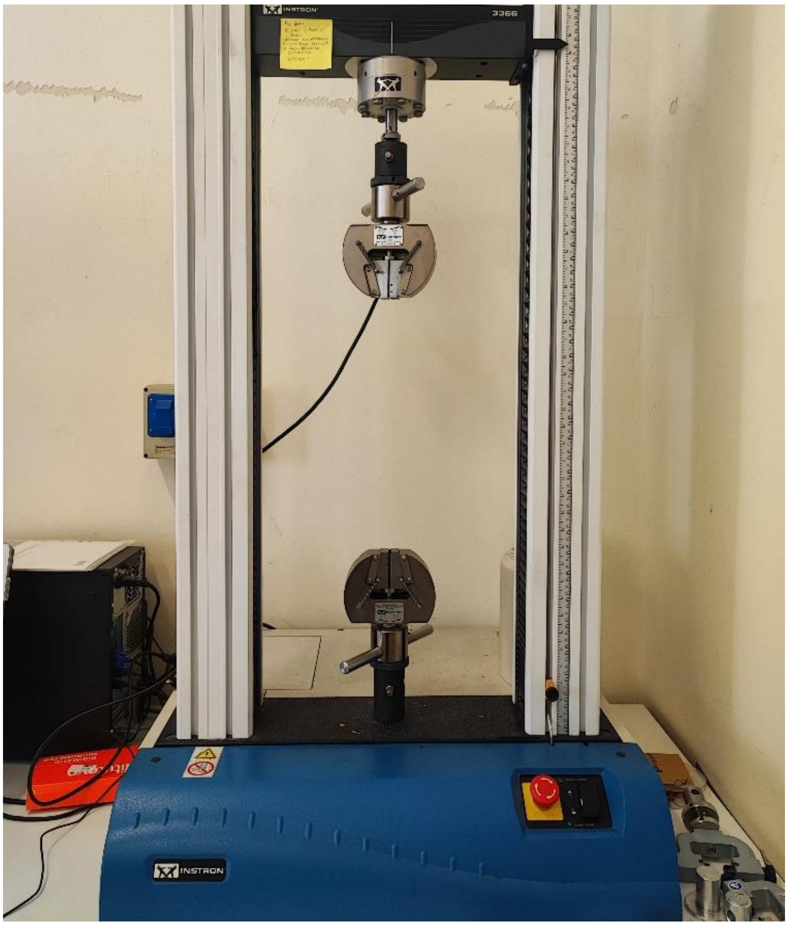

Figure 3.15: Instron Tensile Testing Machine used to analyze the mechanical properties of the functionalized membranes.

3.4 Analysis of the separation capacity for oil/water mixtures

To evaluate the effectiveness of the membranes for oil/water separation, a microfiltration system consisting of a Büchner flask, a Büchner funnel with a guko's conical silicone seal, a porous stainless-steel plate, a PTFE gasket and a graduated cylinder was used. The components were fixed together using an anodized alluminum clamp to ensure the stability of the system, as shown in Figure 3.16. A more detailed schematic representation of the filtration system used is illustrated in Figure 3.17.

Figure 3.16: Microfiltration system used to analyze the SBR-based membranes efficiency of separation of oil/water mixtures.

For the filtration tests, water and hexadecane were used. Water was previously colored with a water-soluble and oil-insoluble blue dye in order to easily distinguish the presence of both liquids. The membrane samples were positioned on the porous stainless-steel plate, ensuring a full coverage of the filtration area. Subsequently, the PTFE gasket and the graduated cylinder were fixed with the clamp before proceeding to pour the liquids under study.

The initial phase of the analysis of the membranes performance consisted in testing the penetration capacity of oil (hexadecane) and dyed water individually, thus, evaluating the wettability properties of the samples. For this purpose, 5 ml of liquid were quickly poured, and the penetration was evaluated for 5, 10 and 30 minutes (if applicable), monitoring the content of liquid deposited in the flask (i.e., passing through the membrane) in terms of volume and weight. The tests were carried out using only gravity as driven force, it was not necessary to apply any pressure, since the liquid flowed properly through the membrane.

The liquid volume was measured using a graduated cylinder (10:1 ml, DIN -ln 20°, ± 0.2 ml, Boro 3.3, Class A), while the weight was measured directly on the balance by making the necessary calibration adjustments.

At the end of the test, the microfiltration system was disassembled to verify the integrity of the membrane used.

The second phase of the tests consisted in evaluating the membrane's capacity to separate water and oil by quickly pouring both liquids in a 1:1 volumetric ratio. In this case, 5 ml of oil (hexadecane) and 5 ml of dyed water were used. The penetration of the liquid was measured, considering the fraction deposited on the flask in terms of volume and weight, but also from a visual point of view. The test time was approximately one hour. Once these values were collected, any water residues present in the oil fraction obtained from the filtration system were allowed to evaporate overnight. Subsequently, the volume and the weight of the remaining liquid fraction was measured again.

Then, in order to study the consistency of the separation efficiency of the membranes with time several filtration cycles were repeated using the same membrane. In particular, as in the previous case, 5 ml of hexadecane and 5 ml of dyed water were poured in each cycle and the mixture was left in the filtration system for 15 minutes. Once the test time was over, the permeate and concentrate contents obtained were weighed and the volume was measured. A total of 20 cycles were performed and at the end of the test the filtration system was disassembled to check the integrity and stability of the membrane.

Finally, separation tests were performed using a dispersion of hexadecane droplets in water, obtained by intensely stirring the oil/water liquid mixture. Thus, the dispersion was poured into the graduated cylinder and the separation capacity of the membranes was analyzed. The optical microscope was used to verify the presence of hexadecane droplets in the initial mixture and in the two fractions obtained after the filtration process, i.e., in the permeate and in the concentrate.

According to the principles described in Section 2.1.4 on the fundamentals of membrane technology, there are certain parameters that allow to evaluate the performance of a membrane in terms of filtration efficiency. Thus, variations of the flux and efficiency expressions were used to quantitatively analyze the filtration system, adapting them according to the parameters obtained during the experimental phase. In particular, the oil flux was calculated using Equation 3.2:

$$\varphi = \frac{V}{ST} \tag{3.2}$$

where φ represents the oil flux (L), S is the effective area of the nanofibrous membrane positioned on the porous stainless-steel plate (m^2) and T is the separation time (h).

Furthermore, the quantity of oil before and after the filtration process was weighed and the separation efficiency (η) was calculated according to Equation 3.3:

$$\eta = \frac{W_1}{W_0} \cdot 100\% \tag{3.3}$$

where W_0 and W_1 are the weight of oil before and after filtration, respectively.

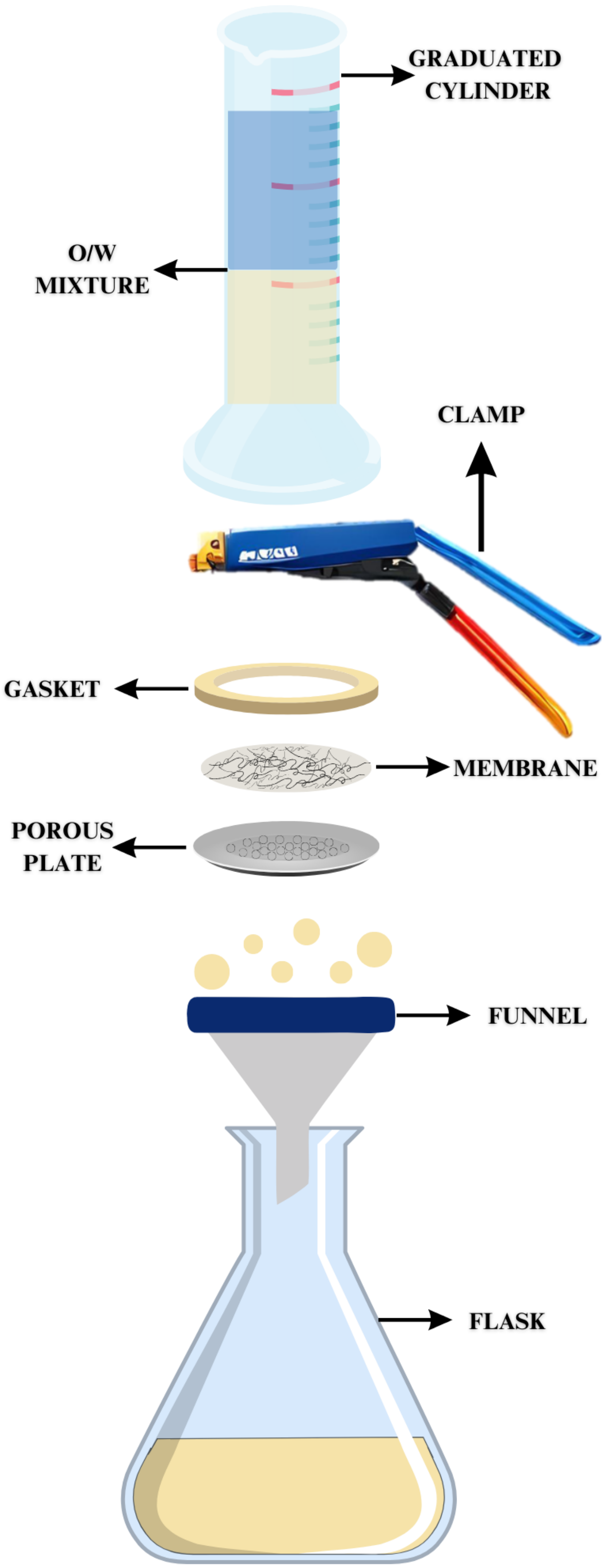

Figure 3.17: Detailed schematic representation of the filtration system.

4 Results and discussion

4.1 Production of the SBR-based electrospun membranes

As discussed in the previous chapters, electrospun membranes were produced using styrene-butadiene rubber (SBR) latex and were appropriately functionalized with a polydimethylsiloxane (PDMS) functionalizing agent to be used as hydrophobic/oleophilic filters for oil/water separation.

In particular, suspension electrospinning of SBR latex (i.e., stable dispersion of rubber nanoparticles in water) was carried out. However, since it was not possible to form a stable jet of latex through electrospinning, it was necessary to use an easily electrospinnable and water-soluble polymer template. Therefore, a small amount of polyethylene oxide (PEO) was added to the solution. An SBR/PEO mass ratio of 10/3 was used, being sufficient to stabilize the electrospinning process of the SBR latex [51]. After electrospinning, the membranes were subjected to UV irradiation at ambient condition: thanks to the presence of the photoinitiators (TPO + Darocur 1173) and the multifunctional thiol crosslinker (TRIS) added to the electrospinning formulation, the thiol-ene photoinduced crosslinking of the system took place. In fact, the photoinitiators could create radical reactive species when exposed to light, and the reactive C=C double bonds (broadly known as “enes”) present in the chemical structure of SBR reacted with the thiol groups of TRIS.

The mechanism followed a free-radical pathway proceeding by a step-growth addition mechanism which is propagated by a chain-transfer reaction involving the thiyl radicals (RS•), as shown in Figure 4.1.

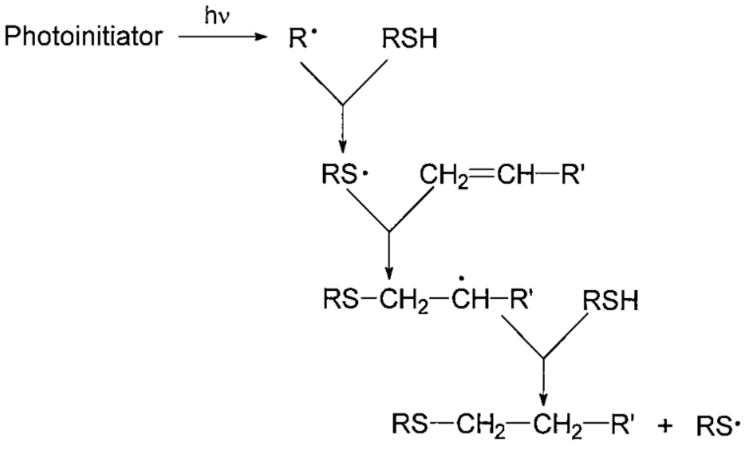

Figure 4.1: Mechanism of thiol-ene prohotinduced crosslinking.

Then, the polymeric network was formed due to the reaction between the polyene (SBR) with the multifunctional thiol crosslinker (TRIS), as shown in Figure 4.2 [62].

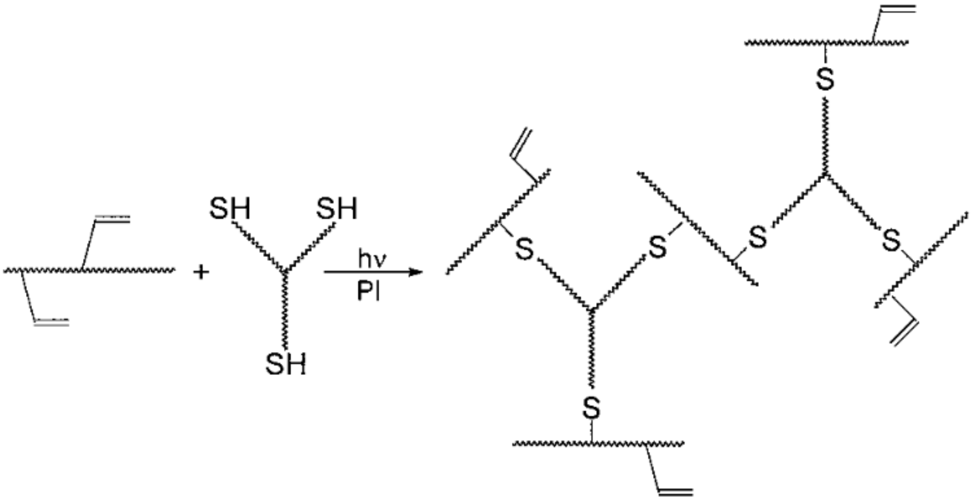

Figure 4.2: Formation of the polymeric network by thiol-ene reaction.

Once a stable crosslinked structure was obtained, a water treatment step was applied to remove PEO from the fibrous mats and obtain nanofibrous membranes made of only crosslinked SBR.

Then, the rubber membranes were functionalized by using a vinyl terminated PDMS and a thiol-ene photo-induced chemical grafting, as illustrated in Figure 4.3. The mats were dunked in a PDMS solution, UV irradiated and washed to remove the unreacted monomer. Light irradiation promoted the reaction of the terminal vinyl groups of the PDMS monomer with the thiol groups of TRIS in excess still active on the nanofibers. The result was the formation of covalent bonds between the PDMS molecules and the SBR-based fibers.

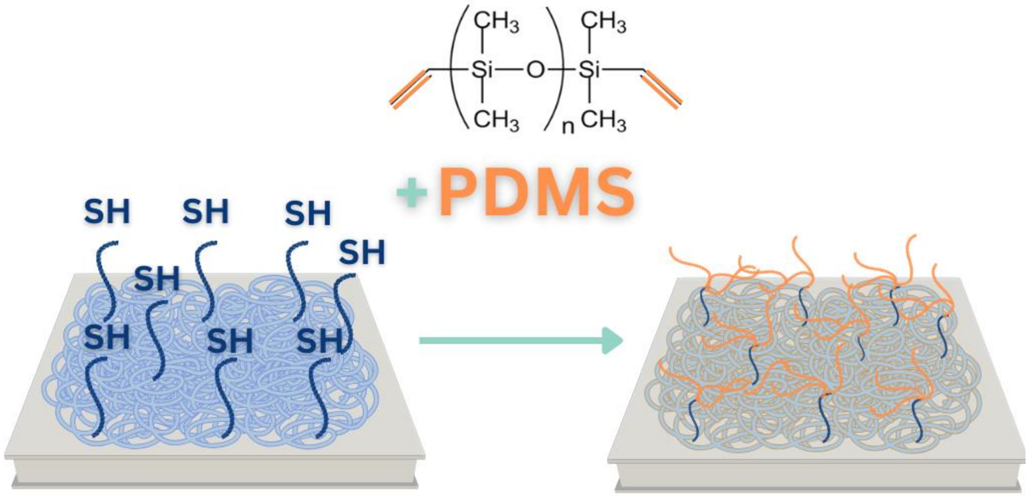

Figure 4.3: Thiol-ene photo-induced chemical grafting of PDMS.

At the end of the production process, free-standing, stable, flexible and insoluble rubber nanofibrous membranes were obtained, as shown in Figure 4.4.

Figure 4.4: Styrene-butadiene rubber (SBR) nanofibrous membranes obtained by electrospinning, photo-induced crosslinking and functionalization with vinyl terminated polydimethylsiloxane (PDMS).

In order to analyze the nanofibrous membranes, characterization techniques were applied in terms of morphology, chemical composition and wettability, as well as quantitative analyses to evaluate the filtration capacity of the membranes. The nanofibrous membranes subjected to the different treatments during the production process were analyzed and the results will be described considering the nomenclature presented in Table 4.1.

Table 4.1. Samples of nanofibrous membranes under analysis.

Sample	**Designation**
PEO electrospun membranes	PM
SBR/PEO electrospun membranes	EM
SBR/PEO electrospun membranes after UV irradiation	EM+UV
SBR electrospun membranes after UV irradiation and water treatment	EM+UV+WT
SBR electrospun membranes after UV irradiation, water treatment and functionalization with PDMS	EM+UV+WT+PDMS

A scheme representing the entire process, from fabrication to application of the nanofibrous membranes, is reported in Figure 4.5.

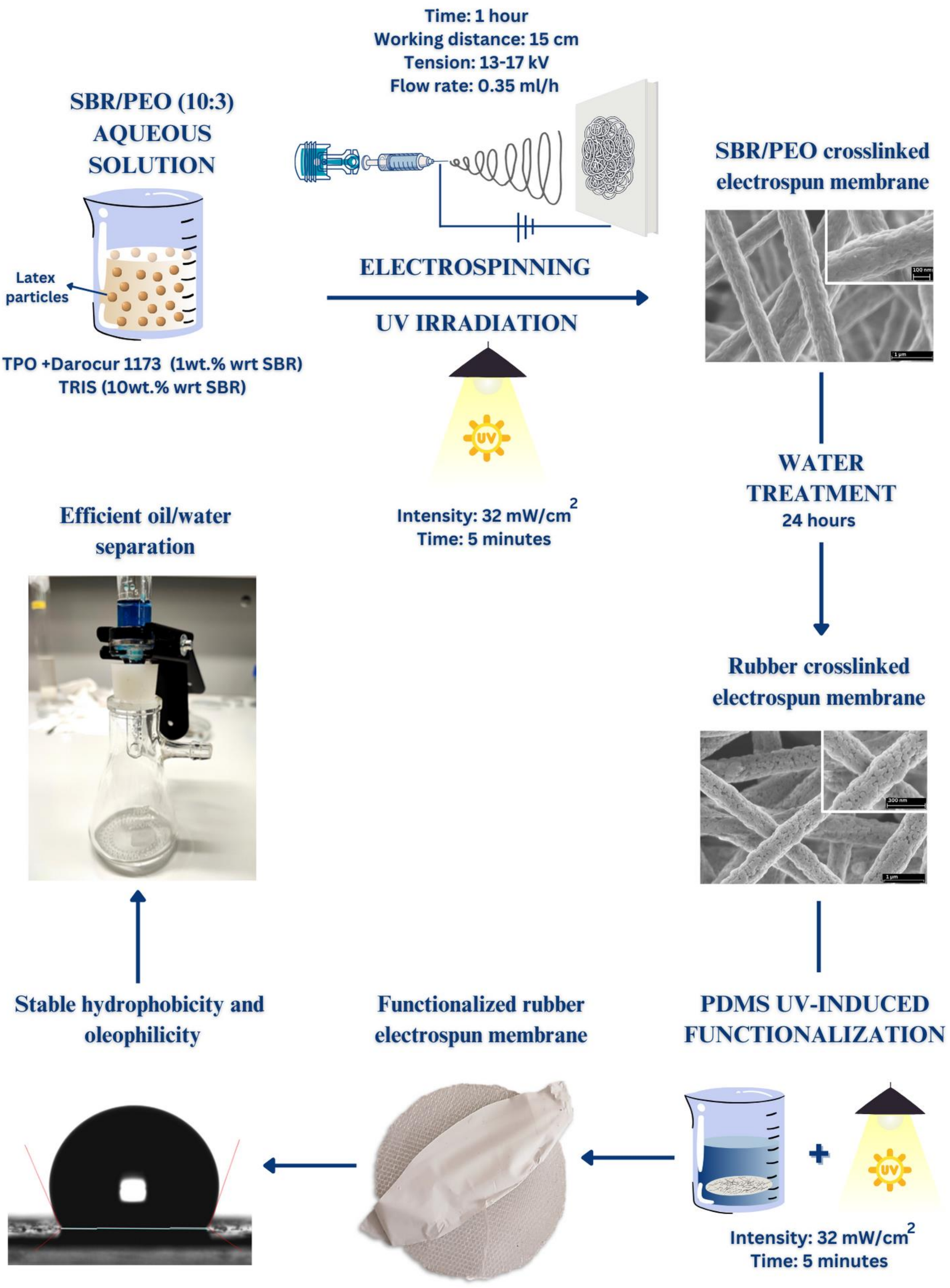

Figure 4.5: Rubber nanofibrous membranes obtained by electrospinning and their application as oil/water filtration systems (experimental process).

4.2 Morphology of the electrospun membranes

Once the samples were obtained, they were first analyzed by optical microscopy. This technique provided general information about the morphology of the electrospun membranes.

Firstly, the easy production of the fibers from an aqueous solution containing only PEO (5 wt. %) was confirmed. The fibers obtained are shown in Figure 4.6 (a) and provide a reference for evaluating the deposition of SBR-based fibers, which in turn are shown in Figure 4.6 (b).

As it is evident from the figures, in both cases, continuous randomly oriented and entangled fibers are obtained. In a first approximation, these optical microscopic images allow to corroborate the correct deposition of the fibers even with a material that in principle would not be electrospinnable, such as SBR, thanks to the use of PEO as a template.

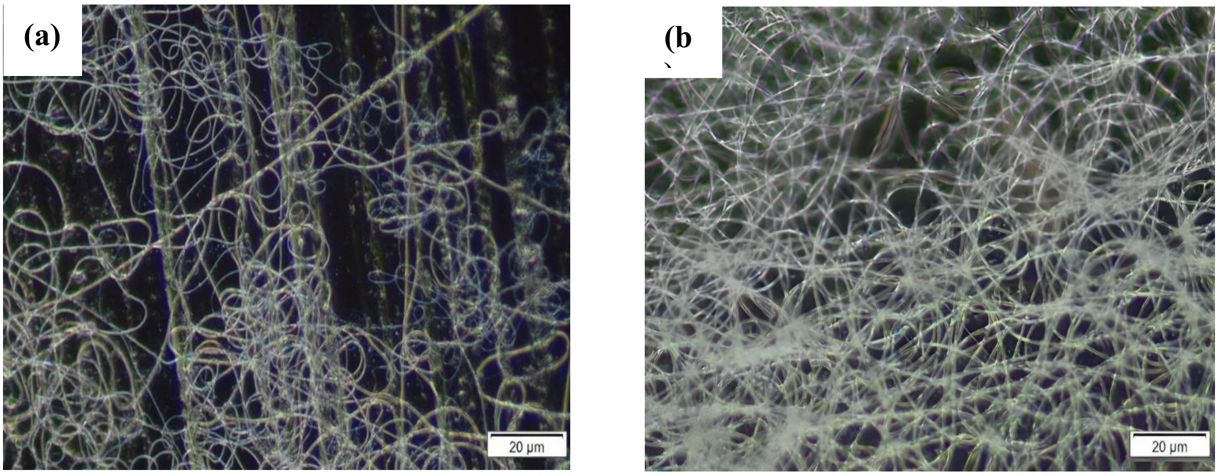

Figure 4.6: Optical microscope image of (a) PM sample (20x) and (b) EM sample (20x).

Furthermore, the different treatments applied to the nanofibrous membranes allowed the preservation of a structure composed of well-defined fibers. In fact, even after UV irradiation and water treatment applied for 24 hours, continuous and interconnected fibers are still observed, despite the removal of the polymer used as template, as shown in Figure 4.7 (a).

On the other hand, Figures 4.7 (b) and 4.7 (c) are a first evidence of the success of the membrane surface modification process. Indeed, it can be noted that after functionalization, a structure formed by interconnected fibers is again obtained, but in this case the fibers have a different surface appearance, due to the presence of the functionalizing agent (PDMS).

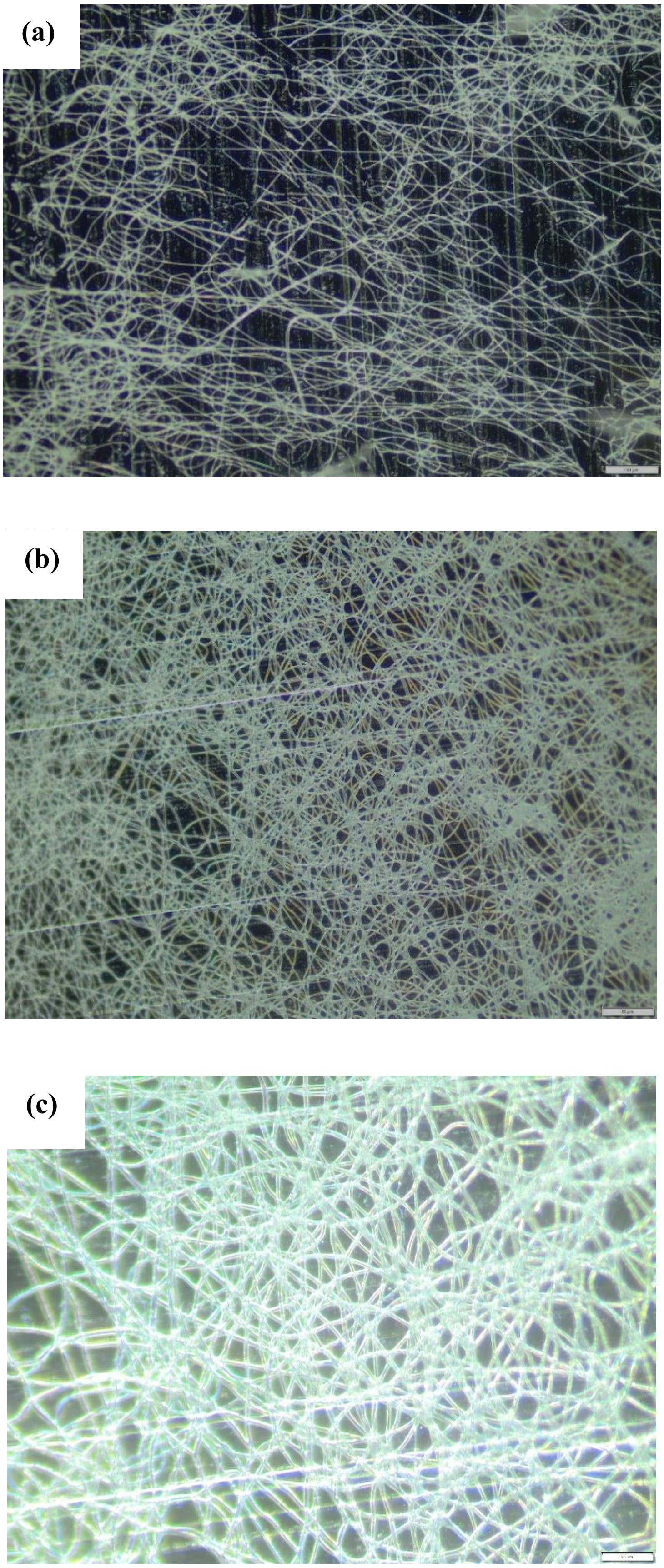

Figure 4.7: Optical microscope images of (a) EM+UV+WT sample (20x). (b) EM+UV+WT+PDMS sample (20x). (c) EM+UV+WT+PDMS sample (50x).

The Field Emission Scanning Electron Microscopy (FE-SEM) technique was used to further analyze the morphology of the fibers. As in the previous case, the membranes were characterized according to the treatments applied and using different magnifications. In particular, the morphology of EM+UV, EM+UV+WT and EM+UV+WT+PDMS samples were analyzed.

Similarly to the optical microscope images, the FESEM analysis made it possible to observe the presence of the fibrous structure even after the different treatments applied, demonstrating that no processes affecting the stability of the nanofibrous membrane were involved. In addition, this technique allowed to observe in greater detail the morphology of the fibers, which appear as well-defined, cylindrical, uniform, and continuous structures. However, quite clear differences were evidenced between the fibers of the membranes subjected to the different treatments.

Firstly, the fibers subjected only to UV irradiation present a surface with a slight roughness, due to the combination of SBR latex with PEO. Therefore, it is possible to affirm that the performance of PEO as an easily and electrospinnable polymeric template was correctly obtained, since the SBR particles are perfectly adhered and compacted in the structure of the fibers, as shown in Figure 4.8 (a) and (b). Moreover, the fact that defined fibers were obtained using rubber as the main component for the electrospinning solution, demonstrates the success of the stabilization process.

Indeed, without the use of a polymeric template and the crosslinking reaction, it would be extremely challenging to obtain a rubber nanofibrous membrane through electrospinning, since the fibers would not be stable due to the SBR flowing that would cause the collapse of the structure. Thus, it is possible to affirm that the crosslinking allows obtaining good quality fibers that maintain an unaltered morphology over time.

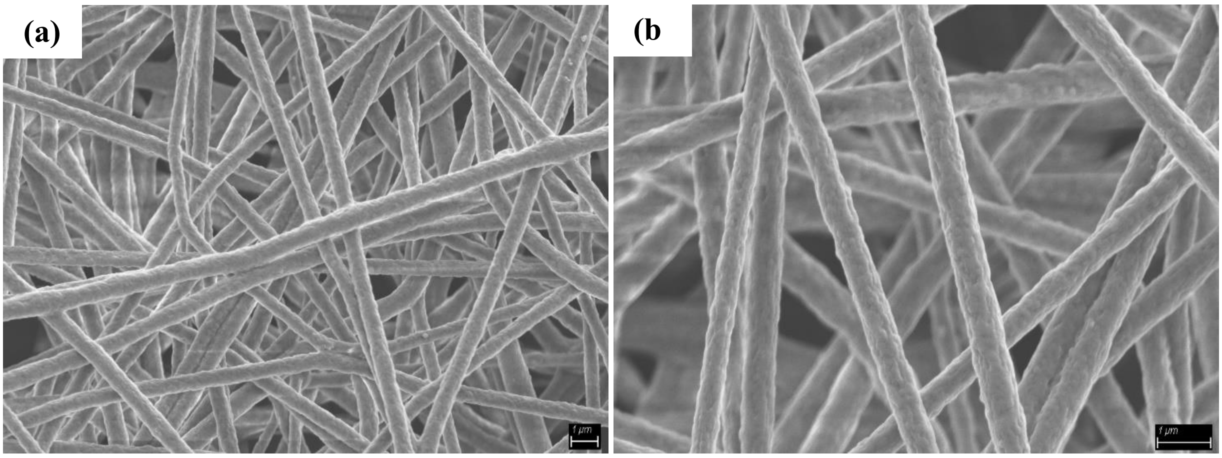

Figure 4.8: FE-SEM images of EM+UV sample (a) 5.00 KX (b) 10.00 KX.

On the other hand, the water treatment to which the membranes were subjected had the purpose of eliminating the polymeric template in order to obtain predominantly SBR fibers.

The observation of the morphology of the membranes after the water treatment for 24 hours confirms the correct elimination of the PEO, since the surface characteristics of the fibers were effectively modified. Fibers with a rougher surface were observed, as shown in Figure 4.9 (a) and (b).

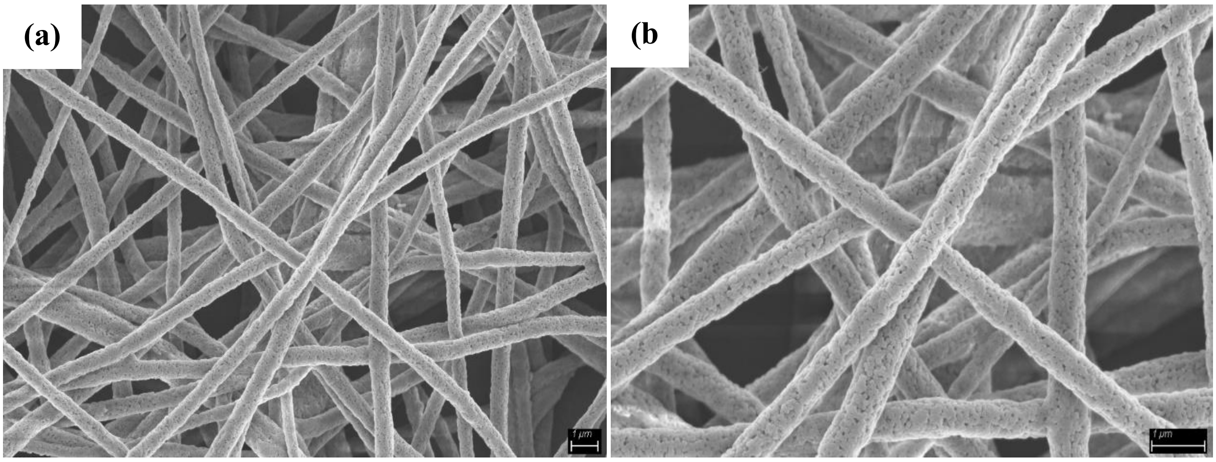

Figure 4.9: FE-SEM images of EM+UV+WT sample (a) 5.00 KX (b) 10.00 KX.

In addition, it was possible to observe that once the template was removed, the fibers remained continuous and stable structures formed by SBR distinct rubber nanoparticles partially fused together, with an average diameter of 101.31 ± 0.61 nm.

The difference between the two morphologies, before and after water treatment, can be clearly observed in Figures 4.10 and 4.11.

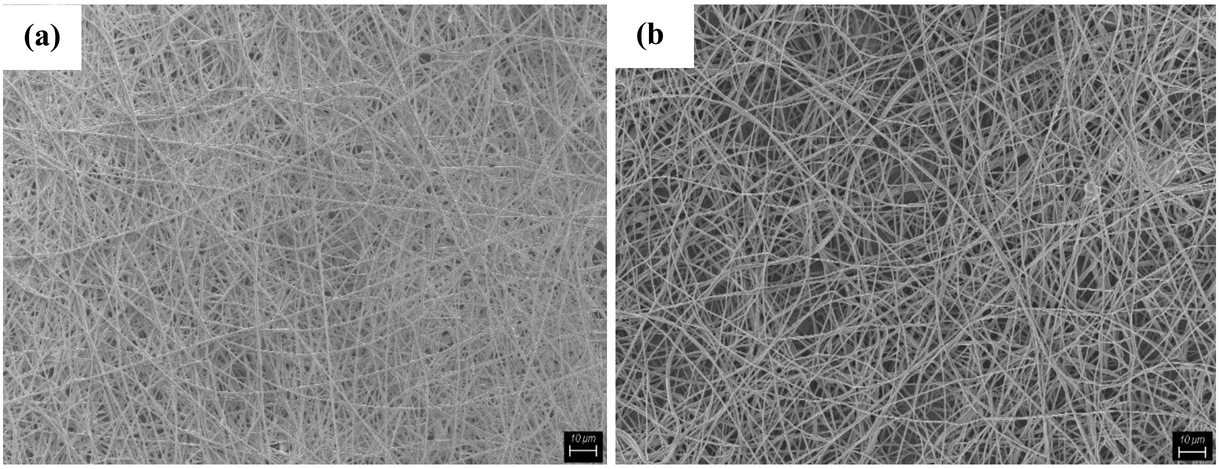

Figure 4.10: FE-SEM images of (a) EM+UV sample (b) EM+UV+WT sample (500 X).

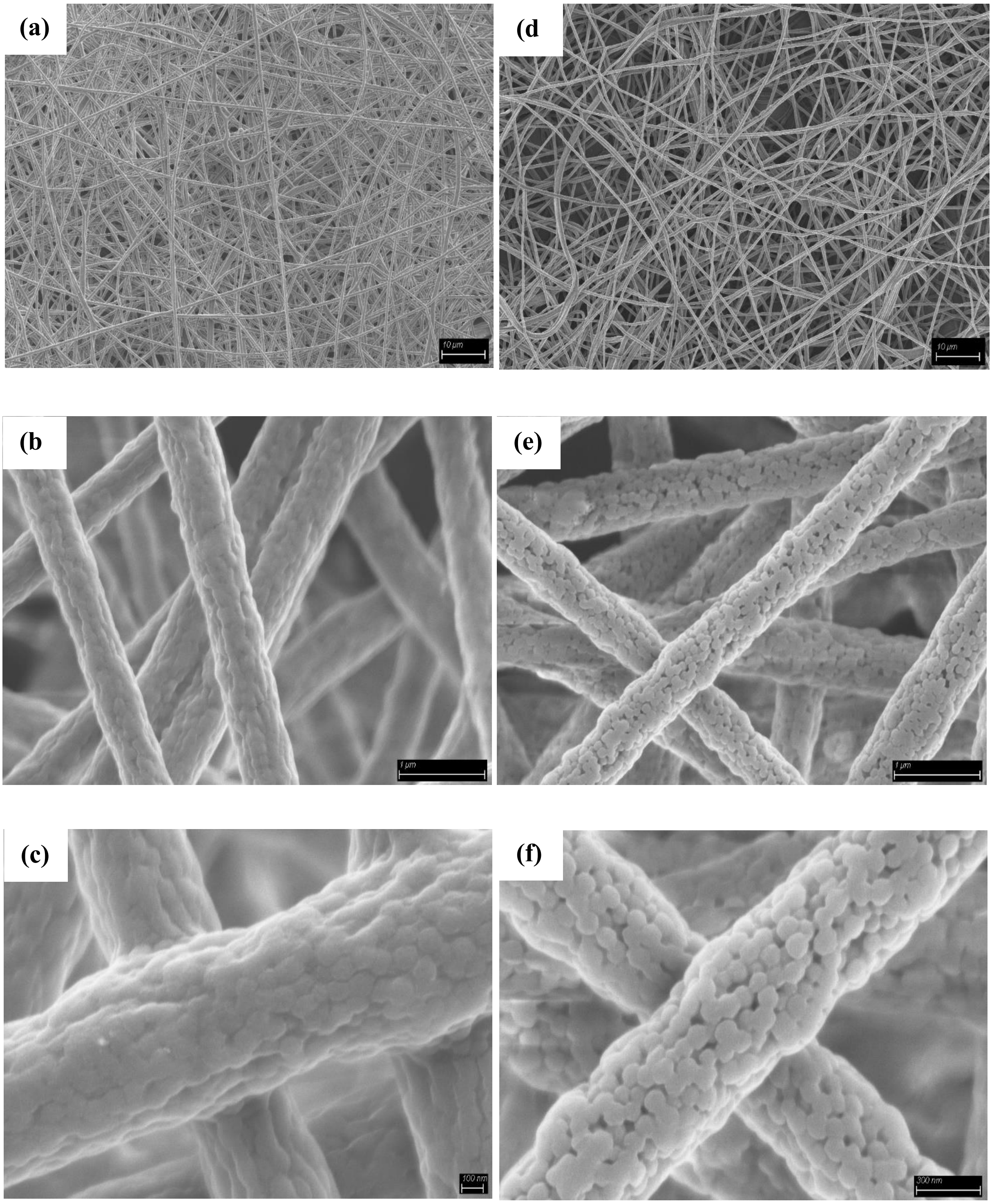

Figure 4.11: FE-SEM images of (a), (b) and (c) EM+UV sample and (d), (e) and (f) EM+UV+WT sample (1.00 KX, 20.00 KX, 50.00 KX respectively).

Overall, it was possible to observe the correct assembly of a membrane that, due to its nanofibrous nature, presents a high percentage of porosity. This structure is obtained due to the entanglement of the fibers and the spaces that are formed between them, as well as the small pores present in the length of each fiber due to the gaps created around the contact points between the nanoparticles.

This represents an interesting result regarding the application of these membranes as systems for the treatment of oil/water mixtures, since the higher specific surface area promotes the separation processes.

The FE-SEM images were also analyzed to study the mean diameter of the fibers as well as the distribution of the diameters in the membranes.

For membranes subjected to UV irradiation, an average fiber diameter of 713.1 ± 6.4 nm was obtained, while for membranes subjected to water treatment, a slightly lower average fiber diameter (638.2 ± 5.3 nm) was determined.

Likewise, the fiber diameter distribution also varied after treatment. Membranes subjected to water treatment show a narrower fiber diameter distribution with respect to untreated fibers, as shown in Figure 4.12, confirming that the removal of the PEO polymeric template results in more uniform and finer fibers.

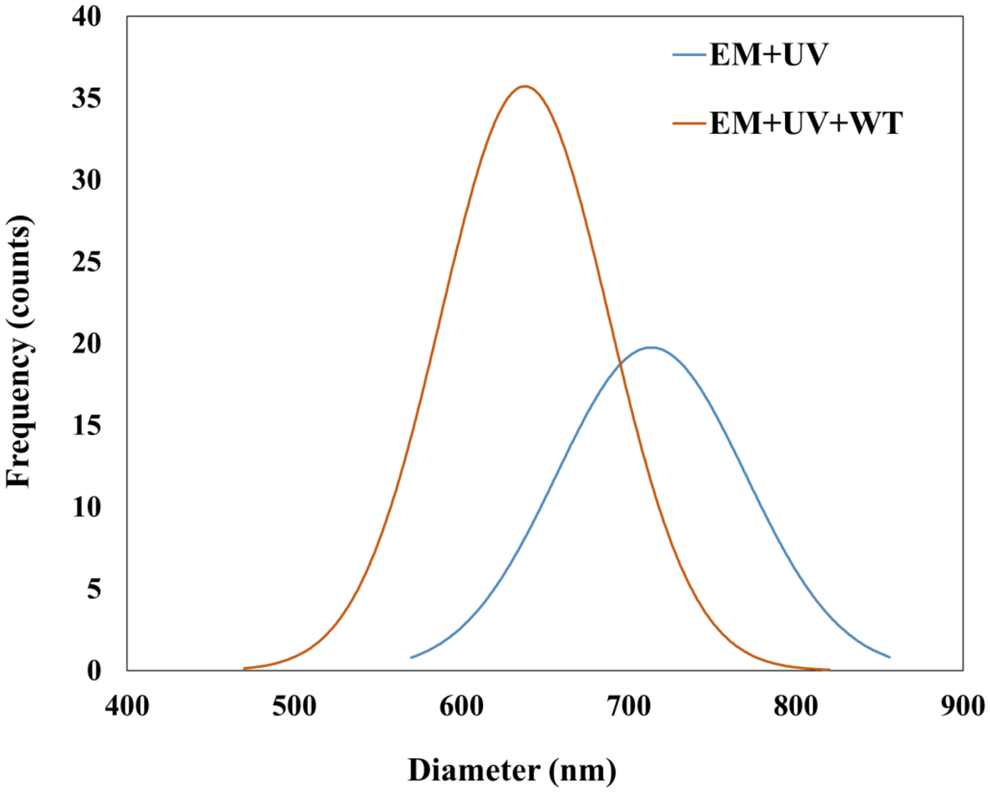

Figure 4.12: Fibers diameter distribution for EM+UV and EM+UV+WT samples.

On the other hand, as previously demonstrated by the optical microscope analysis, FE-SEM images shown that the morphology of the membranes is altered after the functionalization with PDMS. In fact, part of the membrane porosity is covered by a PDMS film, as shown in Figure 4.13 (a), creating a hydrophobic barrier. Furthermore, the functionalizing agent properly covers the fibers, thus, rubber particles are no longer visible, and in some cases it creates a continuous structure, as clearly shown in Figures 4.13 (b), (c), (d) and (e).

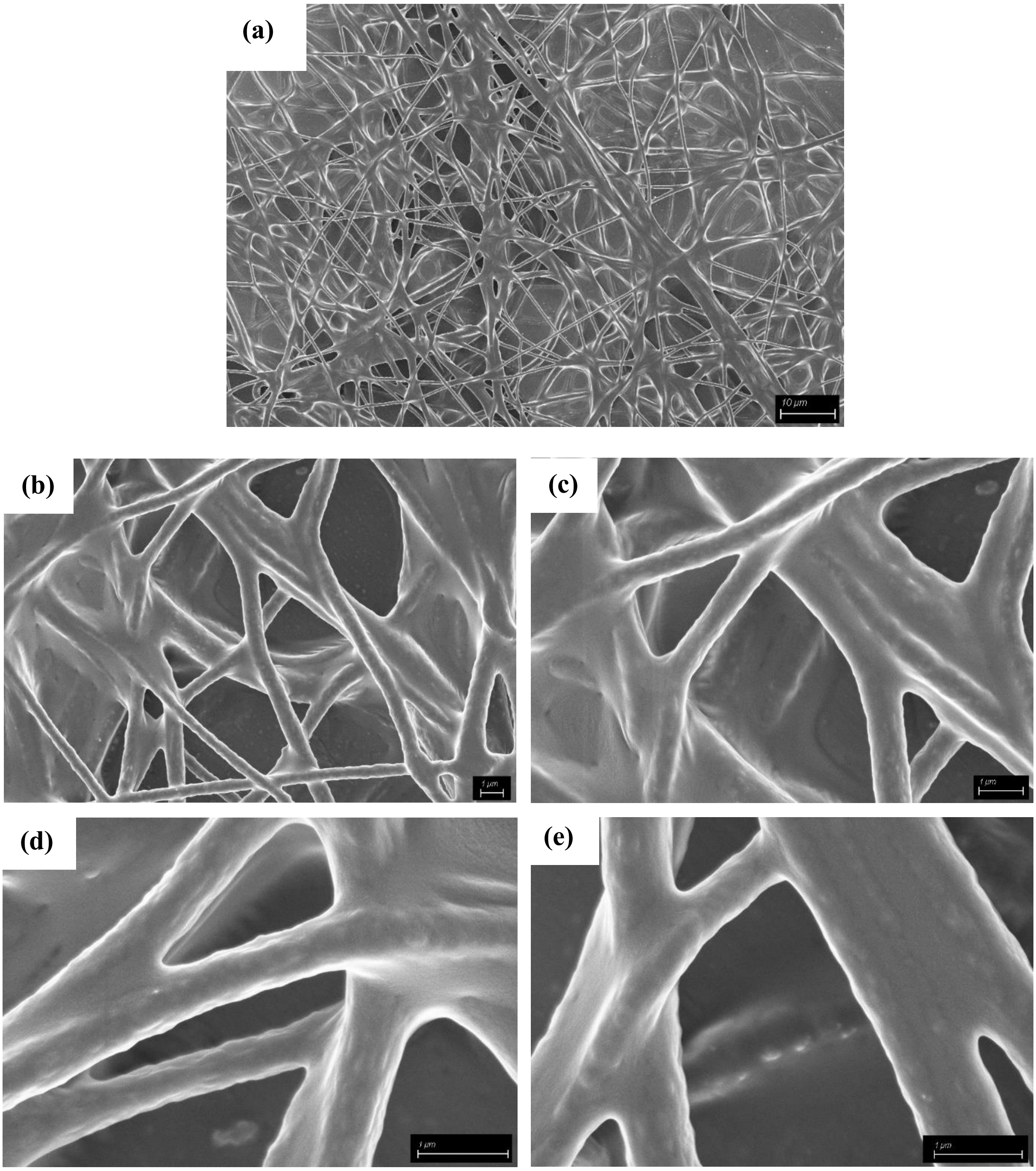

Figure 4.13: FE-SEM images of the EM+UV+WT+PDMS sample: (a) 1.00 KX, (b) 5.00 KX, (c) 10.00 KX, (d) and (e) 20.00 KX.

4.3 Chemical composition of electrospun membranes

In order to identify the chemical composition of the electrospun membranes, the ATR FT-IR spectroscopy was applied. Specifically, the wavenumbers of the characteristic peaks of the materials used for the preparation of the solution were identified considering the membranes immediately after electrospinning (EM), the membranes after the photoinduced crosslinking process through UV light (EM+UV), and the membranes after water treatment and functionalization with PDMS (EM+UV+WT+PDMS).

Figure 4.14 shows the spectrum obtained in the case of the EM sample, while Figure 4.15 corresponds to the spectrum obtained for the EM+UV sample.

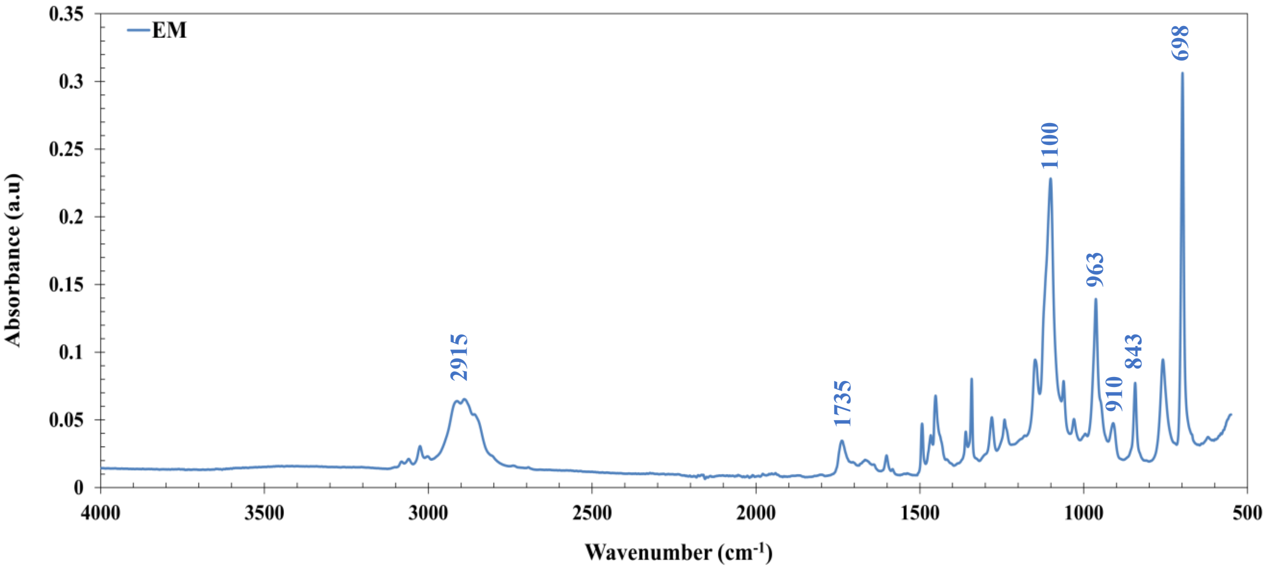

Figure 4.14: ATR FT-IR spectrum of EM sample.

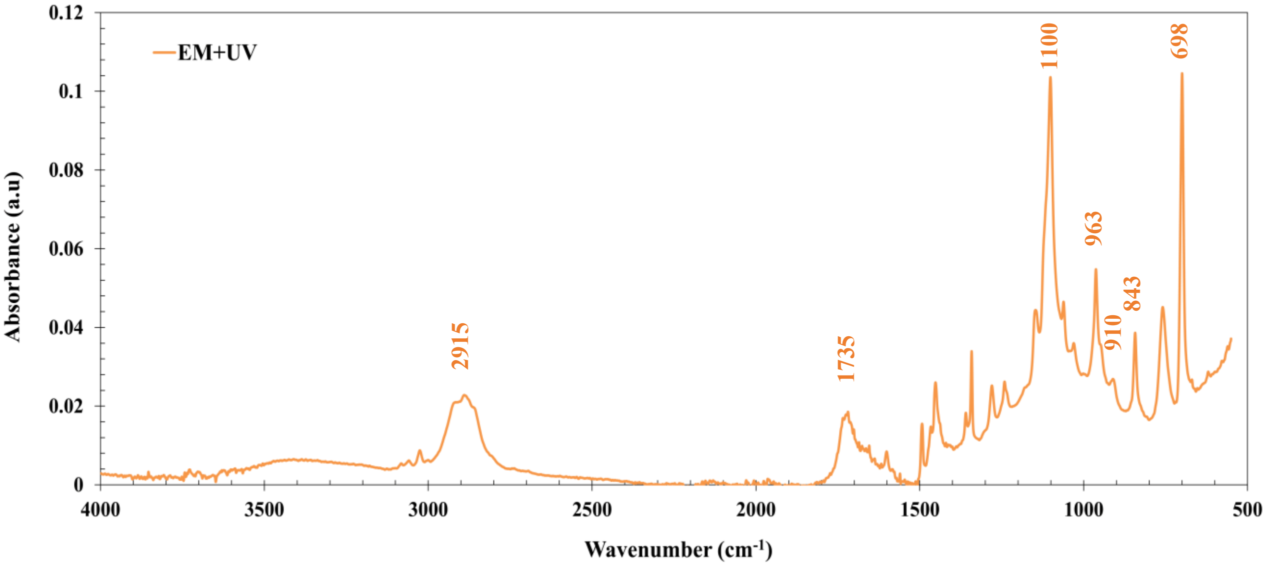

Figure 4.15: ATR FT-IR spectrum of EM+UV sample.

It is possible to observe that the chemical composition of the membranes before and after UV irradiation is substantially the same and the characteristic wavenumbers identified correspond to the different components of the solution used for electrospinning, as summarized in Table 4.2, confirming the presence of both the SBR (characteristic peaks at 698 cm^{-1}, 910 cm^{-1} and 963 cm$^{-1,}$ corresponding to C-H groups of the aromatic ring, vinyl groups and trans butene unsaturations, respectively) and the polymeric template PEO (characteristic peak at 1100 cm^{-1} due to the ether bonds).

Table 4.2. Characteristic wavelengths of electrospun membranes analyzed by ATR FT-IR spectroscopy.

Wavenumber (cm^{-1})	**Characteristic peak**
698	Bending C-H [monosubstituted benzene derivative]
759	1,4 cis-butadiene
843	$-CH_2-CO-$
910	Bending C=C [alkene (vinyl out-of-plane)]
963	Bending C=C [alkene disubstituted (trans)]
1030	Stretching vibrations (cis-PB) C-C
1100	C-O-C (PEO)
1150	P=O
1241	Stretching of C(=O)-O
1342	Stretching of C-O
1451	$CH_2=CH-$
1493	Stretching C=C-C
1601	Vibration of stretches in CH_2 and CH_3 groups
1735	C=O
2915	Elongation of CH groups in styrene aromatic rings
3025	Stretching O-H

The intensity of the peaks, however, showed some variations due to the photoinduced crosslinking process. In fact, considering the chemical structure of the materials used to formulate the electrospinning solution, it is possible to state that the stabilization of the electrospun fibers occurred through a “Click” thiol-ene reaction.

The evidence of the effective development of this type of reaction during the membrane preparation process was verified through the analysis of the ATR FT-IR spectra. Indeed, once the UV radiation was performed, it was possible to identify and study the action of the crosslinking agent through the observation of the variation of C=C double bonds present in the SBR structure. In particular, vinyl and trans butene bonds were considered, centered at 910 cm^{-1} and 963 cm^{-1}, respectively, and in both cases a decrease in intensity was verified, as evidenced in Figure 4.16. This suggests that thiol groups present in the solution promoted an effective photopolymerization process through the SBR reactive groups.

The determination of the areas of the absorption band of the SBR unsaturations normalized with respect to the area of the peak at 698 cm^{-1} (related to the out-of-plane bending of the CH groups in the aromatic ring) allowed to calculate the percentage conversion of the functional groups after UV irradiation.

In the case of vinyl groups, a conversion percentage of 47% was obtained, while in the case of the C=C bonds of the 2-butene backbone, a conversion percentage of 23% was calculated. The difference between both percentages is due to the fact that the vinyl groups present a higher reactivity in the presence of thiyl radicals (RS•) than the 2-butene double bonds [51] and, therefore, the result of the thiol-ene crosslinking process can be monitored with greater certainty by evaluating the decrease in the vinyl unsaturations of the SBR.

Regarding the decrease of the SH thiol groups of the crosslinker, ideally located at 2565 cm^{-1}, it was not possible to calculate the percentage of conversion since the signal was extremely weak, thus complicating the estimation of the area of the absorption band.

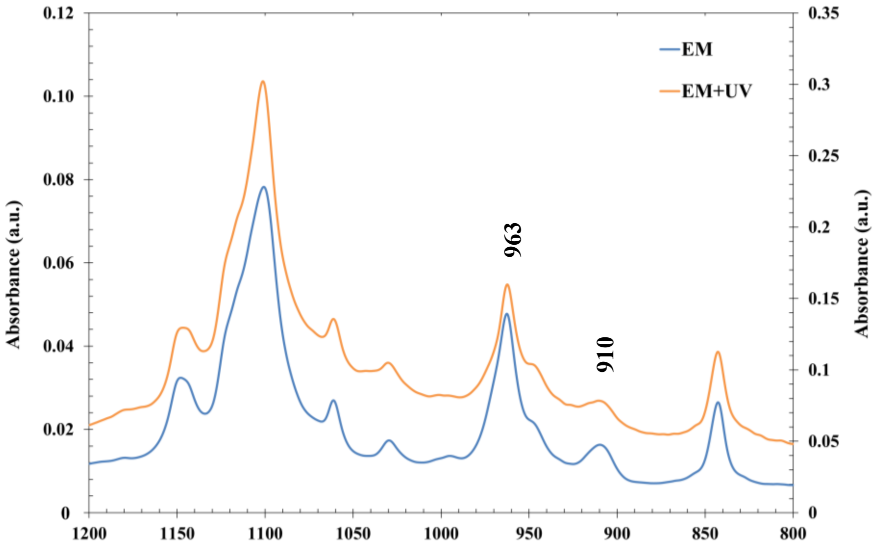

Figure 4.16: Comparison between ATR FT-IR spectra of EM and EM+UV samples.

After water treatment and membrane functionalization with PDMS, the spectrum has clearly shown a modified chemical composition, as illustrated in Figure 4.17. In particular, some of the absorbance bands corresponding to the materials of the initial solution were once again identified.

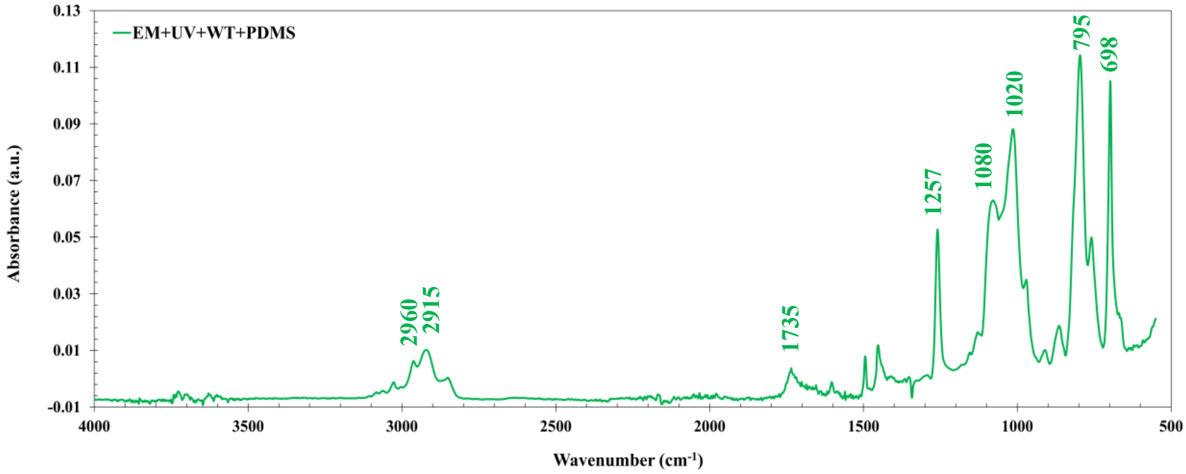

Figure 4.17: ATR FT-IR spectrum of EM+UV+WT+PDMS sample.

It is important to note, however, that the characteristic peaks of PEO associated to ether groups, at 843 cm^{-1} and 1100 cm^{-1}, suffered an important modification. Indeed, as shown in Figure 4.18, none of these absorption bands can be detected in the spectrum, while the intensity of the peaks corresponding to the stretching of the C-H (2915 cm^{-1}) and C=O (1735 cm^{-1}) of PEO showed a decrease in intensity. This shows that most of the PEO was effectively removed through water treatment, which is surely a positive result since it acts only as a template to carry out the electrospinning process of SBR fibers. On the other hand, new additional peaks were also detected (i.e., 795 cm^{-1}, 1020 cm^{-1}, 1080 cm^{-1}, 1257 cm^{-1}, 2960 cm^{-1}), as can be also seen in the comparison of the two spectra shown in Figure 4.18.

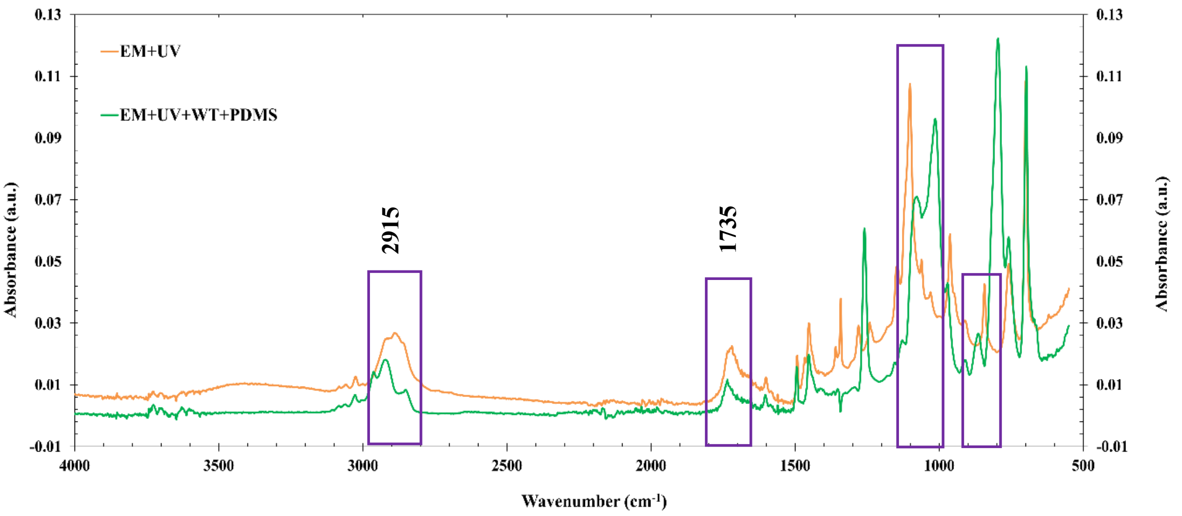

Figure 4.18: Comparison between ATR FT-IR spectra of EM+UV and EM+UV+WT+PDMS samples.

An ATR FT-IR analysis of the functionalizing agent allowed to verify that the presence of the absorbance bands mentioned above is due to the success of the membrane functionalization process, since, as shown in the characteristic wavelengths included in Table 4.3, they correspond exactly to the wavelengths of the PDMS. In fact, considering the direct comparison between the spectrum of the functionalized membrane and the spectrum of PDMS shown in Figure 4.19, it is possible to see the coincidence of the absorbance bands.

Furthermore, the test was performed on both the upper and lower faces of the membrane, obtaining exactly the same spectrum. Therefore, it is possible to affirm that the functionalization proceeded uniformly on the entire surface of the membrane, which could suggest that after the first photoinduced crosslinking process, thiol groups were still available to react with the double bonds available in the functionalizing agent.

Table 4.3. Characteristic wavelengths of PDMS analyzed by ATR FT-IR spectroscopy.

Wavenumber (cm^{-1})	**Characteristic peak**
795	$-CH_3$ rocking and Si-C stretching in Si-CH_3
1020-1080	Si-O-Si stretching
1257	CH_3 deformation in Si-CH_3
2960	asymmetric CH_3 stretching in Si-CH_3

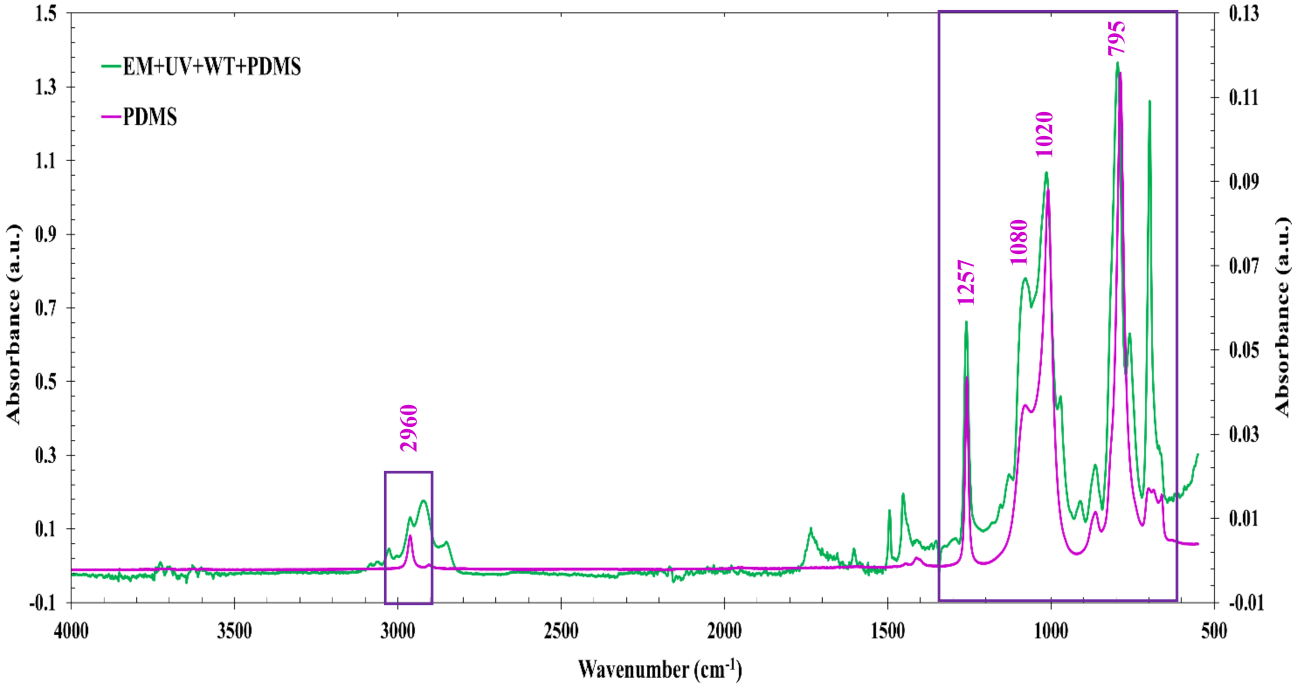

Figure 4.19: Comparison between ATR FT-IR spectra of EM+UV+WT+PDMS sample and PDMS.

4.3 Surface properties of electrospun membranes

One of the techniques to improve the efficiency of membranes for oil/water separation is to modify their surface characteristics in order to obtain special properties such as hydrophobicity and oleophilicity. In the case of the SBR-based nanofibrous membranes under study, both the water treatment to remove PEO and the functionalization with PDMS generated a significant modification in the chemical composition and, therefore, in the surface characteristics of the fibers.

The production of a surface with special characteristics in terms of wettability was studied through the measurement of the contact angle formed by water and oil once deposited on the membranes under different conditions. Also in this case, the EM, EM+UV+WT and EM+UV+WT+PDMS samples were analyzed.

4.3.1 Water in air

Firstly, the contact angle of water in air showed a significant variation once the membranes were subjected to UV irradiation, water treatment and functionalization, as shown in Figures 4.20 and 4.21.

Specifically, the membranes without any treatment presented a maximum contact angle of 63.8 ° as soon as the droplet was deposited, but its behavior was completely unstable over time, showing a fast and progressive decrease and reaching a practically complete wettability of the surface at the end of the test. On the other hand, the membranes subjected to photoinduced crosslinking and water treatment for 24 hours showed a significantly higher contact angle (90.4 °) immediately after droplet deposition that remained nearly constant during the first 10 minutes of testing, demonstrating a higher stability of the droplet. Indeed, this is a further indication of the effective removal of PEO, since, as mentioned above, it is a template easily soluble in water and its presence in the internal structure of the electrospun fibers implies a higher affinity of the membranes with water molecules. Thus, once the polymeric template was removed, the water contact angle with respect to the surface of the membranes was clearly modified. However, although the droplet presented a higher stability over time, the contact angle at the end of the test (10.7 °) represent a very low value with respect to the contact angle that was recorded at the beginning of the test.

Regarding the membranes functionalized with PDMS, a completely different wettability behavior was observed. In fact, in this case, a contact angle of 123.4 ° was recorded as soon as the droplet was deposited, which also remained constant during the entire testing time (30 minutes). Thus, the functionalization resulted in the increase of the contact angle at time zero, but also in a significant improvement of the stability of the wettability over time.

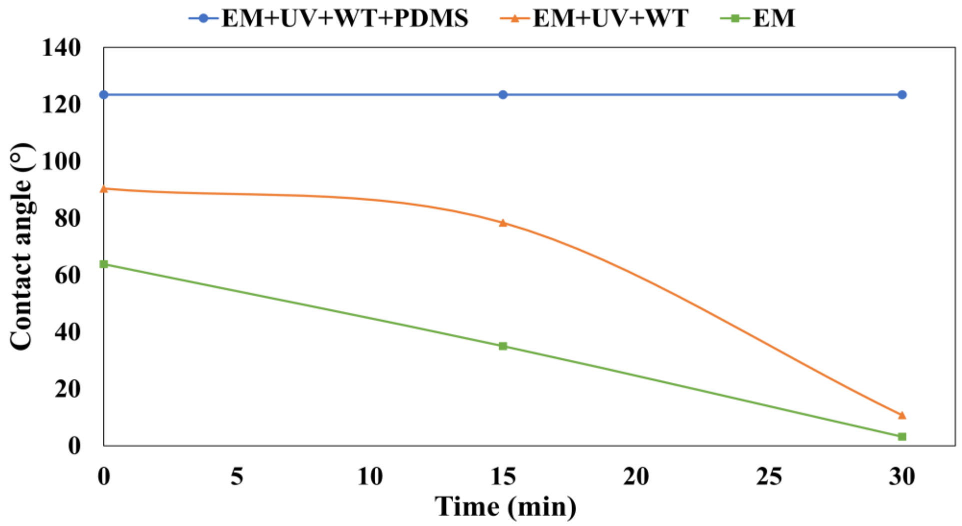

Figure 4.20: Comparison between water-in-air contact angle for EM, EM+UV+WT and EM+UV+WT+PDMS samples.

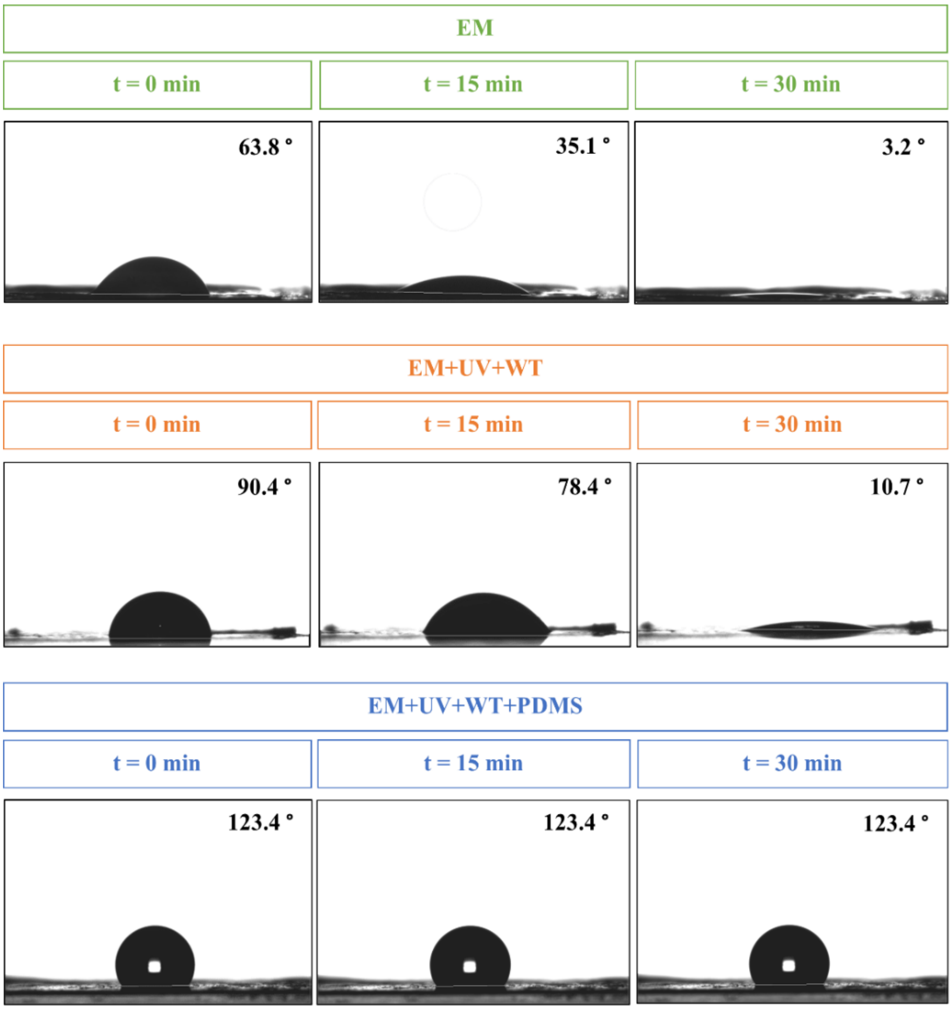

Figure 4.21: Water-in-air contact angle images for EM, EM+UV and EM+UV+WT+PDMS samples.

Considering that the chemical and morphological analysis described above allowed to confirm the success of the functionalization process of the fibers with PDMS, it is possible to affirm that this modification in the wettability behavior of the membrane surface is actually due to the presence of the functionalizing polymer. In fact, PDMS is recognized for being a strongly hydrophobic polymer, a property attributed to its low glass transition temperature of less than -120 °C and its low surface energy [63]. Indeed, once the SBR fibers are functionalized with the liquid siloxane monomer, they are then subjected to photoinduced crosslinking to generate the polymerization of the PDMS chains. Thus, the solid samples present an external hydrophobic surface that limits polar solvents (such as water) from wetting the membranes.

4.3.2 Oil in air

The contact angle of oil (hexadecane) in air was also studied. In the case of membranes without any treatment as well as for membranes subjected to UV radiation, water treatment and functionalization, a distinct oleophilic behavior was observed, as shown in Figure 4.22. In fact, the maximum value of the contact angle was 10.2 °, 12.4 ° and 13.7 ° respectively, but within a few seconds the droplet spread completely, wetting the surface. In all cases, a contact angle lower than 10 ° was obtained at the end of the test, after approximately 60 seconds. Thus, it can be observed that the different treatments and functionalization applied to the membranes, although generating a small variation of the contact angle, did not substantially modify the wettability behavior of oil towards the surface.

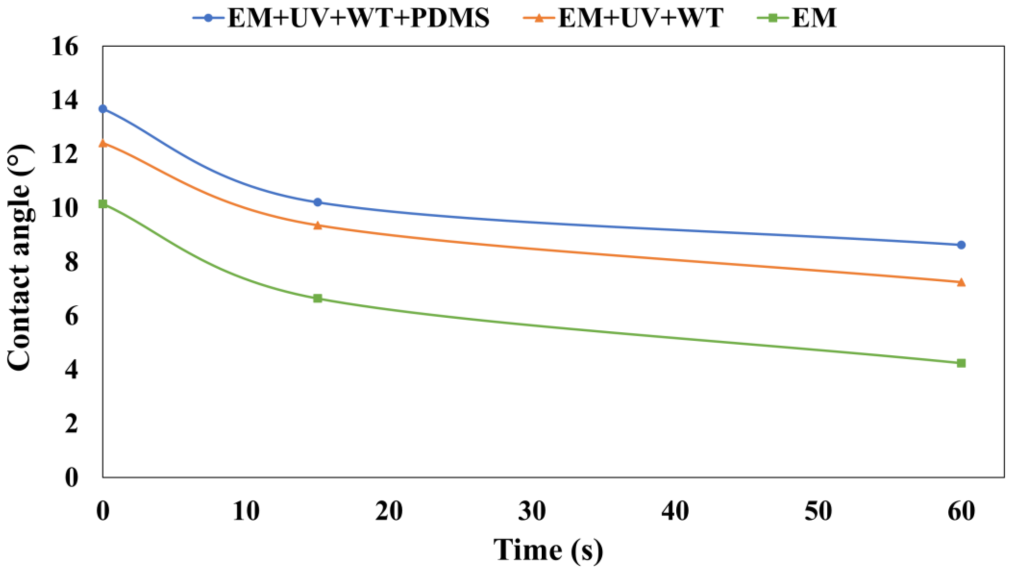

Figure 4.22: Comparison between oil-in-air contact angle for EM, EM+UV+WT and EM+UV+WT+PDMS samples.

4.3.3 Oil in water and water in oil

Another method to evaluate the wettability of the system under study was the measurement of the behavior of a drop of water on the functionalized membranes immersed in hexadecane (water-in-oil contact angle) and of a drop of hexadecane on the membranes immersed in water (oil-in-water contact angle). Interestingly, in the case of oil-in-water, a contact angle of 129.7 ° was obtained, as shown in Figure 4.23 (a), while in the case of water-in-oil a contact angle of 128.9 ° was recorded, as shown in Figure 4.23 (b).

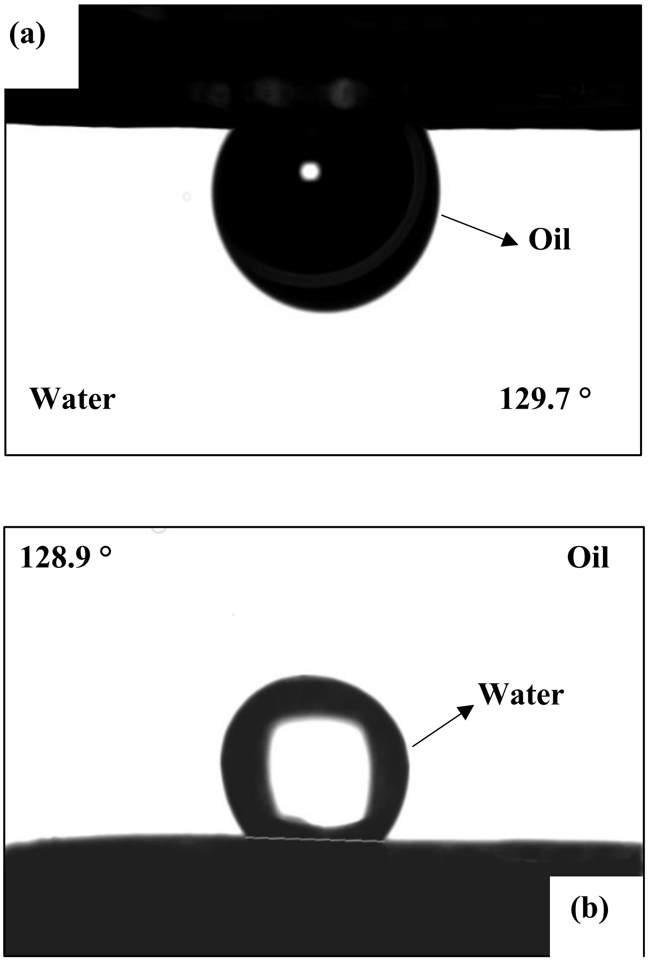

Figure 4.23: (a) Oil-in-water contact angle and (b) Water-in-oil contact angle for EM+UV+WT+PDMS sample.

Moreover, in both cases, a stability of the contact angle was recorded without any variation for 4 hours. For this reason, it was decided to continue with the measurement extending the test time up to 24 hours. The oil-in-water contact angle did not show any variation, presenting the same value at the end of the test, while the water-in-oil contact angle reached a value of 121.6 ° which, however, is still within the range of hydrophobic performance.

To understand the behavior of the water droplet on the surface of the membrane immersed in oil, it must be considered that, as previously demonstrated, oil is completely able to wet the surface of the membrane. Therefore, the liquid penetrates into the porous structure of the sample, without creating a repulsive barrier towards the second liquid (water) and allow it to interact with the surface of the membrane. Conversely, the membranes proved to be hydrophobic in principle, so that when they are immersed in water, the repulsive forces create a barrier effect preventing the oil from interacting directly with the surface, so the behavior of the oil droplet is totally opposite to the case in air conditions. Therefore, the value of the oil-in-water contact angle does not reflect the oleophilicity of the membrane, but rather the interactions between water and oil and the difference between the surface tension of both liquids.

A summary of the contact angle performance of membranes subjected to photoinduced crosslinking, water treatment for 24 hours and functionalized with PDMS is presented in Table 4.4, demonstrating the hydrophobic and oleophilic behavior of the samples obtained.

Table 4.4. Characteristic contact angles for EM+UV+WT+PDMS sample.

Test	**Contact angle (°)**	**Temporal stability**
Oil in air	13.7	< 1 minute Decrease to 10 ° in 60 s
Water in air	123.4	> 30 minutes
Oil in water	129.7	> 24 hours
Water in oil	128.9	Completely stable up to 4 hours. > 24 hours Decrease of approximately 7° in the next 20 hours

4.4 Mechanical properties of the electrospun membranes

The tensile tests were performed on the PDMS-functionalized membranes (EM+UV+WT+PDMS) and allowed to obtain an average value of three important mechanical properties of the materials, i.e., the Young's modulus (E), elongation at break and ultimate tensile strength (UTS), studying the behavior of the samples from the beginning of the tensile stress application until their failure. As shown in Figure 4.24, the sample failure was not severe, thanks to the elastic properties of the materials used in the fabrication of the membranes.

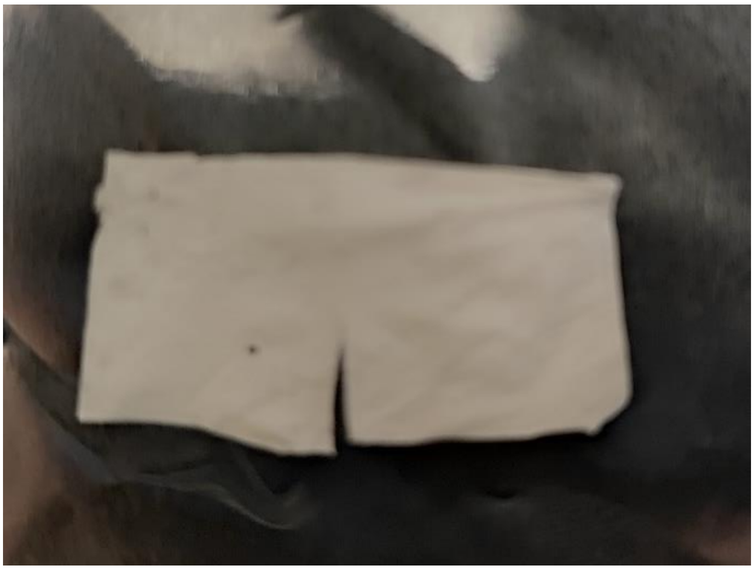

Figure 4.24: EM+UV+WT+PDMS sample after tensile test.

During the test, the sample is subjected to an uniaxial stress state, i.e., stressed only by a perpendicular stress component. The stress-strain curves obtained for the three samples are presented in Figure 4.25.

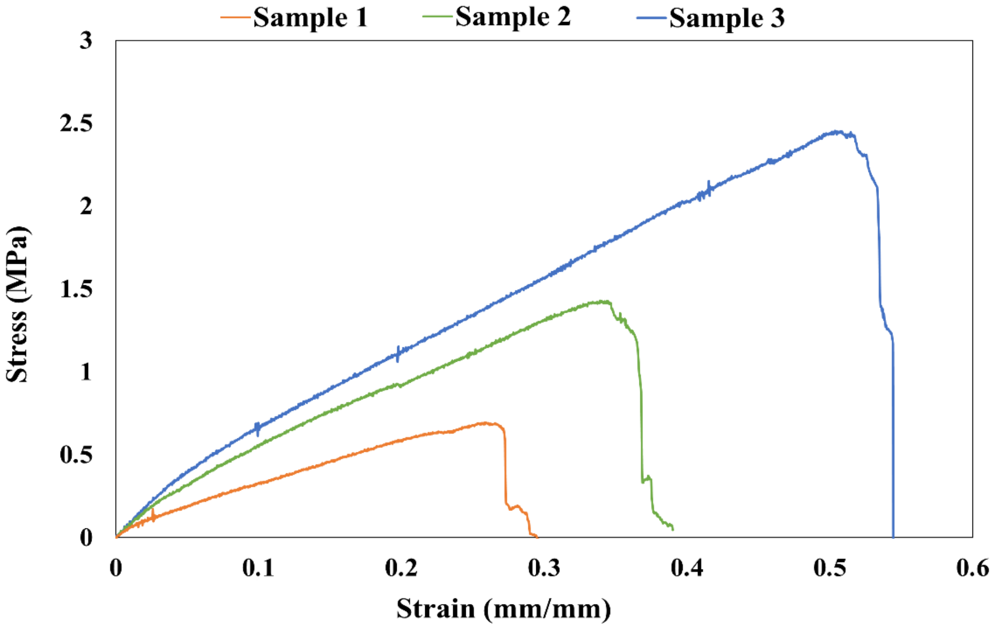

Figure 4.25. Stress-strain curves for EM+UV+WT+PDMS samples.

Firstly, a variation in the mechanical behavior of the samples can be observed. Although the membranes were subjected to the same surface treatments, it is important to consider that each sample was prepared from a different membrane, thus, this result could be an indication of the presence of defects in some of the samples. Furthermore, through quantitative analysis of the data obtained an elastic modulus of 8.3 ± 1.2 MPa, an elongation at break of 45.6% ± 7.7%, and an UTS of 1.7 ± 0.5 MPa were obtained. Interestingly, these values are comparable with those of the non-functionalized membranes [51] and of SBR membranes produced by solution electrospinning coupled with photo-crosslinking [64] , meaning that the morphology of the fibers (e.g., full fibers or fibers formed by rubber nanoparticles) and their chemical functionalization do not strongly influence the mechanical properties of the membranes.

4.4 Performance of the electrospun membranes in oil/water filtration processes

Given the results derived from the characterization tests, the possibility of exploring the potential of SBR electrospun membranes as filtration systems for oil/water mixtures was considered. Indeed, as described above, they exhibit selective wettability properties towards oil and water, as well as being easily tunable to obtain stable structures over time with interesting surface properties for the separation of liquids.

Concerning the possibility of using these membranes for this application, the penetration capacity of oil (hexadecane) and distilled water colored with a blue dye soluble in water and insoluble in oil was tested. The test was performed by pouring each of the liquids individually using the membranes before and after functionalization with PDMS as a filtration device. In particular, the oil was poured first and once no change in the stability of the system was noticed, the water was poured.

The non-functionalized membrane allowed both oil and water to pass through without any resistance. In fact, both liquids penetrated the membrane without applying any extra pressure other than the effect of gravity guaranteed by the filtration system. The result was that both liquids resulted mixed in the flask, as can be seen in Figure 4.26 (a), demonstrating that the sample did not work for oil/water separation. In this case it was not necessary to monitor the system over time, as the liquids flowed immediately upon pouring.

The mixture obtained at the end of the test can be seen in the Figure 4.26 (b), where both hexadecane (transparent) and water (blue) can be clearly identified.

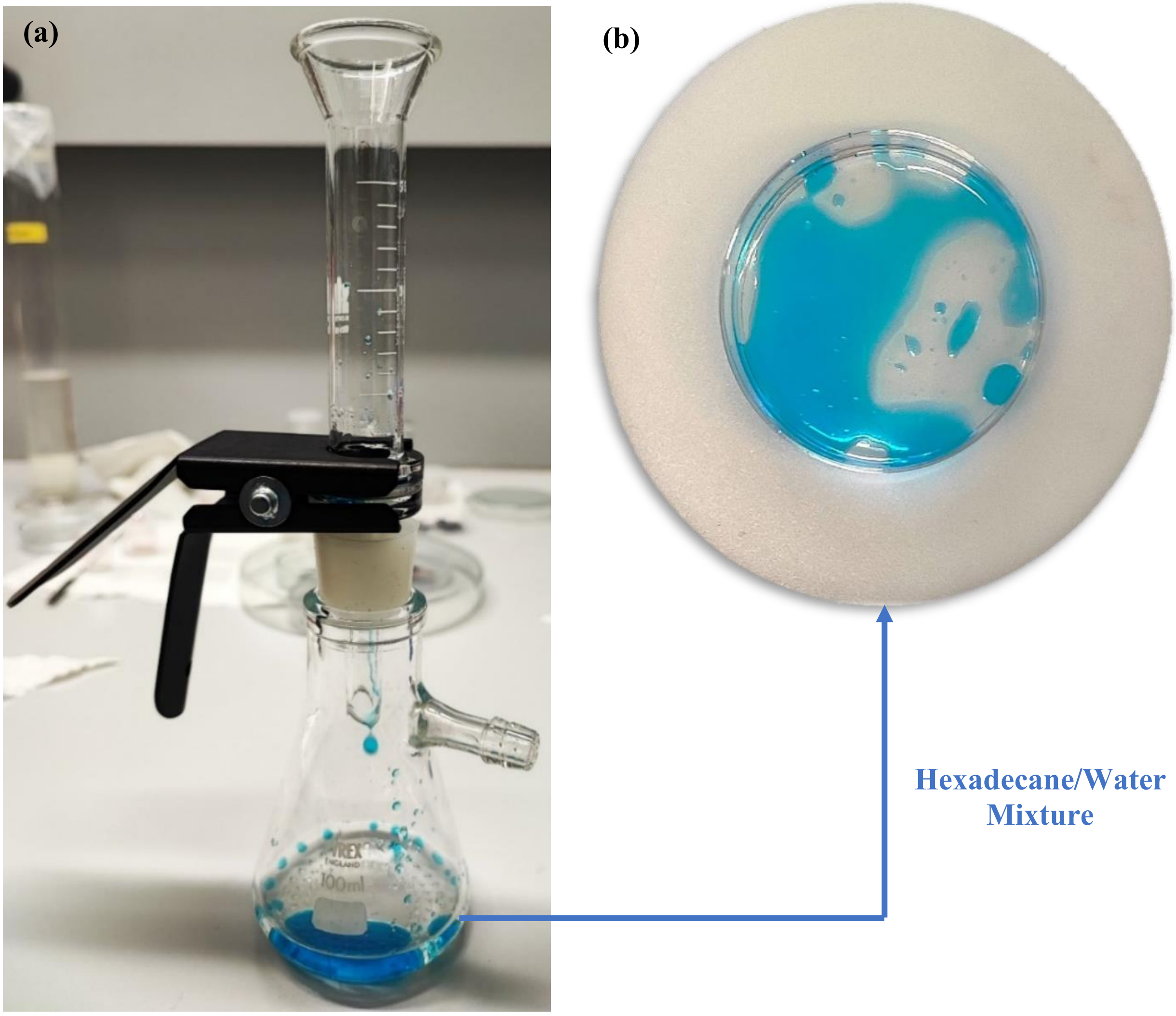

Figure 4.26: (a) Performance in terms of separation capacity of EM sample. (b) Mixture obtained after the test.

In turn, the functionalized membrane allowed hexadecane to pass through correctly, as shown in Figure 4.27 (a), while blocking the passage of water (Figure 4.27 (b)). After observing that the water remained suspended in the graduated cylinder thanks to the action of the membrane, the system was left with the same configuration for one hour, monitoring the state of the permeate and the concentrate after 5, 10, 30 and 60 minutes. The final state of the filtration process at the end of the test is shown in Figure 4.27 (c). During this time, no change was observed in the system and no presence of water droplets was detected in the flask, thus it is possible to state that the membrane performed its function as a filtration device correctly. In fact, Figure 4.27 (d) shows the water and hexadecane obtained after the filtration process.

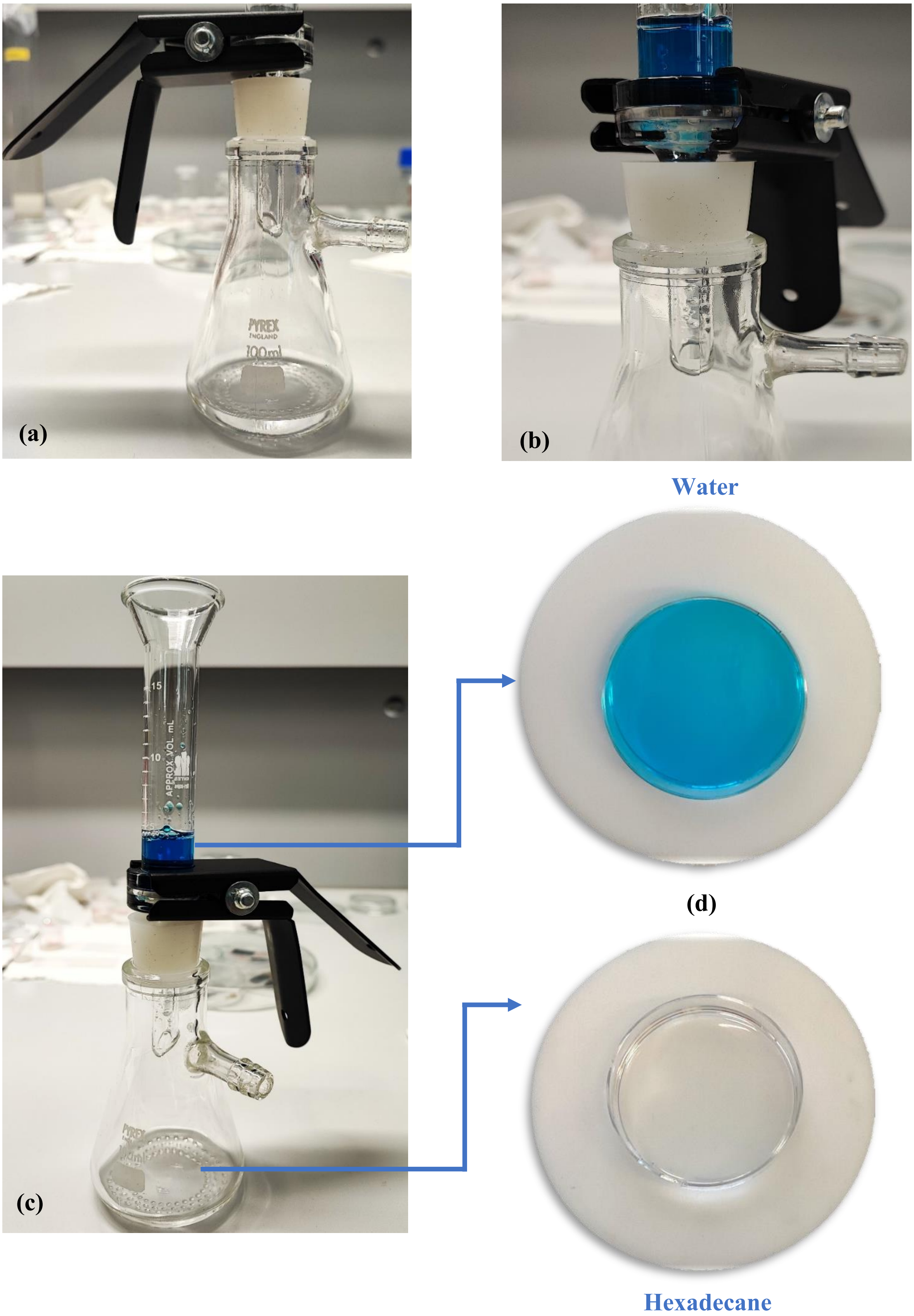

Figure 4.27: (a) Permeation of hexadecane through the EM+UV+WT+PDMS sample (b) Water retention in the graduated cylinder (c) Stable filtration system after 60 minutes (d) Separated water and hexadecane obtained through the filtration set-up.

The volume and weight of the filtered oil was measured and, although no water droplets were visually detected in the hexadecane fraction (as shown in Figure 4.28), possible water residues were allowed to evaporate overnight. Then, the volume and weight of hexadecane were measured again, allowing to estimate an oil flux value (φ) of 993.2 $L \cdot m^{-2} \cdot h^{-1}$ and a separation efficiency value (η) of 99.8 %, which represent a competitive percentage with respect to other membranes used for the filtration of oil/water mixtures and emulsions found in literature [65, 66, 67].

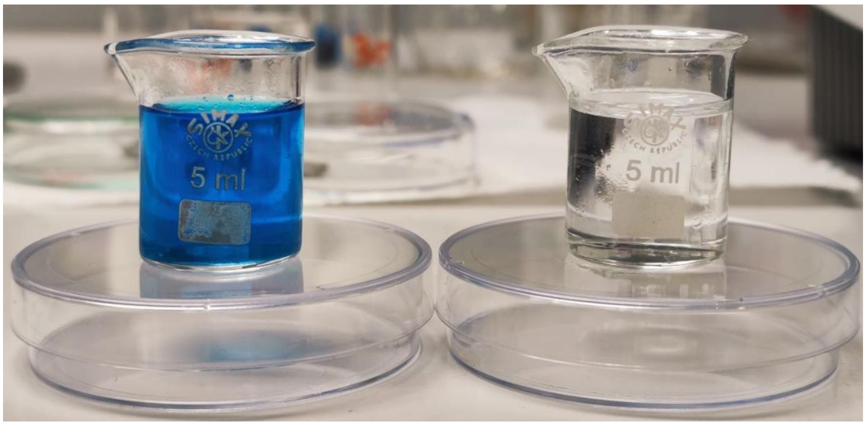

Figure 4.28: Detail of the separated water and hexadecane obtained through the filtration set-up.

To study the consistency of these results, several filtration cycles were repeated using the same membrane, alternately pouring 5 ml of hexadecane and 5 ml of dyed water in each cycle. Results obtained in terms of separation efficiency and oil flux are shown in Figure 4.29, demonstrating a quite stable performance of the functionalized SBR membranes. In particular, after 20 filtration cycles, a separation efficiency value of 99.3 % was calculated, while the average oil flux was 988.4 $L \cdot m^{-2} \cdot h^{-1}$.

Although a small variation was observed with respect to the values obtained in the case of a single cycle, these are still high-performance values. Further investigation of the reasons behind this variation would be interesting, considering aspects such as the optimization of the procedure to perform the filtration tests or possible fouling effects of the membrane.

Finally, separation tests were performed using a dispersion of hexadecane droplets in water, obtained by intensely stirring the oil/water liquid mixture, as shown in Figure 4.30 (a). In this case, it was observed that the separation process was slower (approximately twice the time compared to the case of filtration of the simple mixture), allowing the difference in density between water and hexadecane to partially establish the separation of the mixture in the graduated cylinder. However, it was observed that the membrane was able to separate the mixture as well. In this case, the separation efficiency was 99.4 %, which is comparable to the percentage obtained in the case of the simple mixture. However, being a slower process, the oil flux obtained was considerably lower, with a value of 529.9 L·m^{-2}·h^{-1}. The fraction of filtered oil and water obtained were observed through the optical microscope to evaluate the separation process from a qualitative point of view by studying the presence of oil droplets in the water. Again, an efficient separation of the mixture was observed, as shown in Figure 4.30 (b).

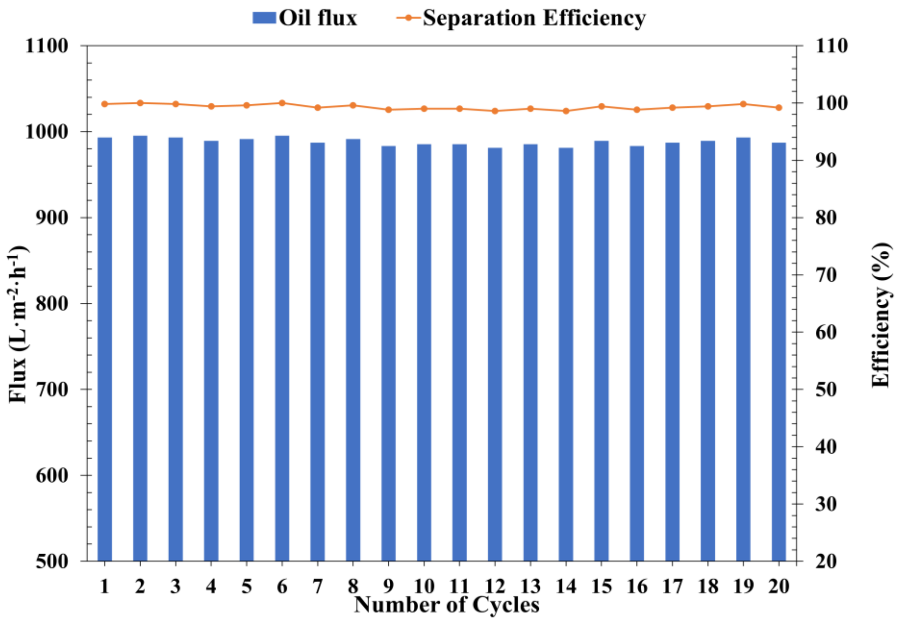

Figure 4.29: Oil flux and separation efficiency of an oil/water mixture using EM+UV+WT+PDMS.

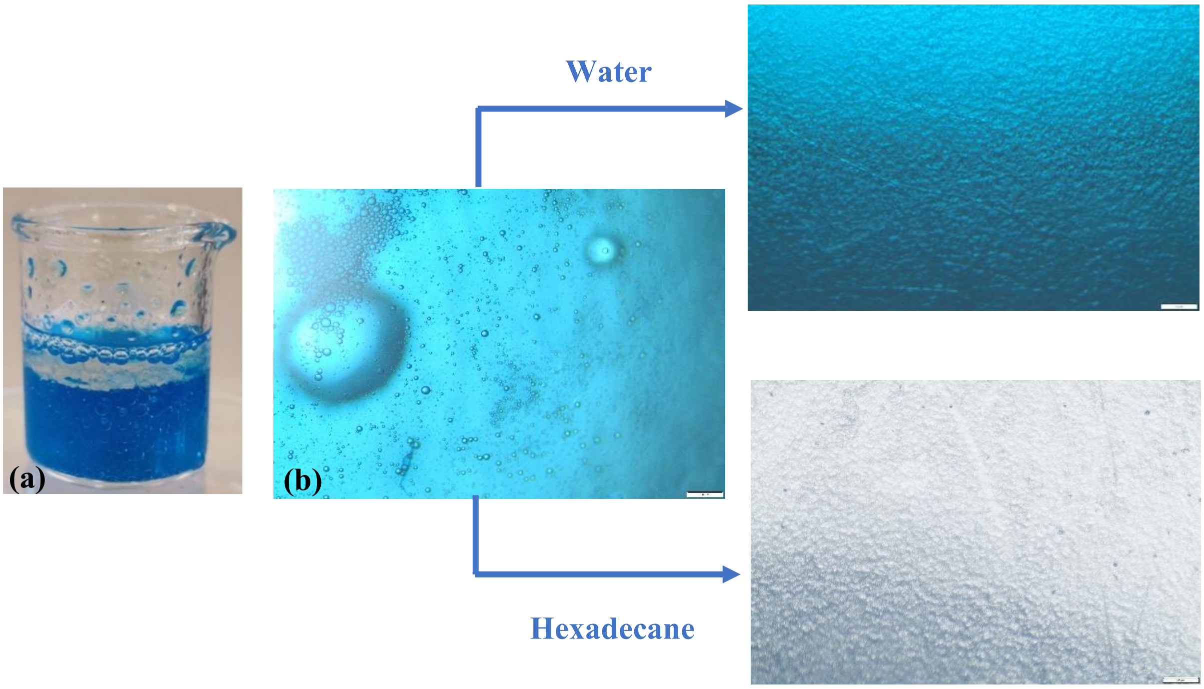

Figure 4.30: (a) Stirred oil/water mixture (b) Optical microscope images of the stirred oil/water mixture and of the water and oil obtained after the filtration process.

5 Conclusion and perspectives

This research work allowed to confirm the possibility of using a rubber (SBR) latex to obtain stable fibrous membranes of nanometric dimensions through the use of green electrospinning, a polymeric template (PEO) and a photoinduced thiol-ene crosslinking reaction. This result represents an interesting approach in the field of rubber electrospinning, as these materials are usually hardly electrospinnable due to the intrinsic characteristics of the solutions to which they give rise, and generally need the use of harsh and toxic solvents to be processed.

ATR FT-IR analysis confirmed the conversion (47 %) upon UV irradiation of the SBR reactive vinyl groups thanks to the presence of a multifunctional thiol crosslinker (TRIS).

In addition, it was possible to verify the correct removal of PEO through a water treatment applied during the production of the membranes, since in the morphological analyses a significant change in the structure of the fibers composing the membranes could be clearly observed. In particular, it was observed that once the polymeric template was removed, continuous nanofibers (with an average diameter of 638.2 ± 5.3 nm) formed by SBR distinct rubber nanoparticles partially fused together, were obtained. Thus, such membranes present a high percentage of porosity, which represents an interesting result regarding their application as systems for the treatment of oil/water mixtures, since the higher specific surface area promotes the separation processes.

Furthermore, with the aim of obtaining membranes with stable hydrophobicity and oleophilicity, a vinyl terminated PDMS functionalizing agent was grafted on the nanofibers through a thiol-ene photoinduced polymerization reaction. It was possible to verify the correct functionalization of the membranes by FT-IR analyses, thanks to the presence of the characteristic absorption bands of the functionalizing agent in their chemical composition (i.e., 795 cm^{-1}, 1020 cm^{-1}, 1080 cm^{-1}, 1257 cm^{-1}, 2960 cm^{-1}).

Contact angle tests demonstrated that the developed PDMS-functionalized rubber nanofibrous membranes are able to maintain their hydrophobicity with time (water contact angle of 123.4 ° after 30 minutes, water-in-oil contact angle of 121.9 ° after 24 hours), as well as presenting a distinctive oleophilic behavior (oil contact angle < 10 °). Finally, the membranes proved to successfully separate oil from water, with an average separation efficiency of 99.3 % and an oil flux of 988.4 $L \cdot m^{-2} \cdot h^{-1}$, both after 20 cycles of filtration of an oil/water mixture, while they showed a separation efficiency of 99.4 % and an oil flux of 529.9 $L \cdot m^{-2} \cdot h^{-1}$ in the case of a simple dispersion of oil droplets in water. These results represent an outstanding application potential for the treatment of polluted oily water with the use of PDMS-functionalized rubber nanofibrous membranes.

It is highly recommended to continue the study of the filtration system considering more complex oil/water mixtures (e.g. with the use of different light and heavy oils or emulsions) and in terms of possible failures due to fouling or mechanical properties of the membranes.

References

[1] Wei, Y., Qi, H., Gong, X. and Zhao, S., (2018). Specially Wettable Membranes for Oil–Water Separation. *Advanced Materials Interfaces*. 5(23), 1800576. [DOI: 10.1002/admi.201800576]

[2] Cleana Water ® (2022). Oil Water Separator Benefits. Accessed on 08/26/2023. [Available online at: https://cleanawater.com.au/information-centre/oil-water-separator-benefits]

[3] Valicor ® (2022). An Introduction to Oily Wastewater Treatment and Oil Recovery Services. Accessed on 08/26/2023. [Available online at: https://www.valicor.com/blog/an-introduction-to-oily-wastewater-and-oil-recovery#:~:text=Oily%20wastewater%20contamination%20affects%20drinking,ability%20to%20produce%20healthy%20crops]

[4] Yu, L., Han, M. and He, F., (2017). A review of treating oily wastewater. *Arabian Journal of Chemistry*. 10, S1913—S1922. [DOI: 10.1016/j.arabjc.2013.07.020]

[5] Abuhasel, K., Kchaou, M., Alquraish, M., Munusamy, Y. and Jeng, Y. T., (2021). Oily Wastewater Treatment: Overview of Conventional and Modern Methods, Challenges, and Future Opportunities. *Water*. 13(7), 980. [DOI: 10.3390/w13070980]

[6] Sawyer, C. N., Perry L. McCarty, Gene F. Parkin (2003). Chemistry for environmental engineering and science. 5th ed. Boston: McGraw-Hill. [ISBN 978-0-07-248066-5]

[7] World Wildlife Fund, WWF® (2023). Water Scarcity. Accessed on 08/26/2023. [Available online at: https://www.worldwildlife.org/threats/water-scarcity]

[8] UNICEF (2020). Water scarcity: Addressing the growing lack of available water to meet children’s needs. Accessed on 08/26/2023. [Available online at: https://www.unicef.org/wash/water-scarcity]

[9] United Nations Educational, Scientific and Cultural Organization, UNESCO (2017). The United Nations World Water Development Report 2017: Wastewater the Untapped Resource. Paris, France. [ISBN : 978-92-3-100201-4]

[10] Kwon, G., Post, E. and Tuteja, A., (2015). Membranes with selective wettability for the separation of oil–water mixtures. *MRS Communications*. 5(3), 475–494. [DOI: 10.1557/mrc.2015.61]

[11] Han, M., Zhang, J., Chu, W., Chen, J. and Zhou, G., (2019). Research Progress and Prospects of Marine Oily Wastewater Treatment: A Review. *Water*. 11(12), 2517. [DOI: 10.3390/w11122517]

[12] Rocha e Silva, F. C. P., Rocha e Silva, N. M. P., Luna, J. M., Rufino, R. D., Santos, V. A. and Sarubbo, L. A., (2018). Dissolved air flotation combined to biosurfactants: a clean and efficient alternative to treat industrial oily water. *Reviews in Environmental Science and Bio/Technology*. 17(4), 591–602. [DOI: 10.1007/s11157-018-9477-y]

[13] Medeiros, A. D. M. d., Silva Junior, C. J. G. d., Amorim, J. D. P. d., Durval, I. J. B., Costa, A. F. d. S. and Sarubbo, L. A., (2022). Oily Wastewater Treatment: Methods, Challenges, and Trends. *Processes*. 10(4), 743. [DOI: 10.3390/pr10040743]

[14] Daiminger, U., Nitsch, W., Plucinski, P. e Hoffmann, S., (1995). Novel techniques for iol/water separation. *Journal of Membrane Science*. 99(2), 197–203. [DOI: 10.1016/0376-7388(94)00218-n]

[15] Ahmad, A. L., Ismail, S. and Bhatia, S., (2005). Optimization of Coagulation−Flocculation Process for Palm Oil Mill Effluent Using Response Surface Methodology. *Environmental Science & Technology*. 39(8), 2828–2834. [DOI: 10.1021/es0498080]

[16] Zhao, C., Zhou, J., Yan, Y., Yang, L., Xing, G., Li, H., Wu, P., Wang, M. and Zheng, H., (2020). Application of coagulation/flocculation in oily wastewater treatment: A review. *Science of The Total Environment*. 142795. [DOI: 10.1016/j.scitotenv.2020.142795]

[17] Mohtashami, R. and Shang, J. Q., (2019). Electroflotation for Treatment of Industrial Wastewaters: A Focused Review. *Environmental Processes*. 6(2), 325–353. [DOI: 10.1007/s40710-019-00348-z]

[18] Rocha e Silva, F. C. P., Rocha e Silva, N. M. P., Luna, J. M., Rufino, R. D., Santos, V. A. and Sarubbo, L. A., (2018). Dissolved air flotation combined to biosurfactants: a clean and efficient alternative to treat industrial oily water. *Reviews in Environmental Science and Bio/Technology*. 17(4), 591–602. [DOI: 10.1007/s11157-018-9477-y]

[19] Le, T. V., Imai, T., Higuchi, T., Yamamoto, K., Sekine, M., Doi, R., Vo, H. T. and Wei, J., (2013). Performance of tiny microbubbles enhanced with “normal cyclone bubbles” in separation of fine oil-in-water emulsions. *Chemical Engineering Science*. 94, 1–6. [DOI: 10.1016/j.ces.2013.02.044]

[20] Santos, M. R. G., Goulart, M. O. F., Tonholo, J. and Zanta, C. L. P. S., (2006). The application of electrochemical technology to the remediation of oily wastewater. *Chemosphere*. 64(3), 393–399. [DOI: 10.1016/j.chemosphere.2005.12.036]

[21] Mohd-Salleh, S. N. A., Mohd-Zin, N. S. and Othman, N., (2019). A Review of Wastewater Treatment using Natural Material and Its Potential as Aid and Composite Coagulant. Sains Malaysiana. 48(1), 155–164. [DOI: 10.17576/jsm-2019-4801-18]

[22] Thines, R. K., Mubarak, N. M., Nizamuddin, S., Sahu, J. N., Abdullah, E. C. and Ganesan, P., (2017). Application potential of carbon nanomaterials in water and wastewater treatment: A review. *Journal of the Taiwan Institute of Chemical Engineers*. 72, 116–133. [DOI: 10.1016/j.jtice.2017.01.018]

[23] Mulder, M., (1996). Basic principles of membrane technology. 2nd ed. Dordrecht: Kluwer Academic.

[24] K, G. V. and Ali, I., (2012). Environmental Water: Advances in Treatment, Remediation and Recycling. Elsevier Science & Technology Books.

[25] Wang, L. K., (2011). Membrane and desalination technologies. New York, NY: Humana Press.

[26] Iorhemen, O., Hamza, R. e Tay, J., (2016). Membrane Bioreactor (MBR) Technology for Wastewater Treatment and Reclamation: Membrane Fouling. *Membranes*. 6(2), 33. [DOI: 10.3390/membranes6020033]

[27] Bongiovanni, R., Nettis, E. and Vitale, A., (2020). Fluoropolymers for oil/water membrane separation. In: Opportunities for Fluoropolymers. Elsevier. pp. 209–246. [DOI: 10.1016/b978-0-12-821966-9.00008-0]

[28] Zhen, G., (2009). Fundamentals and applications of nanomaterials. Boston: Artech House.

[29] Su, B., Tian, Y. and Jiang, L., (2016). Bioinspired Interfaces with Superwettability: From Materials to Chemistry. *Journal of the American Chemical Society*. [DOI: 10.1021/jacs.5b12728]

[30] Myers, D., (1999). Surfaces, Interfaces, and Colloids. Wiley & Sons, Incorporated, John.

[31] III. An essay on the cohesion of fluids, (1805). *Philosophical Transactions of the Royal Society of London*. 95, 65–87. [DOI: 10.1098/rstl.1805.0005]

[32] Makkonen, L., (2016). Young's equation revisited. *Journal of Physics: Condensed Matter*. 28(13), 135001. [DOI: 10.1088/0953-8984/28/13/135001]

[33] Wenzel, R. N., (1936). Resistance of solid surfaces to wetting by water. *Industrial & Engineering Chemistry*. 28(8), 988–994. [DOI: 10.1021/ie50320a024]

[34] Cassie, A. B. D. and Baxter, S., (1944). Wettability of porous surfaces. *Transactions of the Faraday Society.* 40, 546. [DOI: 10.1039/tf9444000546]

[35] Cheng, D. F., Urata, C., Yagihashi, M. and Hozumi, A., (2012). A Statically Oleophilic but Dynamically Oleophobic Smooth Nonperfluorinated Surface. *Angewandte Chemie International Edition*. 51(12), 2956–2959. [DOI: 10.1002/anie.201108800]

[36] Qing, W., Shi, X., Deng, Y., Zhang, W., Wang, J. and Tang, C. Y., (2017). Robust superhydrophobic-superoleophilic polytetrafluoroethylene nanofibrous membrane for oil/water separation. *Journal of Membrane Science*. 540, 354–361. [DOI: 10.1016/j.memsci.2017.06.060]

[37] Feng, L., Zhang, Z., Mai, Z., Ma, Y., Liu, B., Jiang, L. e Zhu, D., (2004). A Super-Hydrophobic and Super-Oleophilic Coating Mesh Film for the Separation of Oil and Water. *Angewandte Chemie International Edition*. 43(15), 2012–2014. [DOI: 10.1002/anie.200353381]

[38] Ye, C., Voet, V. S. D., Folkersma, R. e Loos, K., (2021). Robust Superamphiphilic Membrane with a Closed-Loop Life Cycle. *Advanced Materials*. 33(15), 2008460. [DOI: 10.1002/adma.202008460]

[39] Yang, H.-C., Xie, Y., Hou, J., Cheetham, A. K., Chen, V. e Darling, S. B., (2018). Janus Membrane: Janus Membranes: Creating Asymmetry for Energy Efficiency. *Advanced Materials*. 30(43), 1870328. [DOI: 10.1002/adma.201870328]

[40] Yang, H.-C., Hou, J., Chen, V. e Xu, Z.-K., (2016). Janus Membranes: Exploring Duality for Advanced Separation. *Angewandte Chemie International Edition*. 55(43), 13398–13407. [DOI: 10.1002/anie.201601589]

[41] Wendorff, J., Burgard, M., Greiner, A. e Agarwal, S., (2016). Electrospinning: A Practical Guide to Nanofibers. de Gruyter GmbH, Walter.

[42] Agarwal, S., Greiner, A. e Wendorff, J. H., (2013). Functional materials by electrospinning of polymers. *Progress in Polymer Science*. 38(6), 963–991. [DOI: 10.1016/j.progpolymsci.2013.02.001]

[43] Ramakrishna, S., Greiner, A., Wendorff, J. H. e Agarwal, S., (2012). Electrospinning: Materials, Processing, and Applications. Wiley-VCH Verlag GmbH.

[44] Reneker, D. H. e Yarin, A. L., (2008). Electrospinning jets and polymer nanofibers. *Polymer*. 49(10), 2387–2425. [DOI: 10.1016/j.polymer.2008.02.002]

[45] The New Zealand Institute for Plant and Food Research Ltd (2008). A diagram of the electrospinning process showing the onset of instability. Provided by Joanna Gatford.

[46] Xue, J., Wu, T., Dai, Y. e Xia, Y., (2019). Electrospinning and Electrospun Nanofibers: Methods, Materials, and Applications. *Chemical Reviews*. 119(8), 5298–5415. [DOI: 10.1021/acs.chemrev.8b00593]

[47] Fang, J. e Lin, T., (2016). Fundamentals of Electrospinning & Electrospun Nanofibers. DEStech Publication, Inc.

[48] Stoiljkovic, A., Ishaque, M., Justus, U., Hamel, L., Klimov, E., Heckmann, W., Eckhardt, B., Wendorff, J. H. e Greiner, A., (2007). Preparation of water-stable submicron fibers from aqueous latex dispersion of water-insoluble polymers by electrospinning. *Polymer*. 48(14), 3974–3981. [DOI: 10.1016/j.polymer.2007.04.050]

[49] Gonzalez, E., Barquero, A., Muñoz-Sanchez, B., Paulis, M. e Leiza, J. R., (2021). Green Electrospinning of Polymer Latexes: A Systematic Study of the Effect of Latex Properties on Fiber Morphology. *Nanomaterials*. 11(3), 706. [DOI: 10.3390/nano11030706]

[50] Cui, J., Lu, T., Li, F., Wang, Y., Lei, J., Ma, W., Zou, Y. e Huang, C., (2021). Flexible and transparent composite nanofibre membrane that was fabricated via a "green" electrospinning method for efficient particulate matter 2.5 capture. *Journal of Colloid and Interface Science*. 582, 506–514. [DOI: 10.1016/j.jcis.2020.08.075]

[51] Kianfar, P., Bakry, A., Dalle Vacche, S., Bongiovanni, R., Vitale, A., Green electrospinning of SBR latex combined with photo-induced crosslinking: control of nanofiber composition, morphology and properties. Manuscript in preparation.

[52] Agarwal, S. e Greiner, A., (2011). On the way to clean and safe electrospinning-green electrospinning: emulsion and suspension electrospinning. *Polymers for Advanced Technologies*. 22(3), 372–378. [DOI: 10.1002/pat.1883]

[53] Sarbatly, R., Krishnaiah, D. e Kamin, Z., (2016). A review of polymer nanofibres by electrospinning and their application in oil–water separation for cleaning up marine oil spills. *Marine Pollution Bulletin*. 106(1-2), 8–16. [DOI: 10.1016/j.marpolbul.2016.03.037]

[54] Lin, J., Tian, F., Shang, Y., Wang, F., Ding, B. e Yu, J., (2012). Facile control of intra-fiber porosity and inter-fiber voids in electrospun fibers for selective adsorption. *Nanoscale*. 4(17), 5316. [DOI: 10.1039/c2nr31515g]

[55] Zubov, A., Pokorny, J. and Kosek, J., (2012). Styrene–butadiene rubber (SBR) production by emulsion polymerization: Dynamic modeling and intensification of the process. *Chemical Engineering Journal*. 207-208, 414–420. [DOI: 10.1016/j.cej.2012.06.144]

[56] Thomasnet ®. All About Sbr Rubber - Properties, Applications and Uses. Accessed on 09/01/2023. [Available online at: https://www.thomasnet.com/articles/plastics-rubber/all-about-sbr-rubber/]

[57] Britannica, The Editors of Encyclopaedia (2023). Styrene-butadiene rubber. Accessed on 09/01/2023. [Available online at: https://www.britannica.com/science/styrene-butadiene-rubber]

[58] Massaglia, G., Frascella, F., Chiadò, A., Sacco, A., Marasso, S. L., Cocuzza, M., Pirri, C. F. and Quaglio, M., (2020). Electrospun Nanofibers: from Food to Energy by Engineered Electrodes in Microbial Fuel Cells. *Nanomaterials*. 10(3), 523. [DOI: 10.3390/nano10030523]

[59] Wakschem. Trimetilolpropano tris(3-mercaptopropionato). Accessed on 09/01/2023. [Available online at: https://www.wakschem.com/?product/id24353-cas33007-83-9]

[60] Mata, A., Fleischman, A. J. and Roy, S., (2005). Characterization of Polydimethylsiloxane (PDMS) Properties for Biomedical Micro/Nanosystems. *Biomedical Microdevices*. 7(4), 281–293. [DOI: 10.1007/s10544-005-6070-2]

[61] Kuo, A. C. M. (1999). Poly (Dimethylsiloxane). Polymer Data Handbook 411–435. Oxford University Press, Oxford.

[62] Decker, C. and Nguyen Thi Viet, T., (2000). High-speed photocrosslinking of thermoplastic styrene-butadiene elastomers. *Journal of Applied Polymer Science*. 77(9), 1902–1912. [DOI: 10.1002/1097-4628(20000829)77:9%3C1902::aid-app6%3E3.0.co;2-6]

[63] Zhou, J., Ellis, A. V. and Voelcker, N. H., (2010). Recent developments in PDMS surface modification for microfluidic devices. *ELECTROPHORESIS*. 31(1), 2–16. [DOI: 10.1002/elps.200900475]

[64] Vitale, A., Massaglia, G., Chiodoni, A., Bongiovanni, R., Pirri, C. F. and Quaglio, M., (2019). Tuning Porosity and Functionality of Electrospun Rubber Nanofiber Mats by Photo-Crosslinking. *ACS Applied Materials & Interfaces*. 11(27), 24544–24551. [DOI: 10.1021/acsami.9b04599]

[65] Zhang, W., Shi, Z., Zhang, F., Liu, X., Jin, J. and Jiang, L., (2013). Superhydrophobic and Superoleophilic PVDF Membranes for Effective Separation of Water-in-Oil Emulsions with High Flux. *Advanced Materials*. 25(14), 2071–2076. [DOI: 10.1002/adma.201204520]

[66] Jiang, S., Meng, X., Chen, B., Wang, N. and Chen, G., (2020). Electrospinning superhydrophobic–superoleophilic PVDF-SiO 2 nanofibers membrane for oil–water separation. *Journal of Applied Polymer Science*. 137(47), 49546. [DOI: 10.1002/app.49546]

[67] Ma, W., Zhang, M., Liu, Z., Kang, M., Huang, C. and Fu, G., (2019). Fabrication of highly durable and robust superhydrophobic-superoleophilic nanofibrous membranes based on a fluorine-free system for efficient oil/water separation. *Journal of Membrane Science*. 570-571, 303–313. [DOI: 10.1016/j.memsci.2018.10.035]